Fuzzy Logic Based Space Vector Modulation Direct Torque Control of Induction Motor for Electric Vehicle Application (Case: Daewoo Damas II)

Tsion Tigistu Tadesse

A Thesis Submitted to

The Department of Electrical Power and Control Engineering

School of Electrical Engineering and Computing

Presented in Partial Fulfillment of the Requirements for the Master of Science Degree in Electrical Power and Control Engineering (Power Electronics)

Office of Graduate Studies

Adama Science and Technology University

October 2020

Adama, Ethiopia

Fuzzy Logic Based Space Vector Modulation Direct Torque Control of Induction Motor for Electric Vehicle Application (Case: Daewoo Damas II)

Tsion Tigistu Tadesse

Advisor:

Tafese Asrat (PhD)

A Thesis Submitted to

The Department of Electrical Power and Control Engineering

School of Electrical Engineering and Computing

Presented in Partial Fulfillment of the Requirements for the Master of Science Degree in Electrical Power and Control Engineering (Power Electronics)

Office of Graduate Studies

Adama Science and Technology University

October 2020

Adama, Ethiopia

APPROVAL OF BOARD OF EXAMINERS

We, the undersigned, members of the board of examiners of the final open defense by Tsion Tigistu Tadesse have read and evaluated her thesis entitled "Fuzzy Logic Based Space Vector Modulation Direct Torque Control of Induction Motor for Electric Vehicle Application (Case: Daewoo Damas II)" and examined the candidate. This is, therefore, to certify that the thesis has been accepted in partial fulfillment of the requirement of the Degree of Master of Science in Electrical Power and Control Engineering (Power Electronics).

Name of Student	Signature	Date
Advisor / Supervisor /	Signature	Date
Yoseph Mekonnen (Ph.D)		31/10/20
External Examiner	Signature	Date
Internal Examiner	Signature	Date
Chairperson	Signature	Date
Head of Department	Signature	Date
School Dean	Signature	Date
Postgraduate Dean	Signature	Date

DECLARATION

I hereby declare that this MSc thesis has been composed by myself and that the work has not be submitted for any other degree or professional qualification. And all sources of material used for this thesis have been duly acknowledged.

Name: Tsion Tigistu Tadesse

Signature: ______________________

This MSc Thesis has been submitted for examination with my approval as thesis advisor.

Name: _________________________________

Signature: ______________________________

Date of submission: ______________________

ADVISOR'S APPROVAL SHEET

To: Electrical Power and Control Engineering Department (EPCE)

Subject: Thesis Submission

This is to certify that the thesis entitled "Fuzzy Logic Based Space Vector Modulation Direct Torque Control of Induction Motor for Electric Vehicle Application (Case: Daewoo Damas II)" submitted in partial fulfillment of the requirements for the degree of Masters of Science in Electrical Power and Control Engineering (Power Electronics), the Graduate program of the department of Electrical Power and Control Engineering, and has been carried out by Tsion Tigistu Tadesse, Id number PGR/18384/11, under my supervision. Therefore, I recommend that the student has fulfilled the requirements and hence hereby she can submit the thesis to the department.

______________________	____________________	_______________
Advisor	Signature	Date

ACKNOWLEDGEMENTS

First, I would like to express the deepest appreciation to my thesis advisor **Dr. Tafese Asrat** for his guidance, encouragement, friendly attitude and patience. The door to Dr. Tafese Asrat office was always open whenever I ran into a trouble spot or had a question about my research. You are highly appreciated!

I am also deeply grateful to **Dr. Tefera Terefe** and **Dr. P. Palanivel** for all of their guidance through this process; your discussion, ideas, and feedback have been absolutely invaluable.

I would moreover like to thank **Mr. Minyamer Gelawe (MSc.)** for helping in editing the documentation. I also wish to show my gratitude to anyone who ever shared their knowledge with me.

Finally, I must express my very profound gratitude to my friends and my parents especially my mother Sara Desta and my fiancé Yitaferu Mulatu for providing me with unfailing support and continuous encouragement throughout my years of study and through the process of researching and writing this thesis. This accomplishment would not have been possible without them. Thank you.

ABSTRACT

Recently a lot of effort has been focused on the development of high performance EV drives. This is mainly; to reduce the environmental pollution due to emissions from internal combustion engine driven vehicles, to replace fossil fuels with a renewable energy source due to its fast depletion. Also, it is used to prevent economic damage due to climate change. Induction motor widely used for EV application because of its good self-starting capability, simple and rugged structure, low cost and reliability. In order to have a good dynamic and transient response of the drive an appropriate control algorithm is required. In this regard, direct torque control-based space vector modulation (DTC-SVM) is proposed for the speed control of the induction motor using fuzzy logic controller for the propulsion of EV Daewoo Damas II. In order to achieve this, the mathematical modeling of the three-phase induction motor, SVM, and vehicle dynamics mathematical modeling are done. Also, the system is simulated in MATLAB software tool. The DTC-SVM scheme is a high-performance control of IM drives to improve the ripples of torque and flux in steady state, which is drawback of conventional DTC. DTC-SVM has three controllers; speed controller, flux controller, and torque controller. To improve the performance of the motor fuzzy speed controller proposed and compared with PID controller their steady state and transient response is analyzed for different set speed of the motor. From the result it can be observed that with fuzzy speed controller a better dynamics response can be achieved with 0% overshoot and 0.05sec settling time. Generally, the simulation result show that the response of motor speed with the fuzzy speed controller is more robust, and reaches to the reference value faster than a PID speed controller and also it has low torque ripple of ±2 Nm.

Key words: *Daewoo Damas II, EV, IM, SVM-DTC, Fuzzy logic controller, and PID.*

TABLE OF CONTENTS

LIST OF FIGUERS

LIST OF TABLES

LIST OF ACRONYMS

Abbreviations	Description
AC	Alternating Current
ANFIS	Adaptive Neuro Fuzzy Interference System
CDTC	Conventional Direct Torque Controller
CO_2	Carbon di oxide
DC	Direct Current
DSP	Digital Signal Processing
DSVM	Discrete Space Vector Modulation
DTC	Direct Torque Controller
EV	Electric Vehicle
BLDC	Brushless Direct Current Motor
FOC	Field Oriented Control
IM	Induction Motor
IMD	Induction Motor Drive
IFOC	Indirect Field Oriented Control
PI	Proportional Integral
PID	Proportional Integral Derivative
PWM	Pulse Width Modulation
PMSM	Permanent Magnet Synchronous Motor
SRM	Switched Reluctance Motor
SVM	Space Vector Modulation
VFD	Variable Frequency Drives
VSI	Voltage Source Inverters
V/F	Voltage per Frequency

LIST OF SYMBOLS

A_f	Frontal area of the car
Cd	Drag coefficient
Crr	Rolling resistance friction constant
f	Power source frequency
Fa	Acceleration force
Fd	Aerodynamic (drag) force
Fg	Gradient (pulling) force
Frr	Rolling resistance force
g	Acceleration due to gravity
GR	Gear ratio
Ids, Iqs	Stator current in d-q frame
Idr, Iqr	Rotor current in d-q frame
J	Moment of Inertia
Kd	Derivative gain
Kp	Proportional gain
Ki	Integral gain
Lm	Mutual inductance
Lr	Rotor inductance
Ls	Stator inductance
M	Vehicle mass
P	Pole pair number
Pt	Maximum tractive power
r	Tier radius
Rr	Rotor resistance
Rs	Stator resistance
Superscript '*'	Indicates reference value
Te	Electromagnetic torque of the motor
V	Vehicle speed
Vdr, Vqr	Rotor voltage in d-q frame
Vds, Vqs	Stator voltage in d-q frame

Wr=wm	Rotor speed
θ	Elevating angel
P	Air density
γss	Stator flux position
η	Efficiency

CHAPTER 1

INTRODUCTION

1.1 Background

An electric vehicle does not contain an internal combustion engine like other vehicles with fuels. It has an electric motor and uses a large traction battery pack to power the electric motor. Nowadays these vehicles are becoming very popular due to their quiet operation and harmless emissions. They are considered to be a promising solution for future transportation. The foremost example is Tesla. These vehicles perform the work using a rechargeable battery instead of a fossil fuel like in the conventional combustion engine vehicles.

The first cars were indeed electrical at the end of the 19 and early 20 centuries [1]. Meanwhile, fossil fuel powered cars with internal combustion engine become available in the early 20 centuries than an intense computation began between the two types of vehicles. The fossil fuel powered cars win the computation due to two main reasons. The first reason is because of poor battery technology; electric vehicle has a low range in those days and could never travel the long distance ranged by the gasoline car and only limited charging stations were available [2]. Furthermore, charging them took much longer than refueling gasoline. The second reasons were the mass production of cheaper fossil fuel powered cars made them affordable [1].

Nowadays the technological advancement and increased concern on controlling pollution have given the electric car a tag of future mobility. A Suzuki Carry now called Daewoo Damas II originated from japan is a very well-known vehicle in Ethiopia since it is a general-purpose car it is becoming very popular. Since it is a fuel-based vehicle it has a CO_2 emission of 224g/km which is harmful to the environment. These types of gasoline vehicles should be replaced by electric ones. EV is more advantageous over internal combustion engine automobiles, including a significant reduction of air pollution and gas emissions. In mathematical design of the vehicle; mass of the car, wheel radius and area of the Daewoo Damas II vehicle is considered.

From different components of an electric vehicle, one of the main parts is the electrical motor which makes the wheels to rotate. Either a DC or an AC type motor can be used. In this study, an induction motor is selected due to its reliability, ruggedness, low maintenance, and low cost. IMs are particularly well suited for traction drive environments due to its good self-starting capability, simple and rugged structure, low cost and reliability [3]. One of the major limitations of an electric vehicle is its high cost. BLDC and PMSM are the lighter and most efficient over all motors but they have some down sides namely the fact that they rely on the rear earth metals in order to function which make them very costly which increases the overall cost of the vehicle. The technology advancement in the control of induction motor makes the controller cost effective and better to be used in an electric vehicle.

The introduction of the space vector theory for multi-phase AC machines in 1959, and the theory of pulse width modulation for AC drives in 1964 finally made it possible for AC motors to be used in speed-controlled drives. This was also due to the introduction of the silicon power switches in the 1950s, which made it possible to switch higher currents and voltages at faster speeds [4]. Several control strategies have been used for induction machine drives.

Traditionally scalar control was employed to control the speed of the motor by varying the voltage and applied frequency [4]. It is a simple and economic method that controls the voltage magnitude in proportion to change in the frequency. The idea is to maintain a constant magnetizing current effectively keeping the air-gap flux constant. However, the decoupling effect is not taken into consideration. The change in control parameters of either voltage or frequency also leads to change in torque and flux respectively, as torque and flux are also dependent on voltage and frequency. Moreover, sluggish performance is obtained through the control of voltage magnitude and frequency. The transient performance is not improved through scalar control [4] [5]. In the scalar control technique, there is no control over the torque or flux of the machine.

The alternative to the scaler control techniques is vector control. The problems involved with scalar control were eliminated by the vector control. Vector control is the most popular IMD control techniques which is now used for high impact automotive applications (EV and Hybrid EV). In this case, the torque control is extended to transient states and allows better dynamic performances. Torque and flux controls is possible with vector control in induction motor drive. There are two kinds of vector control method, the FOC and DTC. In 1970, the principle of field-oriented control of IM was proposed. The FOC appeared to have similar performance to the DC machine over a wide range of speed and load conditions, but the performance of a FOC implementation depends critically on a very accurate coordinate transformations and flux angle estimation, which are complex and depending on the variation of machine parameters. For this reason, many studies have been performed into finding various solutions that enable the IM control to have a quick torque response, and to reduce the complexity of FOC.

Another vector control method is DTC it appears to be very convenient for EV applications. DTC has the advantage of not requiring position encoders and uses voltage and current measurements only. It was introduced in the mid-1980s. Besides its simplicity, DTC is able to produce fast torque and flux control and, if the torque and flux can be estimated correctly, DTC become robust. This method appears as a suitable way to improve dynamic performance of IMs as it provides a fast torque response and robustness to motor parameter variations. However, DTC has some problems such as variable switching frequency and a high amount of torque ripple caused by hysteresis controller. Direct flux and torque control with space vector modulation schemes is proposed which improves the classical DTC method.

The DTC-SVM strategies operate at a constant switching frequency. In the control structures, space vector modulation algorithm is used. The type of DTC-SVM strategy depends on the applied flux and torque control algorithm. Basically, the controllers calculate the required stator voltage vector and then it is realized by space vector modulation technique [6].

In this thesis, the speed of an induction motor is controlled for Daewoo Damas II electric vehicle propulsion application using fuzzy speed controller with SVPWM-DTC method. The comparison of PID and fuzzy speed controllers is performed and the result shows that the space vector pulse width modulation direct torque control with fuzzy speed control have a better performance. The flux and torque are estimated from the measured voltage and current of the motor. The electric vehicle dynamics mathematical modeling is performed. The mathematical model and the principle of a three phase IM drive is discussed. The proposed speed control system for application of electric vehicle is designed and simulated using MATLAB Simulink software.

1.2 Statement of the Problem

Daewoo Damas II is a general-purpose gasoline-based vehicle and it is very well known in Ethiopia but it uses an internal combustion engine. In internal combustion engines, fuel is burned inside the cylinder therefore it emits carbon dioxide which is very harmful to the environment. In addition to this the depletion of fossil fuels is increasing at highly alarming rate and its cost also increasing as well. Electric vehicles are a solution to the environmental problems caused by vehicles with internal combustion engines. The advantages of EVs include energy efficiency, no pollution or emits no greenhouse gas, and it uses renewable energy source. However, energy utilizations are the major issues in electric vehicles. Different researchers have been researching about different electric motors and their drive that are used in electric vehicles.

The motor is the main part of the EV. The most important requirements of the EV motors are high efficiency, high dynamic response (fast torque and speed response), high torque at low speeds, high torque/power to size ratio, low production cost, and many more others. The rapid development in the field of power electronics and control techniques has created a space for various types of electric motors to be used in electric vehicles. Induction motor is favored due to its good self-starting capability, simple and rugged structure, low cost and reliability. Due to the nonlinearity of the system the PID controller for the speed control may not achieve the required performance. In order to satisfy the requirement of the EV motor an appropriate control algorithm is required that means the steady state and transient response of the drive should have good dynamic performance. In this regard, one of the AI techniques which is fuzzy logic controller is implemented to improve the problems of a convectional PID controller in the speed control system.

1.3 Objectives of the Thesis

1.3.1 General Objective

The general objective of the thesis is to design the speed controller of an induction motor using space vector pulse width modulation direct torque control based fuzzy logic controller for a four-wheeler Daewoo Damas II electric vehicle.

1.3.2 Specific Objectives

The specific objectives of this thesis are:

- To design the maximum load of the electric vehicle mathematically.
- To design the dynamic mathematical model of 3-phase induction motor.
- To design flux and torque PI controller.
- To design PID and fuzzy logic speed controllers.
- To simulate the system by using MATLAB software.
- To evaluate and analysis the result obtained.

1.4 Motivation of the Study

The fuel engine cars are highly characterized as one of the major polluting sources of the environment. Considering the number of fuel-based vehicles in the planet we live in, it is easy to observe how badly human beings are treating the environment. We are also witnessing the consequence of the mistreatment of the environment as the climate-based problem is paying back its debt in a harsh way. The time nowadays leave the vehicles industry with a single option of producing environment friendly electric vehicles since this kind of vehicles are not only a solution to reduce the climate change crises but it also uses a renewable energy source. Petroleum is a highly manipulated mineral kind so that it is the verge of its lasting era. Ethiopia is investing billions of dollars in electrical infrastructure as the countries potential of hydropower is estimated up to 45000 MW the 2nd highest in Africa next to the democratic republic of Congo [L1]. The country is also endowed with other renewable energy such as wind, geothermal solar, and biomass. Despite all this grace, the country every year spend billion dollars for petroleum importation.

Many countries are planning to stop producing fuel-based vehicles and to start replacing with electric vehicles. Because of environmental pollution and the expense of petroleum products. A lot of researchers have been researching in this area to improve the electric drive control, battery, and fast charger. The battery technology is getting better from time to time which gives hope to use EV easily. The future will have a tremendous market in the region of electric vehicles. Therefore, due to the futurity of electric vehicles technology, it is very interesting to research in this area.

1.5 Scope and Limitation of the Study

This thesis focuses on MATLAB Simulink implementation of the fuzzy logic speed controller, PI torque controller and PI flux controller of the induction motor for electric vehicle propulsion using SVM direct torque control technique. The performance of the IM drive for PID and fuzzy speed controller is discussed. This thesis is limited to the simulation of the system using MATLAB/Simulink. The study does not include the hardware implementation of the proposed system due to the difficulty of obtaining components and high material cost.

1.6 Significance of the Study

EVs solve the issues of air pollution, global warming, and the rapid decrease of the petroleum resources facing the current transportation technology. EVs are also quieter than petrol/diesel vehicles, which means less noise pollution. On a national level, EVs can help with Ethiopian's energy security. At present, Ethiopia is highly dependent on other countries for petroleum imports. EVs are easy to power from local and renewable energy sources, reducing our reliance on foreign oil. This thesis can support the trend started by center of transportation and vehicle engineering department for building up an EVs in Adama Science and Technology University.

1.7 Organization of the Thesis

The outlines of the structure of the thesis is organized into five chapters. The following is an explanation for each chapter.

Chapter 2: Include the background on EV, IM and its drive. The main component of electric vehicle and varieties of electric motors used for electric propulsion application are discussed. The different controlling mechanism of induction motor are presented.

Chapter 3: Describes the methodology followed in this thesis work. The different forces that exert on the EV, dynamic model of induction motor and SVPWM is discussed. The torque and flux PI controllers, and also fuzzy and PID speed controllers designed.

Chapter 4: Explains the simulation result and analysis of the proposed control system. The motor electromagnetic torque and flux are compared with their estimated values. Fuzzy and PID speed controllers are compared.

Chapter 5: Discusses the conclusions and recommendations.

CHAPTER 2

THEORETICAL BACKGROUND AND LITERATURE REVIEW

2.1 Chapter Overview

In this chapter the main component of electric vehicle and varieties of electric motors used for electric propulsion application are discussed. Comparison of electric motor that are used for EV propulsion is performed. The different controlling mechanism of induction motor are reviewed, compared and discussed. Closely related works on speed control of induction motor are reviewed and discussed.

2.2 Key Parts of an Electric Vehicle

Popularity of the electric vehicles has continuously increased worldwide depending on the decreasing petrol sources and increasing emissions. Therefore, many vehicle manufacturers have launched various commercial electric vehicles such as Toyota RAV4 EV, Chevrolet Volt, Tesla Model S and Renault Twizy [7] [8]. Electric powered vehicles mainly consist of four subsystems: Battery, traction motor, motor driver and control units.

The battery unit supplies the required power to both the traction system and the electrical equipment of the vehicle. It is the duty of the battery management system to check the battery level and the temperature so that they do not exceed any critical levels. In the traction system, an electric motor is used which is generally a brushless permanent magnet motor [9] [10], a squirrel cage induction motor [11] [12] [13] or a switch reluctance motor [14]. The motor driver is used for variable speed/torque control of the motor as well as regenerative breaking. The control unit collects all available data from the other components, and performs the high-level control of the vehicle.

The key parts of an electric vehicle are shown in Figure 2.1 which are the charging port with the connector and cable, high voltage structure battery and the low voltage auxiliary battery, an electric motor, and transmission system which are used for propulsion and finally several power electronics convertors that are used for battery charging, driving the motors and for regenerating braking.

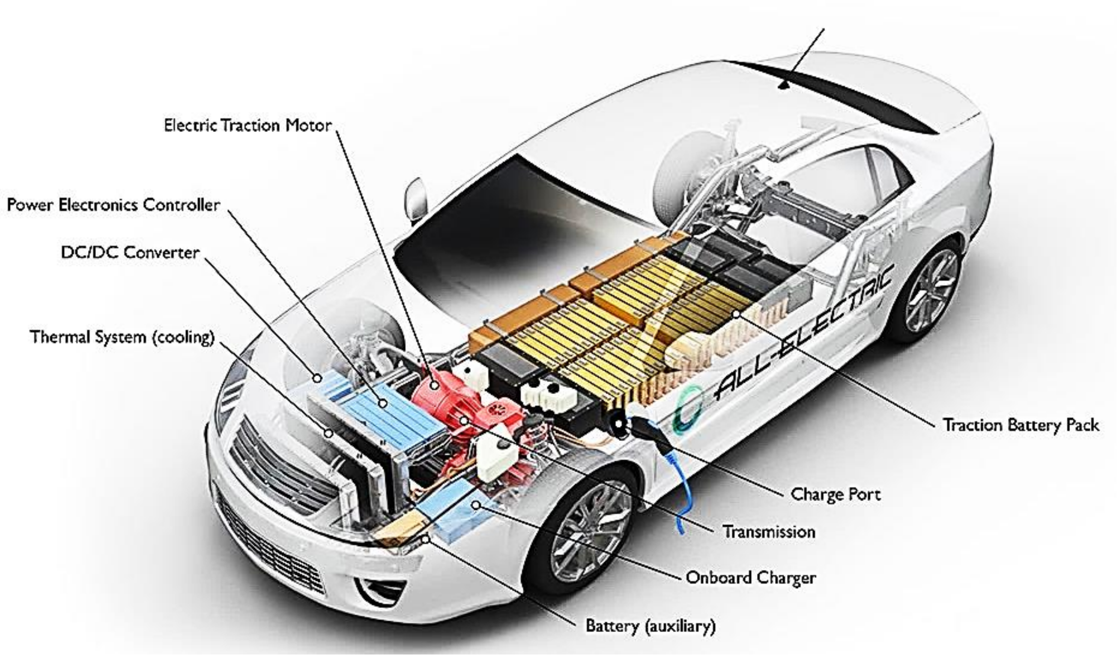

Figure 2.1 Key parts of an electric vehicle [L2]

Battery (all-electric auxiliary): In an electric drive vehicle, the auxiliary battery provides electricity to power vehicle accessories.

Charge port: The charge port allows the vehicle to connect to an external power supply in order to charge the traction battery pack.

DC/DC converter: This device converts higher-voltage DC power from the traction battery pack to the lower-voltage DC power needed to run vehicle accessories and recharge the auxiliary battery.

Electric traction motor: Using power from the traction battery pack, this motor drives the vehicle's wheels. Some vehicles use motor generators that perform both the drive and regeneration functions.

Transmission (electric): The transmission transfers mechanical power from the electric traction motor to drive the wheels.

Power electronics controller: This unit manages the flow of electrical energy delivered by the traction battery, controlling the speed of the electric traction motor and the torque it produces.

Thermal system (cooling): This system maintains a proper operating temperature range of the engine, electric motor, power electronics, and other components.

Onboard charger: Takes the incoming AC electricity supplied via the charge port and converts it to DC power for charging the traction battery. It monitors battery characteristics such as voltage, current, temperature, and state of charge while charging the pack.

Traction battery pack: Stores electricity for use by the electric traction motor.

2.3 Electric Vehicle Batteries

The battery of an electric car can be charged through the use of ordinary grid electricity at a specialized power station. Aside from the conventional lithium-ion battery technologies, there are also other major battery technologies which can be used for electric cars [15]. Current battery technology is designed for extended life (typically about 8 years or 100,000 miles). Mostly used batteries for electric vehicle application are: -

- **Lithium-Ion Batteries:** The lithium ion batteries generally preferred for electric vehicle application mainly driven by its high energy density, no memory effects and relatively the number of charging/discharging cycles of the battery's entire life is long [16] [17]. With the same power and energy capacity the lithium ion batteries have much less weight than its competitors. This battery technology gives extra performance and rang. However, it also carries the highest price tag. Lithium-ion batteries are lighter than Lead acid and Nickel metal. These are also the batteries used in digital cameras and smartphones.

- **Lead Acid Batteries:** This battery technology is also popular. It is the cheapest among the battery technologies. The prospect for the use of lead acid batteries in the electric cars are limited due to the low energy densities, sensitivity to temperature and life cycle.

- **Nickel Metal Hydride Batteries:** This battery technology provides higher output and better performance than lead acid batteries but it costs much more. It has been extensively used for traction purposes and optimized for high energy content.

Figure 2.2 shows the comparison of lithium-ion, lead acid and nickel metal hydride batteries based on power density and energy density. From the figure it can be shown that lithium ion battery has a better power and energy.

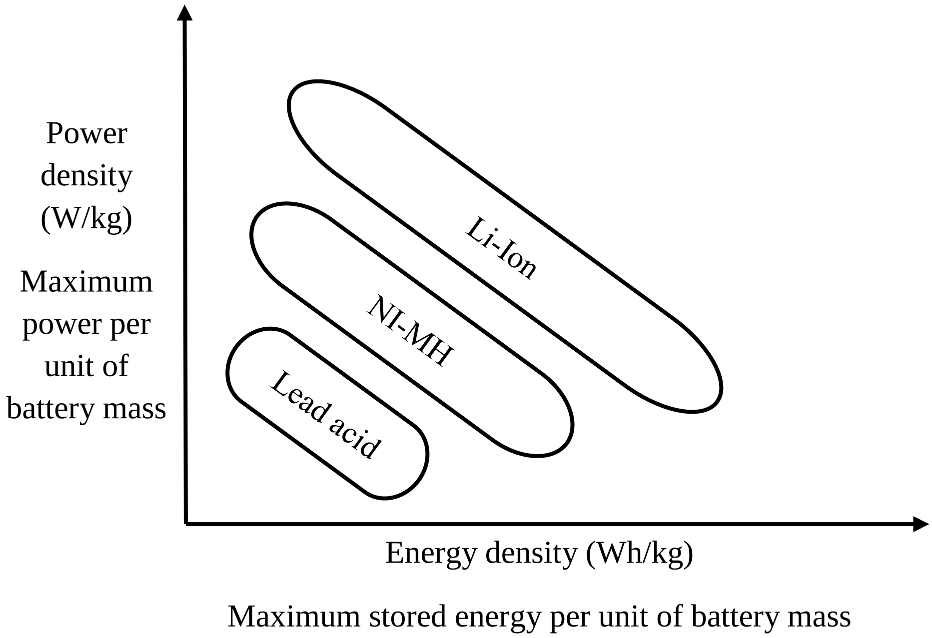

Figure 2.2 Batteries in terms of power density and energy density [16]

2.4 Traction Motor

The core element of the EV, apart from electric vehicle batteries, which replaces the internal combustion engines is an electric motor. The rapid development in the field of power electronics and control techniques has created a space for various types of electric motors to be used in electric vehicles. The electric motors used for automotive applications should have characteristics like [18] [19].

- High efficiency over the wide speed range with constant torque and constant power regions;
- High torque and speed response;
- High torque at low speed for starting and climbing;
- High power density;
- High torque/power to size ratio;
- Robustness and reliability of the motor and its drive;
- Simple design;
- Low maintenance cost (high life expectancy);
- Low production cost etc.

Selection of electric motor for EV is a very important step that requires special attention. In order to select an appropriate motor which can mostly fulfil the EV motor technology requirements, an overall comparison of electric motors is required. A single electric motor cannot fulfill all of the above-mentioned electric vehicle qualification requirements. For example, Induction motor and SR motor has higher constant power in wide speed range than BLDC motor [20]. BLDC and PMSM has high production cost than IM and SR motors due to the cost of the permanent magnet used on the rotor part of this motors.

Electric motors can be structured to use either AC or DC current. AC motors are less expensive and lighter compared to DC motors. They are also more common and they tend to suffer from less mechanical wear and tear. However, AC technology requires a more sophisticated motor controller.

Various types of Electric Motors used in Electric Vehicles:

1. Brushed DC Motor
2. Brushless DC Motor
3. Permanent Magnet Synchronous Motor (PMSM)
4. Three Phase AC Induction Motors
5. Switched Reluctance Motors (SRM)

2.4.1 Brushed DC Motor Drives

High starting torque at low speed capability of the DC brushed motor makes it a suitable option for traction application [19]. These motors may have series or shunt field windings. It was the most widely used motor for traction application in the early 1900s. The advantages of this motor are easy speed control and it can also withstand a sudden increase in load. All these characteristics make it an ideal traction motor. The main drawback of brushed DC motor is a bulky construction, low efficiency, low reliability, and higher need of maintenance, mainly due to the presence of the mechanical commutator and brushes. These motors are used in Indian railways.

2.4.2 Brushless DC Motor

It is similar to DC motors with Permanent Magnets. It is called brushless because it does not have the commutator and brush arrangement. The commutation is done electronically in this motor because of this BLDC motors are maintenance free. BLDC motors have traction characteristics like high starting torque, high efficiency, etc. [21]. BLDC motors are suitable for high power density design approach. The BLDC motors are the most preferred motors for the electric vehicle application due to its traction characteristics. BLDC motors further have two types:

Out-runner type BLDC Motor: In this type, the rotor of the motor is present outside and the stator is present inside. It is also called as Hub motors because the wheel is directly connected to the exterior rotor. This type of motors does not require external gear system. In a few cases, the motor itself has inbuilt planetary gears. This motor makes the overall vehicle less bulky as it does not require any gear system. It also eliminates the space required for mounting the motor. There is a restriction on the motor dimensions which limits the power output in the in-runner configuration. This motor is widely preferred by electric cycle manufacturers like Hullikal, Tronx, Spero, light speed bicycles, etc. It is also used by two-wheeler manufacturers like 22 Motors, NDS Eco Motors, etc. [L3].

In-runner type BLDC Motor: In this type, the rotor of the motor is present inside and the stator is outside like conventional motors. These motors require an external transmission system to transfer the power to the wheels, because of this the out-runner configuration is little bulky when compared to the in-runner configuration. Many three- wheeler manufacturers like Goenka Electric Motors, Speego Vehicles, Kinetic Green, and Volta Automotive use BLDC motors. Low and medium performance scooter manufacturers also use BLDC motors for propulsion. It is due to these reasons it is widely preferred motor for electric vehicle application. The main drawback is the high cost due to permanent magnets. Overloading the motor beyond a certain limit reduces the life of permanent magnets due to thermal conditions.

2.4.3 Permanent Magnet Synchronous Motor (PMSM)

This motor is also similar to BLDC motor which has permanent magnets on the rotor. Similar to BLDC motors these motors also have traction characteristics like high power density and high efficiency [18]. The difference is that PMSM has sinusoidal back EMF whereas BLDC has trapezoidal back EMF due to the construction of the motor. During commutation of BLDC motor has a high torque ripple than PMSM. Permanent Magnet Synchronous motors are available for higher power ratings. PMSM is the best choice for high performance applications like cars, buses. Despite the high cost, PMSM is providing stiff competition to induction motors. PMSM is also costlier than BLDC motors. Most of the automotive manufacturers use PMSM motors for their hybrid and electric vehicles. For example, Toyota Prius, Chevrolet Bolt EV, Ford Focus Electric, zero motorcycles S/SR, Nissan Leaf, Hinda Accord, BMW i3, etc. use PMSM motor for propulsion [L3].

2.4.4 Three Phase AC Induction Motor

Induction motor is the most mature technology among the various commutator less there are two types of induction motor namely the wound rotor and cage rotor. Because of high cost needed for maintenance and lack of sturdiness, the wound rotor induction motor is less attractive. Actually, the cage rotor induction motor is loosely named as induction motor [22]. It's excellent field-weakening performance and low manufacturing costs make it a competitive candidate for EV motor drives.

Nowadays, IMs can achieve similar torque speed control as the DC motor drives [18]. For example, the speed range can be extended beyond the base speed, as shown in Figure 2.3, using field weakening as the field vector can be decoupled from torque vector by vector control. From [3] it can be concluded that induction motor drives are favored in EV propulsion applications because of their low cost, high reliability, mature manufacturing and power converter technologies. However, their drawbacks are requiring complex inverter circuit and control of the motor is difficult.

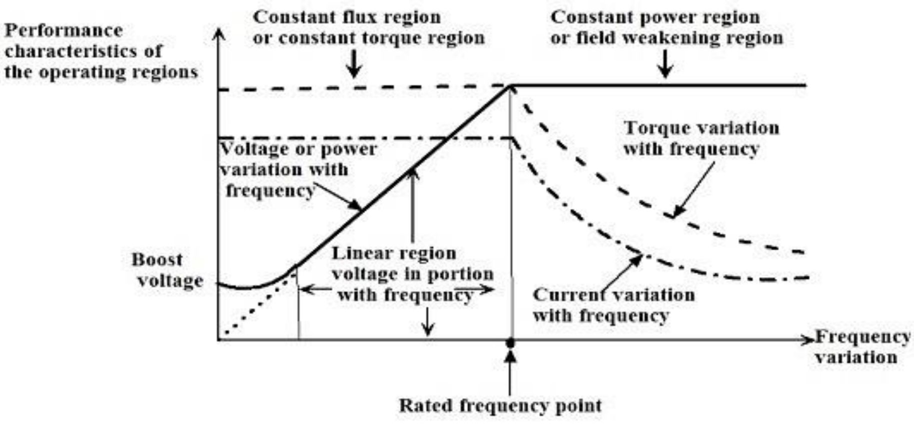

Figure 2.3 Three phase IM torque speed characteristic under vector control [23][L3].

Tesla Model S is the best example to prove the high-performance capability of induction motors compared to its counterparts. Even Mahindra Reva e2o uses a three-phase induction motor for its propulsion [L3]. Major automotive manufacturers like TATA motors have planned to use induction motors in their cars and buses. The two-wheeler manufacturer TVS motors will be launching an electric scooter which uses induction motor for its propulsion. Induction motors are the preferred choice for performance oriented electric vehicles due to its cheap cost. The other advantage is that it can withstand rugged environmental conditions. Due to these advantages, the Indian railways has started replacing its DC motors with AC induction motors [L3].

2.4.5 Switched Reluctance Motor (SRM)

Switched Reluctance Motors is a category of variable reluctance motor with double saliency. Switched Reluctance motors are simple in construction and robust. The rotor of the SRM is a piece of laminated steel with no windings or permanent magnets on it. This makes the inertia of the rotor less which helps in high acceleration. The robust nature of SRM makes it suitable for the high-speed application. SRM also offers high power density which are some required characteristics of electric vehicles [19]. The biggest drawback of the SRM is the complexity in control and increase in the switching circuit. It also has some noise issues. Once SRM enters the commercial market, it can replace the PMSM and Induction motors in the future [L3].

2.5 Performance Comparison of Motors

The PMSM and BLDC are a popular candidate because of their high-power density, high efficiency and compact volume. But the disadvantage is the magnetic materials used in these motors are really expensive, and they need to be well maintained for the reason of magnet corrosion or demagnetization. The SRM is another promising candidate for EV applications, because of its simple structure, fault tolerant operation, and wide speed range at constant power. However, the disadvantages of the SRM are its high torque ripples and low efficiency. Intelligent, reliable and commercialized control systems of AC induction motors are being developed based on power electronic devices and digital signal processing (DSP) technology. From [3] it can be concluded that induction motor is considered as the best candidate for the most of EVs applications. Induction motor drives are well suited for cost sensitive mass production EV applications. Figure 2.4 shows the performance comparison of different electric motor out of 5. Table 2.1 summarizes the application of different electric motor used in different EV manufacturing company.

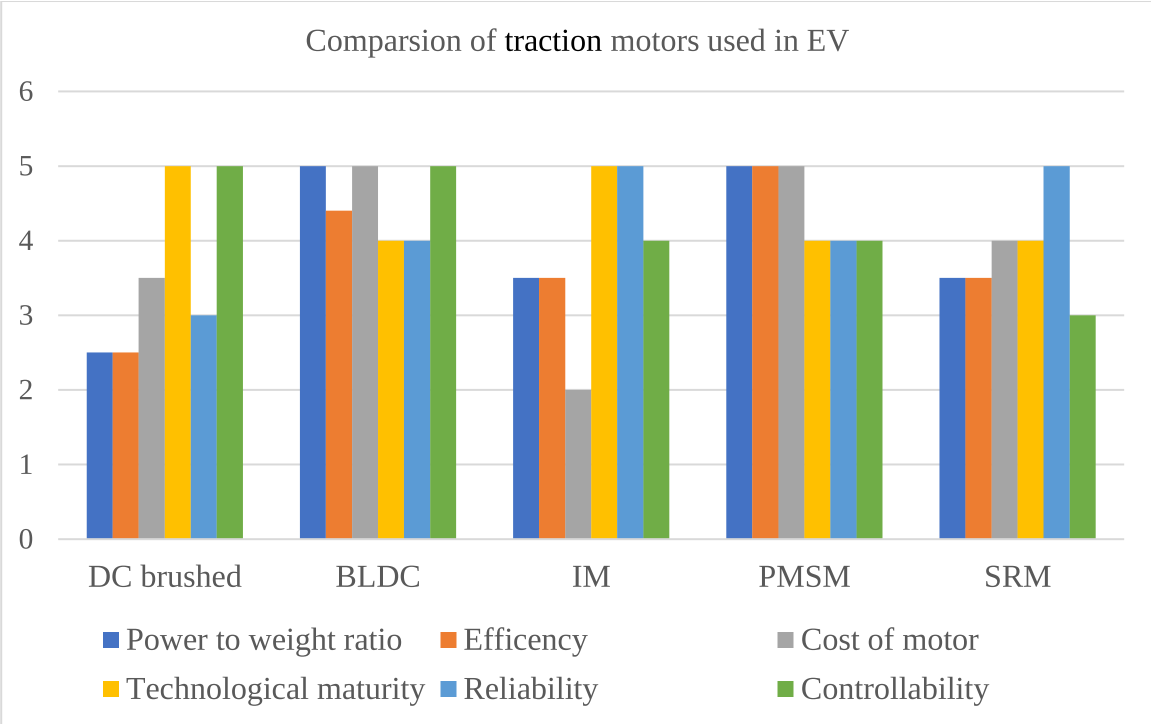

Figure 2.4 Performance comparison of different electric motors used in EV [24] [25] [26]

Table 2.1 Different EV manufacturer and motor type they used [25] [21] [L3]

Nọ	Manufacturer company	EV name	Electric motor used	Country
1	Toyota	Toyota RAV 4	PMSM	Japan
		Prius		
2	Nissan	Tino	PMSM	Japan
3	Mazda	Mazda Bongo	Shunt DC Motor	Japan
4	Holden	ECOmmodore	SRM	Australia
5	Renault	Kangoo	IM	France
6	Chevrolet	Silverado	IM	USA
7	Daimler Chrysler	Durango	IM	Germen/USA
8	BMW	X5	IM	Germen
9	Tesla	Model S/X	IM	USA
10	Kinetic Green	e-auto Safar	BLDC	India
11	Volta Automotive	Model- C650	BLDC	India
12	Honda	Honda EV Plus	BLDC	Japan

2.6 Speed Control of IM

Control techniques are used to make an AC motor follow a given data at desired performance. IM control methods can be divided into scalar and vector control [27]. The general classification of the variable-frequency methods is presented in Figure 2.5.

2.6.1 Scaler Control

Scaler control only controls the magnitude of a variable. However, an induction motor has a rotating magnetic field produced by three magnetic fields therefore, the position of those fluxes should have been controlled this drawback can be eliminated by vector control method. The V/f method, which is the most common scalar method, maintains the stator flux at a constant level by increasing the voltage and frequency of stator simultaneously so that the rate of voltage/frequency remains constant. This method operates correctly during steady-state operation. The V/f method is used to control the motor up to rated speed. In order to control the motor above rated speed, the flux must be weakened so that the motor operates within rated voltage and current capacities.

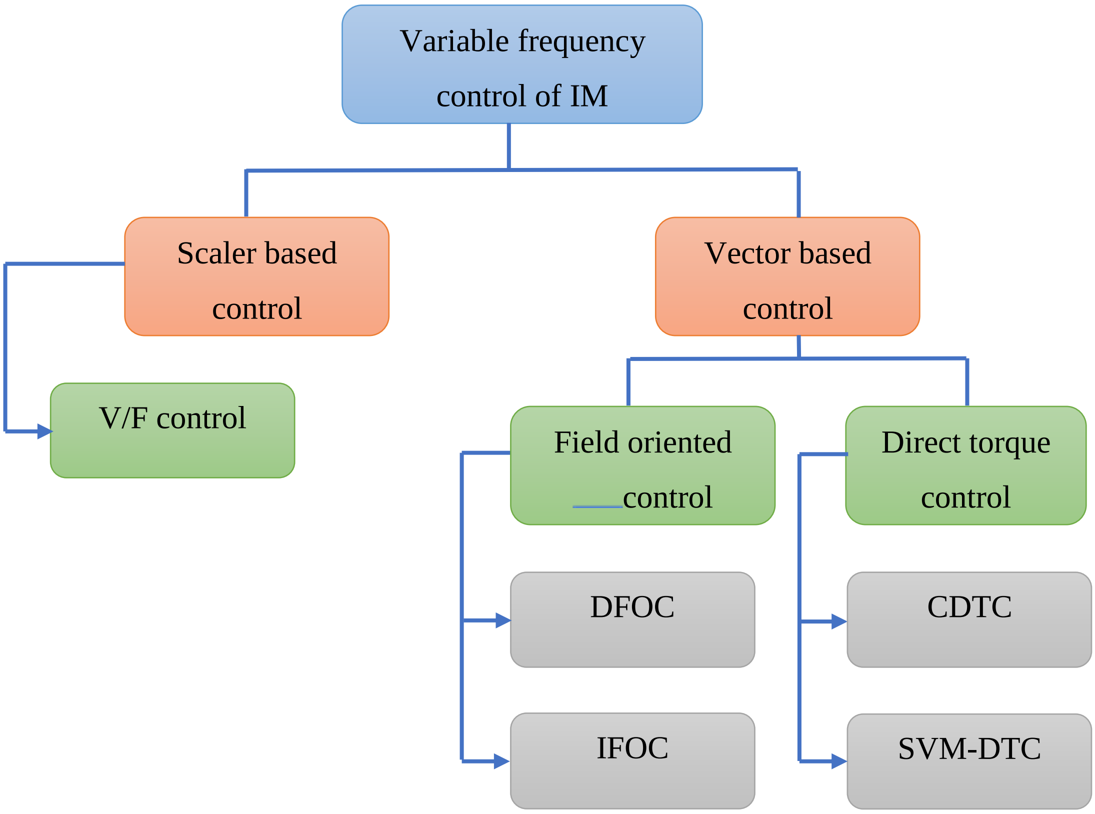

Figure 2.5 Classification of IM control methods [27]

2.6.2 Vector Control

In vector control method IM behaves like a separately excited DC motor since vector control method decouples the flux and torque controls. Purpose of vector control technique is controlling torque and flux independently by making two components of stator currents independent one from other and linearization of torque characteristics of motors. Therefore, the vector control method is preferred to the scalar method, which will be also used in this thesis. Vector control classified in to two; field-oriented control and direct torque control.

2.6.2.1 Field Oriented Control

FOC is the first technology to control the "real" motor control variables of torque and flux. With decoupling between the stator current components (magnetizing flux and torque), the torque producing component of the stator flux can be controlled independently. Decoupled control, at low speeds, the magnetization state of motor can be maintained at the appropriate level, and the torque can be controlled to regulate the speed.

The field-oriented control consists of controlling the stator currents represented by a vector. This control is based on projections that transform a three-phase time and speed dependent system into a two coordinate (d and q frame) time invariant system [28]. These transformations and projections lead to a structure similar to that of a DC machine control. FOC machines need two constants as input references: the torque component (aligned with the q coordinate) and the flux component (aligned with d coordinate).

The main feature of the field-oriented control (FOC) method is the coordinate transformation. Stator phase currents are measured. These measured currents are fed into the Clarke transformation block. The outputs of this projection are entitled $i_{s\alpha}$ and $i_{s\beta}$. These two components of the current enter into the Park transformation block that provide the current in the d, q reference frame. The i_{sd} and i_{sq} components are contrasted to the references: $i_{sd\ ref}$ (the flux reference) and $i_{sq\ ref}$ (the torque reference). These transformations require a rotor flux angle γ_{sr}.

The outputs of the PI controllers are $U_{sd\ ref}$ and $U_{sq\ ref}$. They are applied to the inverse Park transformation block. The outputs of this projection are $U_{s\alpha c}$ and $U_{s\beta c}$ are fed to the SVPWM algorithm block. The outputs of this block provide signals that drive the inverter. Here both Park and inverse Park transformations need the rotor flux position. Hence rotor flux angle is essence of FOC. Depending on calculations of this angle there are two different kind of field-oriented control methods. Those are direct field oriented control (DFOC) and indirect field-oriented control (IFOC) methods.

In DFOC strategy rotor flux vector is either measured by means of a flux sensor mounted in the air-gap or by using the voltage equations starting from the electrical machine parameters. For DFOC an estimator or observer calculates the rotor flux angle γ_{sr}. Inputs to the estimator or observer are stator voltages and currents. An example of the DFOC system is presented in Figure 2.6.

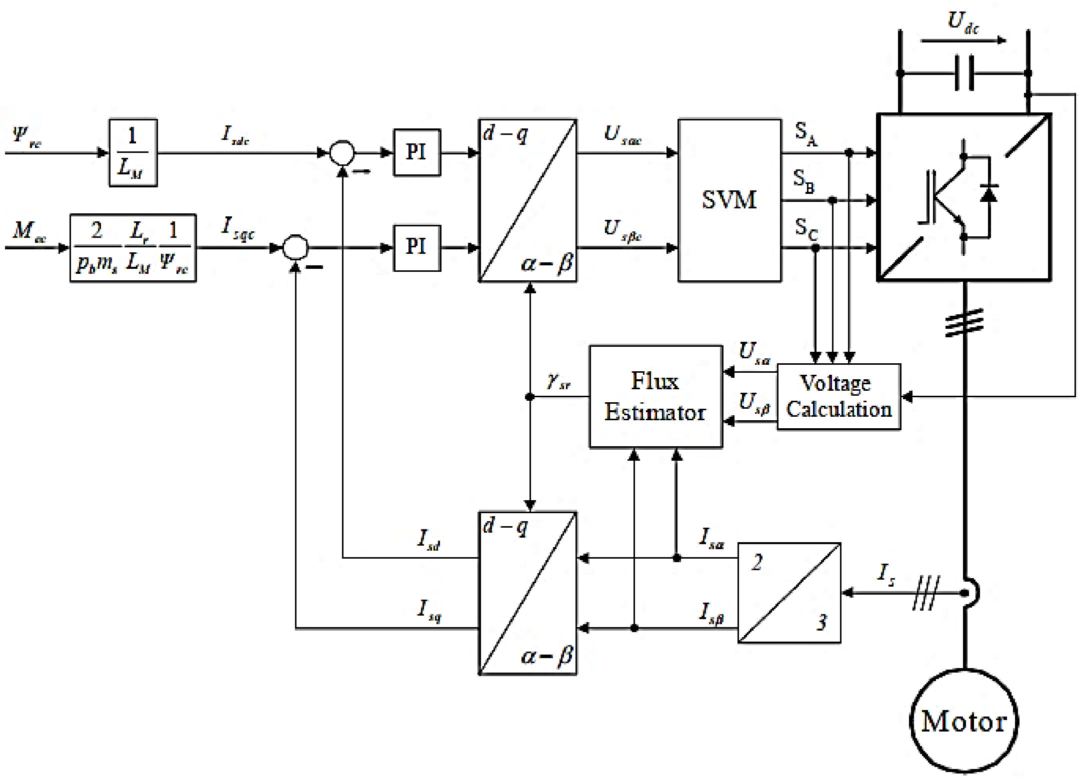

Figure 2.6 Block diagram of the Direct Field Oriented Control [28]

In case of IFOC rotor flux vector is estimated using the field-oriented control equations from reference i_{sdc}, i_{sqc} currents and it also requires a rotor speed measurement. An example of the IFOC system is presented in Figure 2.7. Among both schemes, IFOC is more commonly used because in closed-loop mode it can easily operate throughout the speed range from zero speed to high-speed field-weakening.

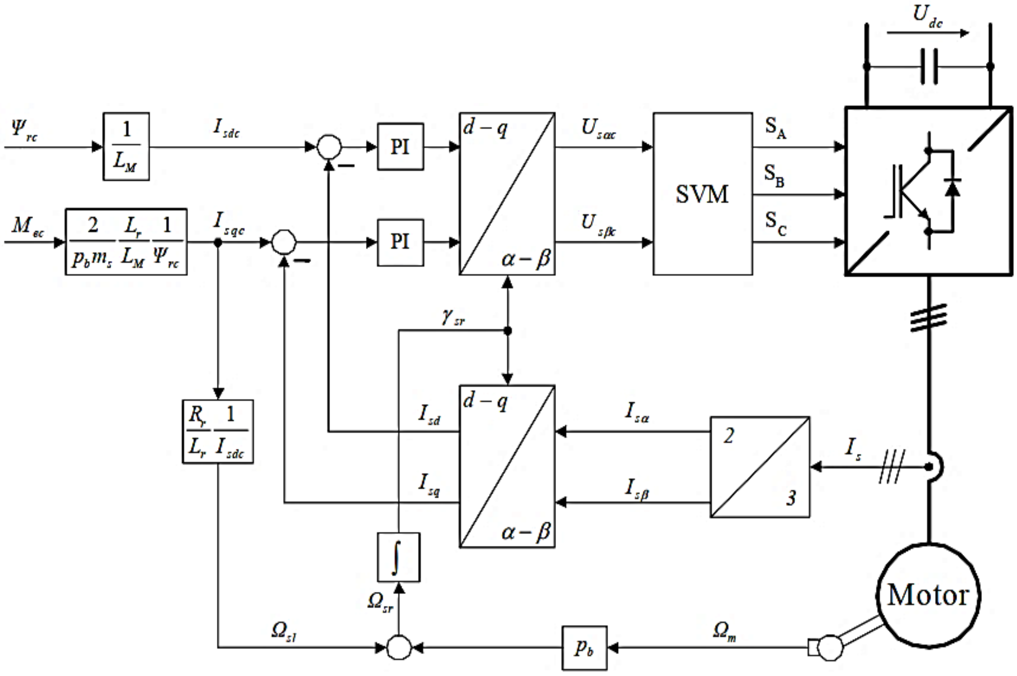

Figure 2.7 Block diagram of the Indirect Field Oriented Control (IFOC) [28]

2.6.2.2 Direct Torque Control

DTC is based on the decoupled control of flux and torque like vector control. It provides a very quick and precise torque response without the complex field-orientation block and the inner current regulation loop. The electromagnetic torque and stator flux are estimated in DTC technique only from the stator currents and voltage and it is independent of the parameters of the motor except for the stator resistance. FOC is highly dependent on the parameter of the motor.

The direct torque control is different from field-oriented control in such a way, that it does not control the flux through the current control, but it directly controls the flux itself. The direct torque control is also different from field-oriented control in the sense that the reference frame here is stator flux instead of rotor flux used in field-oriented control. The input to the direct toque controller is the torque error, error in magnitude of the stator flux space vector, and the angle of the stator flux space vector, from which the states of the power switches are determined. Based on this information, a certain voltage vector or combination of voltage vectors is directly applied to the inverter with a certain average timing. This gives the induction motor drives a very fast response. The voltage vector selection strategy using a switching table is widely researched and commercialized because it is very simple in concept and easy to be implemented. However, the DTC strategy using a switching table has some drawbacks. Switching frequency varies according to the motor speed and the hysteresis bands of torque and flux. It also causes high ripples in the flux and torque that leads to an acoustic noise which degrades the control performances. The ripples in the torque generate additional noise and vibrations and therefore cause disturbances in the rotating shaft. In direct torque control method switching the inverter directly controls flux and torque of the motor variables. Figure 2.8 shows block diagram of the CDTC. The stator flux φ_s and the electromagnetic torque T_e are the estimated values which are compared with the reference signals φ_s^* and T_e^* respectively.

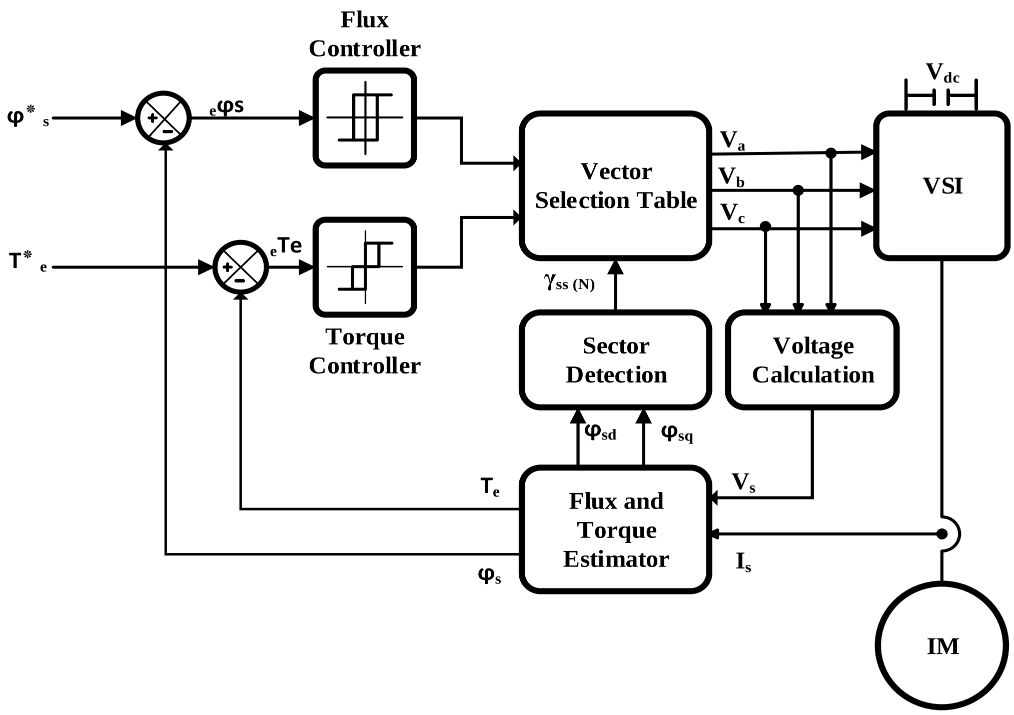

Figure 2.8 Block diagram of the CDTC [28]

The flux $e\varphi_s$ and torque eT_e errors are input to the flux and torque hysteresis controllers respectively. Form flux and torque estimator φ_{sd}, φ_{sq} and the stator flux position $\gamma_{ss}(N)$ can be obtained. The appropriate voltage vector selected using the digitized output variables $d\varphi$, dT and the stator flux position sector $\gamma_{ss}(N)$ from switching table. Thus, the pulses V_a, V_b, V_c that controls the power switches in the inverter generated from the selection table. The disadvantages of classical DTC are caused by hysteresis controllers and switching table used in a structure. Therefore, new DTC-SVM method replaces switching table by space vector modulator and linear PI controllers are used like in the FOC scheme. However, the current control loops are eliminated. The DTC-SVM method is discussed in detail in Section 3.7.

2.7 Comparison of Induction Motor Control Algorithms

In Table 2.2 FOC, CDTC and SVM-DTC compared, due to many advantages, SVM-DTC stands out in different applications.

Table 2.2 Comparison of vector control of induction motor [28]

<table>
<tr><th></th><th>FOC</th><th>CDTC</th><th>SVM-DTC</th></tr>
<tr><td>Advantages</td><td>• Modulator
• Constant switching frequency
• Unipolar inverter output voltage
• Low switching losses
• Low sampling frequency
• Current control loops</td><td>• Structure independent on rotor parameters, universal for IM and PMSM
• Simple implementation of sensor less operation
• No coordinate transformation
• No current control loops</td><td rowspan="2">• Structure independent on rotor parameters, universal for IM and PMSM
• Simple implementation of sensor less operation
• No coordinate transformation
• No current control loops
• Modulator
• Constant switching frequency
• Unipolar inverter output voltage
• Low switching losses
• Low sampling frequency</td></tr>
<tr><td>Disadvantages</td><td>• Coordinate transformation
• A lot of control loops
• Control structure depended on rotor parameters</td><td>• No modulator
• Bipolar inverter output voltage
• Variable switching frequency
• High switching losses
• High sampling frequency</td></tr>
</table>

2.8 Closely Related Works on IM Speed Control

Researchers reported several papers on induction motor speed control by using different methods and algorithms. The authors in [29] proposed and developed a design of electric vehicle which is propelled by three phase cage induction motor and powered by solar energy station. In this the induction motor speed is controlled by constant V/F control method and space vector pulse width modulation algorithm. The proposed vehicle has a weight of 500kg. The research work was implemented in MATLAB/Simulink. Also, the hardware implementation was developed using DSP kit and it showed that the drive is able to operate the vehicle at different speeds under flat and uphill road condition. However, during uphill condition the current required was quite high. The author suggested a better drive to improve the performance of the induction motor used in EV. A 37kW induction motor controlled with v/f speed control method is proposed by author [30] the result shows a ripple in speed response and the settling time is around 1 sec.

The improvement of the dynamics and transient responses of an induction motor were investigated in [31] by decoupling of the components. A proportional integral (PI) controller was used to control the torque while flux is controlled by a derivative controller. In this paper, variation in speed range is obtained for the application of electric vehicles. The model was simulated in the MTALAB to implement the proposed DTC scheme to analyze the effectiveness and improved behavior of the system.

In [31] research work the proposed DTC method is validated in different operating conditions of the electric vehicle and compared with the conventional DTC control to justify the improved transient and dynamic behavior of the IM. The proposed DTC control scheme is implemented on considered IM drive system. The results are analyzed for the conventional as well as proposed DTC scheme in the same scenario. The result analysis reflected that the conventional DTC scheme has suffered from poor transient and dynamic response. Also, the torque waveform having ripple content and steady state error. On the other hand, results validate the improved behavior of the IM drive system with the proposed DTC scheme. The transient and dynamic responses are better as compared to conventional one since the reference speed is tracked by actual speed only at 0.2s as compared conventional DTC which takes 0.4s. Also, the ripple content and steady state error are reduced with the proposed control scheme. However, the results reflect that the proposed DTC method needs further improvement.

To control the speed of an induction motor the application of a new multilevel inverter for DTC based induction motor drive is studied in [32]. The proposed multilevel inverter uses multiple series units of switching cells to achieve staircase voltage waveform with low harmonic distortion. Topology and operation of the suggested multilevel inverter is studied. The requirements imposed by a direct torque control (DTC) strategy on multilevel inverters are studied and then, a control strategy is applied. The simulation results verify; near sinusoidal stator voltage and current, very low ripples and good regulations of torque and stator flux but the disadvantage of this arrangement is the complexity of the drive and its high cost.

The paper in [33] proposes an adaptive neuro fuzzy interference system (ANFIS) based speed control of two induction motors (one for each rear wheel) for the application of EV. A speed network control is used to control each motor torque. The speed of each rear wheel is controlled using speed difference feedback. Since the two rear wheels are directly driven by two separate motors, the speed of the outer wheel will need to be higher than the speed of the inner wheel during steering. The inverters share the same dc bus. The reference speed is obtained by the accelerator pedal command. The model was simulated in the MTALAB to implement the proposed method to analyze the effectiveness and behavior of the system. Simulation results demonstrate that ANFIS controller is better than the classical PI controller in performance. The PI and ANFIS controller compared for no load and loaded condition and the result shows that ANFIS controller tracks the speed command with relatively small steady state error when compared to PI controller. The ANFIS speed controller settles to its command speed after 2.3 sec at no load and when the motor is loaded the proposed control system settles at 0.29 sec.

CHAPTER 3

METHODOLOGY

3.1 Chapter Overview

In this chapter, different forces that exert on the EV are calculated and also the dynamic model of induction motor is discussed. In the next part, out of the different PWM techniques SVPWM discussed in detail due to its advantage over other modulating techniques. The torque and flux PI controllers, and also fuzzy and PID speed controllers discussed for the speed control of the induction motor. Finally, the system is simulated by using MATLAB software.

3.2 Methods

In order to attain the general and specific objectives of the study, the following methods and techniques are followed. First the closely related works are reviewed. Then the necessary data used throughout this work is collected and analyzed. The specifications value of the Daewoo Damas II have taken from the manufacturing company. Induction motor specifications have taken from literatures and its manufacturing company. The modeling of IM drive with its speed controller is developed.

Then the system is simulated by using MATLAB/Simulink/Code. The result of the simulation is compared for PID and fuzzy speed control algorithms. In general, the method followed throughout the research study can be summarized in Figure 3.1. The collected data is analyzed mathematically and graphically for developing system modeling. The maximum power requirement of electric car is determined by considering mass of the car, wheel radius and area of the Daewoo Damas II. The induction motor control drive is designed using SVM-DTC techniques. The maximum speed of the designed EV is reduced in order to reduce the motor and battery size.

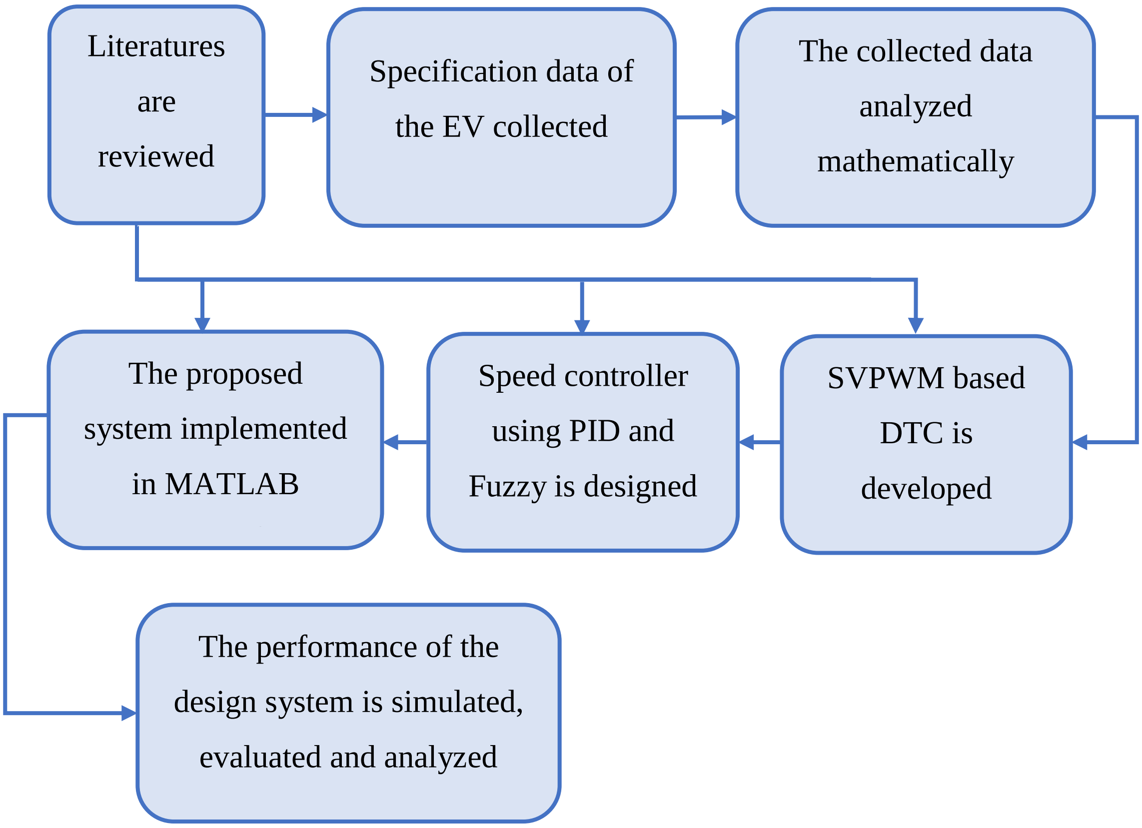

Figure 3.1 Block diagram of the research methodology

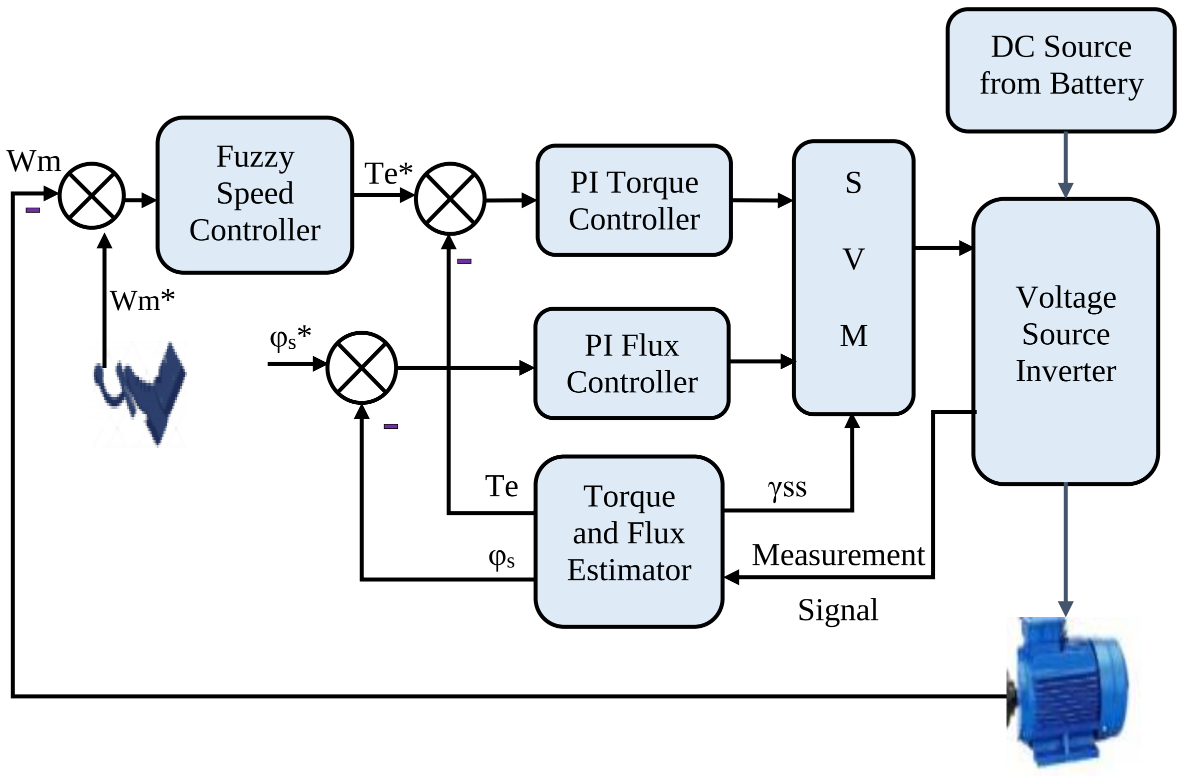

Figure 3.2 Block diagram of the proposed control system

The working principle of the block diagram shown in Figure 3.2 explained in the following manner: First, the difference of the reference speed, which is directly applied by the pedal of the vehicle, and rotor speed is controlled by using a speed regulator for this fuzzy speed controller is proposed. Then based on the speed error speed controller calculates reference torque value. The measured current and voltage transformed using park transformation and fed to estimator block. The reference values of torque and flux are compared with estimated values. Based on the errors flux and torque PI controllers calculate command voltage vector.

The derivation of stator flux defines the control of torque and flux. Stator flux position γss is a function of stator flux vectors. The torque and flux controller output together with the stator flux position γss fed to the space vector pulse width modulation which generates the gate pulses for the voltage source inverter switches. The implemented voltage source inverter is supplied by DC voltage from vehicle battery system.

3.3 Analysis of an Electric Vehicle Dynamics

Drivetrain of a vehicle is series of component that dispatches power to driving wheels. In internal combustion engine vehicles, the main parts of drivetrain include traction engine, clutch, transmission with gear, shafts, and wheels. On the other hand, electric vehicle is simplified with electric motor, single speed transmission and wheels [34]. Figure 3.3 shows the typical configuration of electric vehicle. As illustrated, the electric motor rotates and generates torque on its shaft to deliver power to wheels through transmission and differential. The single speed transmission is used for speed reduction and associated torque multiplication.

In general, differential mechanism basically allows each wheel to spin freely while providing power to each wheel. In order to the vehicle to turn the outer wheels must spin faster than the inner wheels. Differential plays an important role in case of front wheel drive or rear wheel drive vehicles but it is absent in 4-wheel motor drive electric vehicle since the rotation of wheels of such kind of vehicle can be controlled independently. Achieving the reverse gear is easy in electrical vehicle it is done by changing the order of power phase.

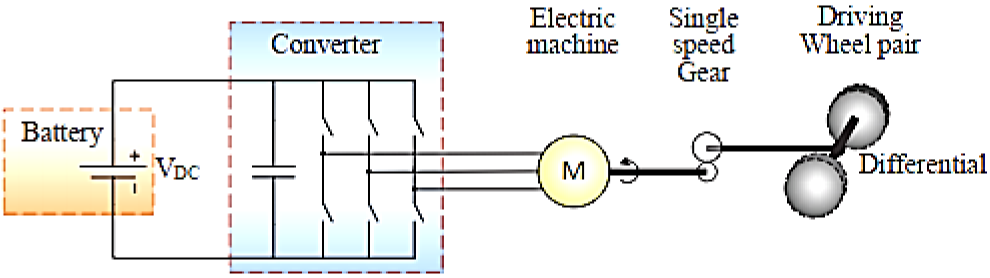

Figure 3.3 Electric vehicle drivetrain configuration [34]

During the vehicle motion, different forces exerted on the EV. Those are rolling, aerodynamic or wind, gradient resistance, acceleration force, and so on. Some of the major forces that exerted on EV are shown in Figure 3.4. The force propelling the electric vehicle has to overcome this force in order to move. To select the required motor power rating and other specification of tractive motor, the total force required for driving the vehicle must be calculated. Specification of Daewoo-Damas-II can be found in Appendix D.

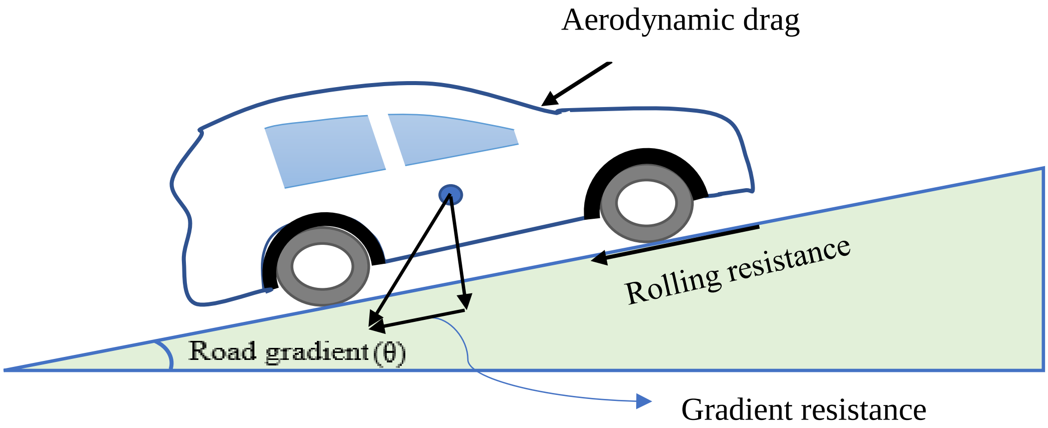

Figure 3.4 Different forces exerted on the EV

3.3.1 Rolling Resistance Force (F_{rr})

Rolling resistance force is the resistance provided due to friction of tires and the track. It is produced by the hysteresis of the tires at the contact surface with the roadway. This force can be minimized by keeping the tires as much inflated as possible [35] [36] [37]. The tractive force must overcome the rolling resistance force. The value of rolling resistance force can be calculated from:

$$F_{rr} = C_{rr} * M * g * \cos(\theta) \tag{3.1}$$

where F_{rr} is rolling resistance force in N, C_{rr} is rolling resistance friction constant, M is total vehicle mass in kg, g is acceleration due to gravity in m/s^2 and θ is elevating angel.

$$F_{rr} = 0.01 \times 1360kg \times 9.81\frac{m}{s^2} \times \cos(23) = 122.8N$$

The coefficient of friction for different surface have a different value Table 3.1 shows the coefficient of friction for different contact surface of the tiers.

Table 3.1 Coefficient of friction for different types of surface [38].

Contact surface type	Coefficient of friction
Concrete(good/fair/poor)	0.01/0.015/0.02
Asphalt(good/fair/poor)	0.012/0.017/0.022
Macadam(good/fair/poor)	0.015/0.022/0.037
Snow / dirt	0.025/0.037
Mud(firm/medium/soft)	0.037/0.09/0.15
Grass(firm/soft)	0.055/0.075
Sand(firm/soft/dune)	0.06/0.15/0.3

The power required to overcome the rolling resistance force can be calculated as: -

$$P_{rr} = F_{rr} * V = 122.8N \times \frac{85,000m}{3600s} = 2.89kW \tag{3.2}$$

Where V is the vehicle speed in (m/s). The power required to overcome the rolling resistance force is $2.89\,kW$.

3.3.2 Gradient (Pulling) Force (F_g)

When a vehicle goes up or down a slope, its weight produces a component, which is always directed to the down ward direction. It is the resistance due to slope of the road [35]. It is the form of gravitational force that tends to pull the vehicle back when it is climbing an inclined surface. The grade resistance acting on the vehicle can be calculated as: -

$$F_g = M * g * \sin(\theta) \tag{3. 3}$$

Where F_g is rolling resistance force in N, M is vehicle mass in kg, g is acceleration due to gravity and θ is elevating angel.

$$F_g = 1360\text{kg} \times 9.81 \frac{\text{m}}{\text{s}^2} * \sin(23) = 5212\text{N} \quad (3.4)$$

The power required to overcome the gradient force is: -

$$P_g = F_g * V = 5212\text{N} \times \frac{42{,}500\text{m}}{3600\text{s}} = 61.5\text{kW} \quad (3.5)$$

In Equation (3.5) the speed of the vehicle is assumed half of the maximum speed (i.e. 42.5 km/hr) to increase the torque when climbing the hill.

3.3.3 Aerodynamic (Drag) Resistance Force (F_d)

Vehicle traveling at a particular speed in air encounters a force resisting its motion, this force referred to as aerodynamics drag. The forward motion of the vehicle pushes the air in front of it. However, the air cannot instantaneously move out of the way resulting in high air pressure in addition, the air behind the vehicle cannot instantaneously fill the space left by the forward motion of the vehicle.

The motion has therefore created two zones of pressure that oppose the motion of a vehicle by pushing it forward (high pressure in front) and pulling it backward (low pressure in the back). Aerodynamic force is the result of viscous resistance and pressure distribution over the body of the air working against the motion of the vehicle [39]. The aerodynamic drag resistance is given by:

$$F_d = \frac{1}{2} \times \rho_a \times C_d \times A_f \times (V + V_{wind})^2 \quad (3.\ 6)$$

Where C_d is coefficient of drag, ρ_a is air density in kg/m^3, V is vehicle speed in m/s and A_f is frontal area of the vehicle in m^2 and V_{wind} is air speed in m/s.

$$F_d = \frac{1}{2} \times 1.2041 \frac{\text{kg}}{\text{m}^3} \times 0.25 \times 2.688\text{m}^2 \times \left(23.6 \frac{\text{m}}{\text{s}}\right)^2 = 225.3\text{N} \quad (3.\ 7)$$

The power required to overcome the aerodynamic resistance force is: -

$$P_d = F_d * V = 225.3\text{N} \times \frac{85{,}000\text{m}}{3600\text{s}} = 5.3\text{kW} \quad (3.\ 8)$$

Figure 3.5 shows that the aerodynamic force increases with the square of the speed of the car. From Equation (3.6) it can be observed that the drag force is directly proportional to the sum of the wind and the car speed square. For the speed of the car vires from 0 km/hr to 85 km/hr the force increases from 0 to 225.3N. The wind speed is assumed to be zero since its very low when compared to the speed of the car.

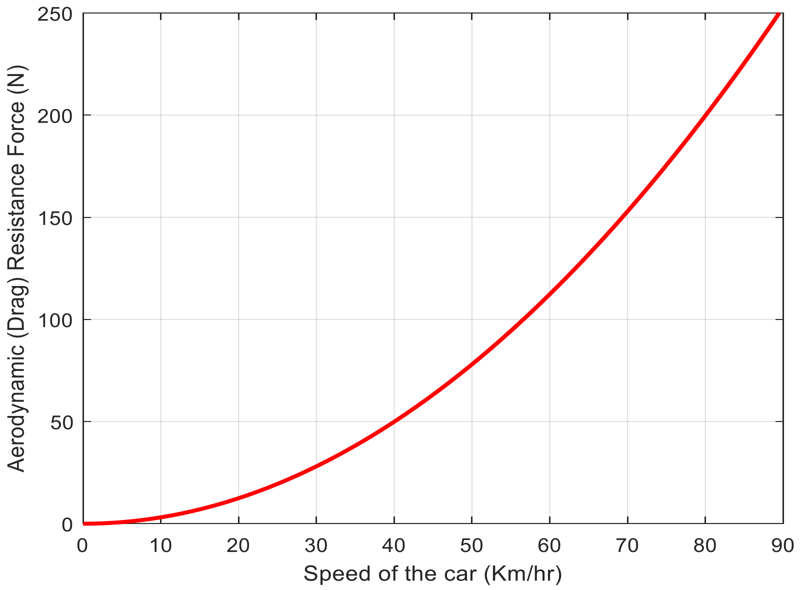

Figure 3.5 Aerodynamic dragging force versus speed of the car in km/hr

3.3.4 Acceleration Force (Fa)

It is the force defined by newton second law. This force helps the vehicle to reach a predefined speed from rest in specified period of time. The main forces that acts on the vehicle when it travels at a constant speed are the rolling resistance force, the gradient force and the aerodynamic force. But while the vehicle is accelerating or decelerating the effect of force due to inertia also acts up on the vehicle [40].

There are also other forces to consider in designing the vehicle dynamics like equivalent inertial force (during acceleration) - (including linear and rotational inertias, due to vehicle mass and rotating component of gear train and wheels) aerodynamic lift force, wheel force, and others. Usually, they are minimum compared to the other forces mentioned above and can be considered as a maximum of 1.5 kW. Therefore, the maximum tractive power required to move the vehicle is the sum of all power.

$$P_T = 2.89kW + 61.5kW + 5.3kW + 1.5kW = 71.19kW \quad (3.9)$$

Electric motor with output power rating 71.19kW should not be selected. The losses due transmission of power to the wheel must be included. Therefore, the mechanical power output required to drive the vehicle is given by Equation (3.10).

$$P_{driving} = \frac{P_{max}}{\eta_{transmision\ of\ gear\ system}} = \frac{71.19kW}{0.95} = 75kW \tag{3. 10}$$

The power required to drive the vehicle in HP: -

$$P_{driving\ (hp)} = \frac{P_{driving\ (watt)}}{745.699872} = \frac{75kW}{745.699872} = 100HP \tag{3. 11}$$

Therefore, the motor can be selected from the information of the driving output power.

When a vehicle moves in a flat road the gradient force will be zero since the road gradient angle θ is zero and its sin becomes 0. Therefore, the only force that acts on the vehicle are rolling resistance force, aerodynamic force and acceleration force. In Figure 3.6 a vehicle with its full load accelerating at 1.8 m/s^2 in a flat road is considered and it can be observed that the power required to overcome the forces is 70kW which is below the calculated maximum power. With this design the car can accelerate from rest to its top speed within 13 sec.

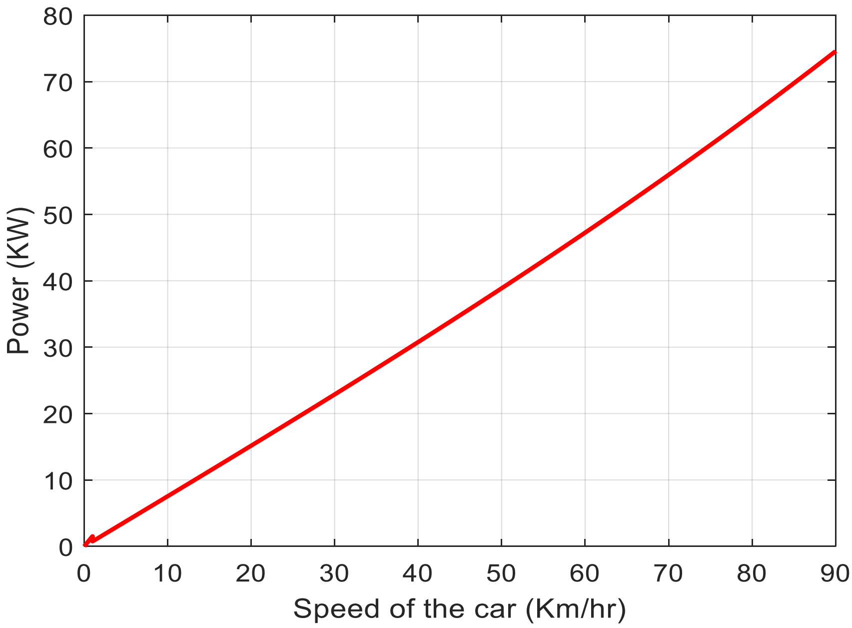

Figure 3.6 Consumed power versus speed of the vehicle (km/hr)

From the knowledge of the calculated total motive force and the maximum power, the motor with the specification listed in Table 3.2 is selected. The motor’s peak power should satisfy vehicle’s dynamic needs.

Table 3.2 Parameter specification of IM used in this thesis [41]

Parameters	Value
Number of pole pair	2
Frequency	50Hz
Power factor	0.875
Efficiency at rated	94 %
Control input rated voltage	400 V
Rated motor current	131.6 A
Rated motor power	75 kW/ 100hp
Ratted motor torque	483Nm
Rated speed	1482 rpm
Stator winding resistance	35.52m Ω
Rotor winding resistance	2.11 Ω
Stator inductance	0.335mH
Rotor inductance	0.335mH
Mutual inductance	237.3mH
Inertia moment of the rotor	0.01kg·m^2
Nominal stator flux	0.9Wb

In propulsion, applications the induction motor has to operate at speeds higher than the rated one, the field (flux) weakening is required which denotes the strategy by which the motor's speed can be increased above the rated speed. Up to the rated speed the motor operates in constant torque region. After the rated speed the motor operates in constant power region and the torque starts to reduce in order to keep the motor power constant. These characteristics of the motor is very desirable to limit the starting current of the motor by limiting the inrush current while providing the power required. Figure 3.7 shows the torque verses speed characteristics of the selected motor.

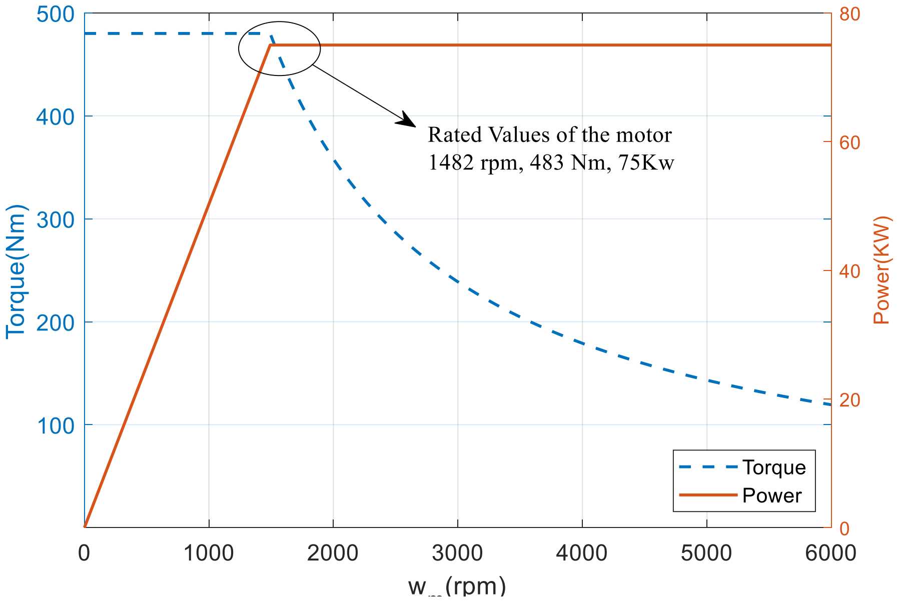

Figure 3.7 Torque versus speed characteristics of the IM

3.3.5 Torque Required

The motor in its normal mode of operation provide constant torque up to its base speed. At this point, the motor reaches its rated speed and rated power.

From Equation (3.12), the power can be determined

$$P = T \times \omega \qquad (3.12)$$

Where P is total power delivered from the motor to the wheels, ω is the angular speed of the motor. The motor speed in rad/s can be calculated as: -

$$\omega_{motor} = \frac{2 \times \pi \times N}{60} = \frac{2 \times 3.14 \times 1482\text{rpm}}{60} = 155.12\text{rps} \qquad (3.13)$$

Where N is the rated speed of the motor in rpm.

From Equation (3.12) and (3.13) the motor torque can be calculated as

$$T_{motor} = \frac{P_{total}}{\omega_{motor\,(rps)}} = \frac{75\text{kW}}{155.12\text{rps}} = 483.5\text{Nm} \qquad (3.14)$$

The wheel angular speed depends on the radius of the tier and can be obtained by using the formula in Equation (3.15).

$$\omega_{wheels} = \frac{V}{r} = \frac{23.6m/s}{0.2764m} = 85.38rps \tag{3.15}$$

Where V is the speed of the car in m/s and r is the radius of the tier.

The torque required in the wheels can be calculated as:

$$GR = \frac{T_{wheels}}{T_{motor}} = \frac{\omega_{motor}}{\omega_{wheels}} \tag{3.16}$$

Where T_{wheels} and ω_{wheels} is the torque and angular speed of the wheels respectively. T_{motor} and ω_{motor} is the rated torque and the rated speed of the motor.

$$GR = \frac{\omega_{motor}}{\omega_{wheels}} = \frac{155.12rps}{85.38rps} = 1.82$$

Therefore, the torque in the wheels is

$$T_{wheels} = T_{motor} \times GR = 483.5Nm \times 1.82 = 879.97Nm \tag{3.17}$$

In order to move a 1360 kg mass car at 85 km/hr or 23.6 m/s, induction motor with the rating of 100hp, 1482 rpm and 483 Nm and a transmission with a gear ratio of 1.82 is required. The selected motor can deliver 879.97 Nm torque at the wheels with 0.2764 radius tier.

3.3.6 Battery Sizing

In order to move the car 80km per charge the required battery size can be calculated as:

$$\frac{P_{total}}{V_{car}} = \frac{75,000W}{85km/hr} = 882Whr/km \tag{3. 18}$$

With 400v pack battery voltage the Ah used per km can be calculated as: -

$$\frac{882Whr/km}{400v} = 2.2Ah/km \tag{3. 19}$$

To find the Ah rating of the battery the Equation in (3.19) will be multiplied by km per charge of car.

$$2.2Ah/km \times 80km \times 1.2 = 211.2Ah \tag{3. 20}$$

1.2 is to restrict the battery to 80% of usage so we can still have 20% charge left after the drive. There must be 20% left using all the stored energy in the battery will damage the battery through time. With 220 Ah batteries and a voltage pack of 400v the car will move 80km per charge at 85km/hr.

Table 3.3 Battery specifications

Parameters	Value
Cell type	Lithium-ion
Total battery power pack	88kWh
Capacity	220Ah
Rated voltage	400V
Nominal voltage	3.2V

Table 3.4 shows the Daewoo Damas II electrical vehicle specifications.

Table 3.4 Daewoo Damas II electrical vehicle specifications

Parameter	Symbol	Value
Maximum Power (p)	P	75kW/100hp
Maximum speed of the car	km/hr	85
Wheel base	B	1.839m
Length × Width× Height	L× W× H	3.485 × 1.400 × 1.92 m
Coefficient of rolling friction	C_{rr}	0.01
Vehicle mass	M	1360kg
Air density	ρ	1.2041 kg/m^3
Frontal area	A_f	2.688m^2
Aerodynamic drag coefficient	C_d	0.25
Tire radius	r	0.2764m
Gravitational acceleration	g	9.81m/s
Maximum gradient angle	degree	23^0

3.4 Mathematical Model of Induction Motor

In an induction motor, an electricity is inducted in the rotor by magnetic induction rather than a direct electrical connection [42]. An induction motor has two main parts the stator and the rotor. The stationary (stator) and the rotating (rotor) part of the motor is separated by an air gap which means there is no mechanical contact between the rotor and the stator. The stator is made from very tin highly permeable steals that are stacked together and laminated inside a steel or cast-iron frame.

The rotor of a squirrel cage induction motor consists of aluminum bars which are short-circuited by connecting them to two end rings so that rotor generates the induction current and magnetic field by itself therefor IM is a self-starting machine. When three-phase ac power is given to the stator a three-phase current passes through the winding and produces a rotating magnetic field which causes the rotor to turn. The coils in the stator connected 120^0 apart from each other. The torque produced from the rotor is obtained by electromagnetic induction from the magnetic field of the stator winding. The rotational speed of the magnetic field is known as the synchronous speed.

A wire carrying current produces a magnetic field around it since the rotor bars are short-circuited, a large circulating current will be generated in the rotor bars [43]. When the short-circuited rotor bar interacts with the revolving magnetic field the current will be induced in the loop since it's exposed to a changing magnetic field then the resultant torque will be produced by the Lorentz' law, which states that the direction of this induced current will be such that the magnetic field created by the induced current opposes the initial changing magnetic field which produced it. A tangential electromagnetic force will be then generated on the rotor bars, and the sum of forces on each rotor bar produces a torque that eventually drives the rotor in the direction of the rotating field. Therefore, electrical energy is transformed into mechanical energy.

The rotating speed of the magnetic field which defined as synchronous speed, related to the number of poles of the induction motor and the frequency of the power source [44].

$$n_{syn} = \frac{120f}{p} \text{rpm} \tag{3. 21}$$

where f is the power source frequency in Hz, P is the number of poles and n_{syn} is the synchronous speed in revolutions per minute.

When three-phase ac power is connected to the stator the rotor will accelerate rapidly from rest, to keep up with the rotating stator flux. If rotor speed is the same as the magnetic field speed since both are rotating at the same speed, the rotating loop will always experience a constant magnetic field so there wouldn't be any induced emf and current this means zero force on rotor bars. So, the rotor will gradually slow down but as it slows down the rotor loop will experience varying magnetic fields. So, induced current and force will rise again and the rotor will speed up. In short, the rotor will never be able to catch up with the speed of the magnetic field it rotates at a specific speed which is slightly less than synchronous speed. This is why induction motors are also called asynchronous motors [44]. The difference between the stator and rotor speed is defined as the slip speed:

$$n_{slip} = n_{sync} - n_m \tag{3.22}$$

Where n_{slip} is the slip speed n_{sync} is the speed of the rotating magnetic field n_m is the mechanical shaft speed of the motor

Also, a slip ratio can be defined as:

$$s = \frac{n_{sync} - n_m}{n_{sync}} \tag{3. 23}$$

If the rotor runs at synchronous speed s = 0 and If the rotor stops moving s = 1.

Coordinate transformations simplify the modeling, analysis, and control design of the induction motor. Using a coordinate transformation, a three-phase variable can be transferred into a two-phase variable; also, a stationary variable can be transferred into a rotational one. This transformation usually includes Clarke and Park transformation consecutively implementing these two transforms simplifies computations by converting AC voltage waveform into DC signals.

Clarke transformation:

The Clarke transformation converts a three-phase system to two components in an orthogonal stationary frame αβ. The αβ representation uses two orthogonal axes (90 degrees apart) to represent any given space vector or phasor. The α axis is placed along the 'a' axis as shown in Figure 3.8 and the beta(β) axis is placed perpendicular to the alpha(α) axis.

$$\begin{pmatrix} v_\alpha \\ v_\beta \end{pmatrix} = \frac{2}{3}\begin{pmatrix} 1 & \frac{-1}{2} & \frac{-1}{2} \\ 0 & \frac{\sqrt{3}}{2} & \frac{-\sqrt{3}}{2} \end{pmatrix}\begin{pmatrix} v_a \\ v_b \\ v_c \end{pmatrix} \tag{3.24}$$

The factor 2/3 in Equation (3.24) makes the amplitude of any space phasor, which represents a three-phase balanced system, equal to the amplitude of two-phase system.

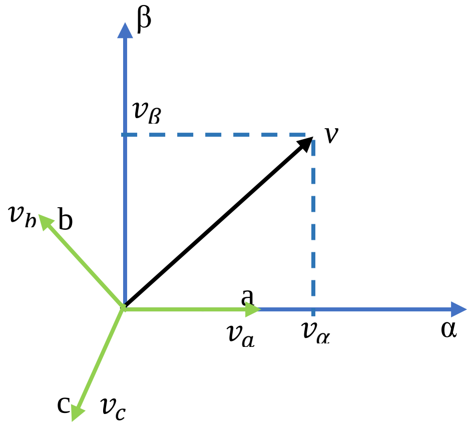

Figure 3.8 Clarke transformation of three-phase voltage

Park transformation:

The Park transform converts the two components from the Clarke transformation in the αβ frame to an orthogonal rotating reference frame (dq). d stands for direct and q stands for quadrature component. Park transformation of two-phase voltage is shown in Figure 3.9.

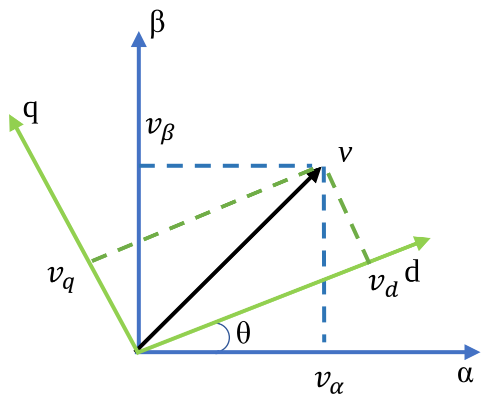

Figure 3.9 Park transformation of two-phase voltage

The dq representation greatly simplifies control of the induction motor because PI controller design can be simply used to track constant dc references rather than sinusoidal references.

$$\begin{pmatrix} v_d \\ v_q \end{pmatrix} = \begin{pmatrix} \cos\theta & \sin\theta \\ -\sin\theta & \cos\theta \end{pmatrix} \begin{pmatrix} v_\alpha \\ v_\beta \end{pmatrix} \quad (3.25)$$

For simplicity, the following simplifying assumptions are made for the considered induction motor [45].

- The three-phase motor is symmetrical.
- The air gap is uniform.
- The effects of magnetic saturation, iron losses, and eddy currents are neglected.
- The coil resistances and reactance are taken to be constant.
- Motor stator and rotor windings are sinusoidally distributed.
- The harmonics in voltages and currents are neglected.

The induction motor modeling usually contains three parts: flux equations, voltage equations, and torque equations.

3.4.1 Flux Equation

There are three kinds of fluxes: stator flux, rotor flux, and mutual flux. The stator flux and rotor flux vectors can be expressed in terms of stator current and rotor current given below:

$$\varphi_{ds} = L_s I_{ds} + L_m I_{dr} \quad (3.26)$$

$$\varphi_{qs} = L_s I_{qs} + L_m I_{qr} \quad (3.27)$$

$$\varphi_{dr} = L_r I_{dr} + L_m I_{ds} \quad (3.28)$$

$$\varphi_{qr} = L_r I_{qr} + L_m I_{qs} \quad (3.29)$$

Where L_s is stator inductance, L_r is rotor inductance, L_m is mutual inductance, φ_{ds} and φ_{qs} are stator flux vector in d and q axis respectively, φ_{dr} and φ_{qr} are rotor flux vector in d and q axis respectively, I_{ds}, I_{qs} and I_{dr}, I_{qr} are the stator and rotor current in d and q axis respectively.

3.4.2 Voltage Equations

The voltage equations of induction motors can be described in different coordinate frames. The reference frame can be revolving or stationary, can be attached to the stator or rotor. The possible choices for d-q axes frames in ac machines are the stationary frame (stator reference frame), the rotor, and rotates at the speed of the rotor (rotor reference frame) and a frame rotating at synchronous speed. (synchronously rotating reference frame) or field frame [46].

The following equation is based on a general reference frame. Models in other reference frames can be obtained as a particular case of this general model.

The stator and rotor voltage equations can be expressed as:

$$v_{ds} = R_s i_{ds} + \frac{d\varphi_{ds}}{dt} - \omega_g \varphi_{qs} \tag{3.30}$$

$$v_{qs} = R_s i_{qs} + \frac{d\varphi_{qs}}{dt} + \omega_g \varphi_{ds} \tag{3.31}$$

$$v_{dr} = R_r i_{dr} + \frac{d\varphi_{dr}}{dt} + \left(p\omega_r - \omega_g\right)\varphi_{qr} \tag{3.32}$$

$$v_{qr} = R_r i_{qr} + \frac{d\varphi_{qr}}{dt} + \left(\omega_g - p\omega_r\right)\varphi_{dr} \tag{3.33}$$

Where ω_g is the reference frame angular velocity and ω_r is the rotor angular speed.

Substituting Equation (3.26) and (3.27) into Equation (3.30) and (3.31), the stator voltage equations can be rewritten as:

$$v_{ds} = R_s i_{ds} + \frac{d}{dt}\left(L_s I_{ds} + L_m I_{dr}\right) - \omega_g \left(L_s I_{qs} + L_m I_{qr}\right) \tag{3.34}$$

$$v_{qs} = R_s i_{qs} + \frac{d}{dt}\left(L_s I_{qs} + L_m I_{qr}\right) + \omega_g \left(L_s I_{ds} + L_m I_{dr}\right) \tag{3.35}$$

Substituting Equation (3.28) and (3.29) into Equation (3.32) and (3.33), the rotor voltage equations can be rewritten as:

$$v_{dr} = R_r i_{dr} + \frac{d}{dt}\left(L_r I_{dr} + L_m I_{ds}\right) + \left(p\omega_r - \omega_g\right)\left(L_r I_{qr} + L_m I_{qs}\right) \tag{3.36}$$

$$v_{qr} = R_r i_{qr} + \frac{d}{dt}\left(L_r I_{qr} + L_m I_{qs}\right) + \left(\omega_g - p\omega_r\right)\left(L_r I_{dr} + L_m I_{ds}\right) \tag{3.37}$$

From the four voltage equations, the relationship of voltages and currents in the general reference frame can be given in matrix form as shown in Equation (3.38).

$$\begin{bmatrix} v_{ds} \\ v_{qs} \\ v_{dr} \\ v_{qr} \end{bmatrix} = \begin{bmatrix} R_s + L_s \frac{d}{dt} & -\omega_g L_s & L_m \frac{d}{dt} & -\omega_g L_m \\ \omega_g L_s & R_s + L_s \frac{d}{dt} & \omega_g L_m & L_m \frac{d}{dt} \\ L_m \frac{d}{dt} & (p\omega_r - \omega_g) L_m & R_r + L_r \frac{d}{dt} & (p\omega_r - \omega_g) L_r \\ (\omega_g - p\omega_r) L_m & L_m \frac{d}{dt} & (\omega_g - p\omega_r) L_r & R_r + L_r \frac{d}{dt} \end{bmatrix} \begin{bmatrix} i_{ds} \\ i_{qs} \\ i_{dr} \\ i_{qr} \end{bmatrix} \quad (3.38)$$

3.4.3 Torque Equations

The equation for electromagnetic torque in terms of flux linkages and current in any reference frame can be obtained using the quantities in that frame and is given by:

$$T_e = \frac{3}{2} p \left(\varphi_{ds} i_{qs} - \varphi_{qs} i_{ds} \right) \quad (3.\ 39)$$

Also, the system motion equation is given by:

$$T_e = T_L + J \frac{d\omega_r}{dt} \quad (3.\ 40)$$

Where T_e is the electromagnetic torque, T_L is the load torque, ω_r is the rotor rotating speed, and p is the poles pair number, and J is rotors moment of inertia.

3.5 Voltage Source Inverter

Power electronic control is becoming more and more important and a large share of motors are equipped with frequency converters to enable motor speed control and to reduce the energy consumption of motor systems. The two-level voltage source converter is the most used configuration to supply three-phase motors [47]. The three-phase two-level VSI consists of six active power semiconductor switches. Different power devices for electric propulsion are used out of them IGBT is almost exclusively used for modern EVs due to its advantage over the others.

The basic configuration of the inverter is shown in Figure 3.10. The converter consists of the three legs with semi-conductor switches.

The inverter is supplied by a DC voltage source. The power semiconductors switches are controlled in an on-off fashion. There are three different legs each leg is connected to its respective phase. There is a 120-degree phase shift between each phase. The switches in each leg must not turn on at the same time otherwise the circuit will be shorted resulting in undefined states in the VSI and thus undefined ac output line voltages. Applying a gating pulse and removing it will turn the switch on and off respectively. The middle points of the inverter legs are connected to the induction motor.

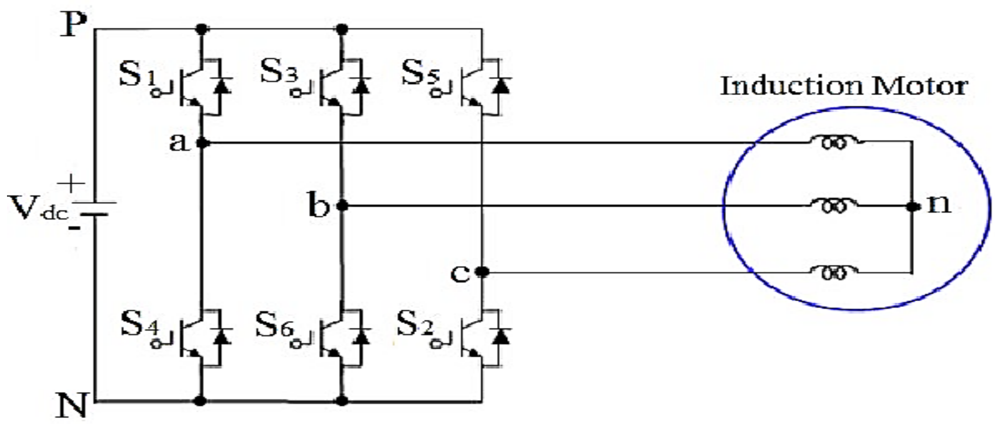

Figure 3.10 The topology of two-level voltage source inverter [48]

There are eight valid switch states which are given in Table 3.5. Two of them (7 and 8) are called zero switch states to produce zero AC line voltages. In this case, the AC line currents freewheel through either the upper or lower components. The remaining states (1 to 6) are called non-zero switch states to produce non-zero AC output voltages. The resulting AC output line voltages consist of discrete values of voltages that are V_{dc}, 0, and $-V_{dc}$.

The output voltage from an inverter can also be adjusted by exercising control within the inverter itself. The most efficient method of doing this is by pulse-width modulation control. In this method, a fixed dc input voltage is given to the inverter and a controlled ac output voltage is obtained by adjusting the on and off periods of the inverter components. This is the most popular method of controlling the output voltage.

The actual power flow in each motor phase is controlled by the duty cycle of the respective switches. To obtain a suitable duty cycle for each switches technique pulse width modulation is used. PWM is based on the sequential switching of active and zero vectors. From different types of PWM control techniques, SPWM and SVPWM are the most popular.

Table 3.5 Valid switching states and output line to line voltage of three-phase VSI [49]

State	Switching state	Line to line voltage		
		V_{ab}	V_{bc}	V_{ca}
1	S_1, S_6, and S_2 are on [100]	V_{dc}	0	$-V_{dc}$
2	S_1, S_3, and S_2 are on [110]	0	V_{dc}	$-V_{dc}$
3	S_4, S_3, and S_2 are on [010]	$-V_{dc}$	V_{dc}	0
4	S_4, S_3 and S_5 are on [011]	$-V_{dc}$	0	$-V_{dc}$
5	S_4, S_6 and S_5 are on [001]	0	$-V_{dc}$	V_{dc}
6	S_1, S_6, and S_5 are on [101]	V_{dc}	$-V_{dc}$	0
7	S_4, $S_{6,}$ and S_2 are on [000]	0	0	0
8	S_1, $S_{3,}$ and S_5 are on [111]	0	0	0

3.5.1 Sinusoidal Pulse Width Modulation

Sinusoidal modulation is based on a triangular carrier signal. In this method, three reference signals V_a, V_b, and V_c are compared with the triangular carrier signal, which is common to all three phases as shown in Figure 3.11. In this way, the logical signals S_A, S_B, S_C are generated, which define the switching instants of the power switch.

3.5.2 Space Vector Pulse Width Modulation

In the SVPWM technique, instead of using a separate modulator for each of the three phases, the complex reference voltage vector is processed as a whole. Therefore, the interaction between the three motor phases is considered. SVPWM generates less harmonic distortion in the output voltages and currents in the windings of the motor load and provides more efficient use of the DC supply voltage in comparison with sinusoidal modulation techniques. Since SVPWM provides a constant switching frequency; the switching frequency can be adjusted easily. Although SVPWM is more complicated than sinusoidal PWM, it may be implemented easily with modern DSP based control systems. SVPWM can be implemented in MATLAB Simulink with simple 5 steps.

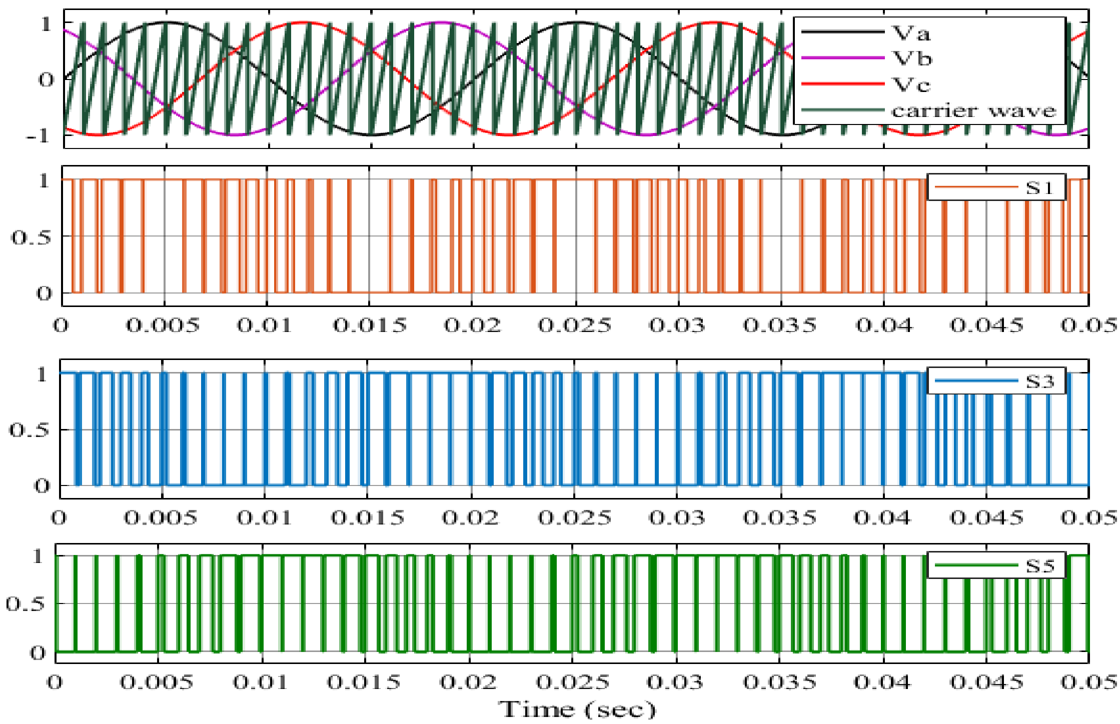

Figure 3.11 Sinusoidal PWM with generated gate pulses

Step 1: Calculating the position θ and magnitude of V_{ref}

To calculate the magnitude and position of the reference voltage the three-phase voltages will be transformed into two phases using Clarke transformation. For a balanced system with the information of the two-phase voltages, the third one can be obtained since their sum equals zero. But for the SVM-DTC method from Figure 3.17, it can be seen that the input to the SVM is the dq voltage vectors therefore instead of Clarke transformation inverse Park transformation is used. MATLAB code in the Appendix C.

$$\begin{pmatrix} V_\alpha \\ V_\beta \end{pmatrix} = \begin{pmatrix} \cos\theta & -\sin\theta \\ \sin\theta & \cos\theta \end{pmatrix} \begin{pmatrix} V_d \\ V_q \end{pmatrix} \tag{3. 41}$$

After finding the value of V_α and V_β the position and magnitude of V_{ref} can be calculated as

$$V_{ref} = \sqrt{\left(V_\alpha^2 + V_\beta^2\right)} \tag{3. 42}$$

$$\theta = \tan^{-1}\left(\frac{V_\beta}{V_\alpha}\right)$$

Where V_{ref} is the refence voltage and θ is the position of the reference voltage.

Step 2: Determining sectors

From Figure 3.12 it can be seen that if the V_{ref} is in sector 1 the angle θ is between 0 to 60. Since the reference voltage rotates in space at an angular velocity of $2\pi f_1$ where f_1 is the fundamental frequency of the inverter output voltage, the reference voltage can be located in any one of the six sectors.

Therefore, using the position θ the location of V_{ref} can be determined. The zero and active vectors in Figure 3.12 do not move in space, and thus they are referred to as stationary vectors. Figure 3.13 shows the Simulink block representation of sector determination.

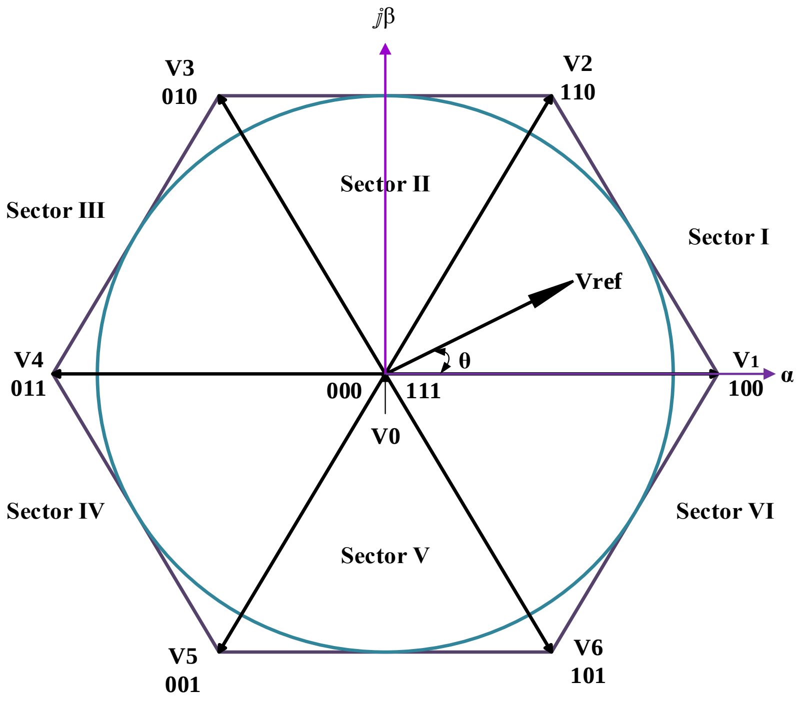

Figure 3.12 Space vector diagram for the two-level inverter.

A space vector can be generally expressed in terms of the three-phase voltages in the abc plane.

$$V(t) = \frac{2}{3}\left(V_{an}(t)e^{j0} + V_{bn}(t)e^{j2\pi/3} + V_{cn}(t)e^{j4\pi/3}\right) \tag{3. 43}$$

Every six active vectors can be obtained by substituting the corresponding line to neutral voltage from Table 3.6 into Equation (3.43). For example, for switching vector 1 0 0 substituting V_{an}=$2/3\,Vd$, V_{bn} = - $1/3Vd$ and V_{cn} = - $1/3\,Vd$.

$$V_1 = \frac{2}{3}\left(\frac{2}{3}V_d e^{j0} - \frac{1}{3}V_d e^{j2\pi/3} - \frac{1}{3}V_d e^{j4\pi/3}\right)$$

$$V_1 = \frac{2}{3}\left(\frac{2}{3}V_d - \frac{1}{3}V_d\left(\frac{-1}{2} + j\frac{\sqrt{3}}{2}\right) - \frac{1}{3}V_d\left(\frac{-1}{2} - j\frac{\sqrt{3}}{2}\right)\right)$$

$$V_1 = \frac{2}{9}V_d\left(2 + \frac{1}{2} - j\frac{\sqrt{3}}{2} + \frac{1}{2} + j\frac{\sqrt{3}}{2}\right)$$

$$V_1 = \frac{2}{3}V_d e^{j0} \tag{3. 44}$$

Following the same procedure, all six active vectors can be derived as: -

$$V_k = \frac{2}{3}V_d e^{j(k-1)\frac{\pi}{3}} \quad k=1, 2, ..., 6 \tag{3. 45}$$

Table 3.6 Valid switching states and output line to neutral voltage of three-phase VSI [49]

Voltage Vector	Switching vectors			Line to neutral voltage		
	a	b	c	V_{an}	V_{bn}	V_{cn}
V_0	0	0	0	0	0	0
V_1	1	0	0	$2/3\,V_d$	$-1/3\,V_d$	$-1/3\,V_d$
V_2	1	1	0	$1/3\,V_d$	$1/3\,V_d$	$-2/3\,V_d$
V_3	0	1	0	$-1/3\,V_d$	$2/3\,V_d$	$-1/3\,V_d$
V_4	0	1	1	$-2/3\,V_d$	$1/3\,V_d$	$1/3\,V_d$
V_5	0	0	1	$-1/3\,V_d$	$-1/3\,V_d$	$2/3\,V_d$
V_6	1	0	1	$1/3\,V_d$	$-2/3\,V_d$	$1/3\,V_d$
V_7	1	1	1	0	0	0

The relationship between the space vectors and their corresponding switching state is shown in Table 3.7.

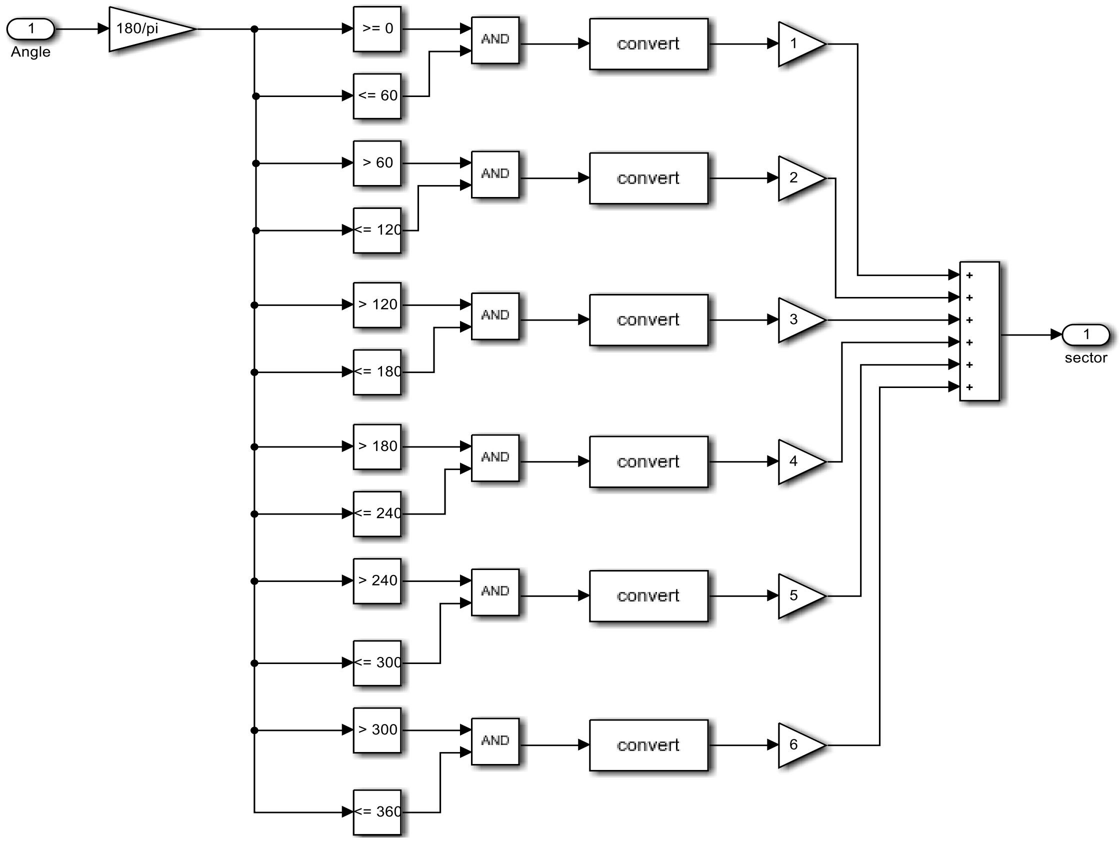

Figure 3.13 Sector determination MATLAB Simulink block diagram

Step 3: Modulation index calculation

The modulation index can be determined by using the Equation (3.46).

$$M_a = \frac{\sqrt{3}V_{ref}}{V_d} \tag{3.46}$$

The maximum value of M_a is 1 therefore, V_{ref} becomes:

$$V_{ref,\,max} = \frac{V_d}{\sqrt{3}} \tag{3.47}$$

The maximum fundamental line to line voltage (rms) produced by the SVPWM scheme can be calculated as:

$$V_{ref,max} = \sqrt{3}\frac{V_{ref,max}}{\sqrt{2}} = \frac{\sqrt{3}}{\sqrt{2}}\left(\frac{V_d}{\sqrt{3}}\right) = 0.707V_d \qquad (3.48)$$

Equation (3.47) indicates that for a given dc bus voltage the maximum inverter line to line voltage generated by the SVPWM scheme is 70.7% of the applied DC bus voltage.

Table 3.7 Space vectors and their corresponding switching state

Space vectors	Switching state	On state switches	Off-state switches	Vector definition
V_0	0 0 0	S_1, S_3, S_5	S_4, S_6, S_2	$v_0 = 0$
V_1	1 0 0	S_1, S_6, S_2	S_4, S_3, S_5	$v_1 = \frac{2}{3}v_d e^{j0}$
V_2	1 1 0	S_1, S_3, S_2	S_4, S_6, S_5	$v_2 = \frac{2}{3}v_d e^{j\frac{\pi}{3}}$
V_3	1 1 0	S_4, S_3, S_2	S_1, S_6, S_5	$v_3 = \frac{2}{3}v_d e^{j\frac{2\pi}{3}}$
V_4	0 1 0	S_4, S_3, S_5	S_1, S_6, S_2	$v_4 = \frac{2}{3}v_d e^{j\frac{3\pi}{3}}$
V_5	0 0 1	S_4, S_6, S_5	S_1, S_3, S_2	$v_5 = \frac{2}{3}v_d e^{j\frac{4\pi}{3}}$
V_6	1 0 1	S_1, S_6, S_5	S_4, S_3, S_2	$v_6 = \frac{2}{3}v_d e^{j\frac{5\pi}{3}}$
V_7	1 1 1	S_4, S_6, S_2	S_1, S_3, S_5	$v_0 = 0$

Step 4: Dwell time calculation:

The dwell time calculation is based on the volt-second balancing principle. V_{ref} can be approximated by two adjacent active vectors and one zero vectors. For example, when V_{ref} falls into sector I as shown in Figure 3.14, it can be synthesized by V_1, V_2, and V_0. Based on which the switching states of the inverter can be selected and gate signals for the active switches can be generated.

The volt second balancing equation is given by:

$$V_{ref}T_s = V_1T_a + V_2T_b + V_0T_0 \qquad (3.49)$$
$$T_s = T_a + T_b + T_0$$

Where T_a, T_b and T_0 are dwell times for the vectors V_1, V_2 and V_0 respectively.

Substituting space vectors V_1, V_2, and V_0 from Table 3.7 and for $\vec{V}_{ref} = V_{ref} e^{j\theta}$ in to Equation (3.49) the dwell time T_a, T_b, and T_0 can be calculated as in Equation (3.55), (3.53), and (3.56) respectively.

$$V_{ref} e^{j\theta} T_s = \frac{2}{3} V_d T_a + \frac{2}{3} V_d e^{j\frac{\pi}{3}} T_b + 0$$

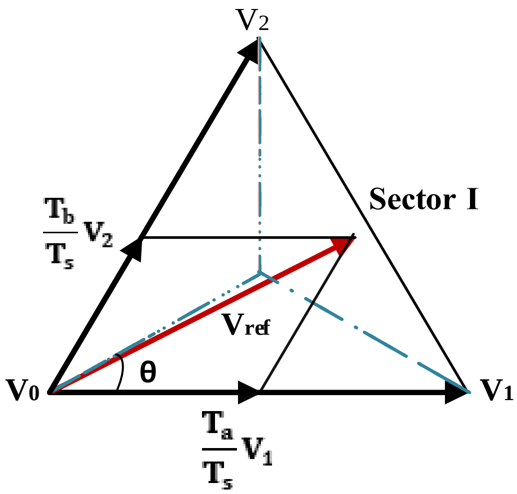

Figure 3.14 V_{ref} synthesized by V_1, V_2, and V_0

$$V_{ref} \left(\cos\theta + j\sin\theta\right) T_s = \frac{2}{3} V_d T_a + \frac{2}{3}\left(\cos\frac{\pi}{3} + j\sin\frac{\pi}{3}\right) V_d T_b$$

$$V_{ref} \left(\cos\theta\right) T_s + V_{ref}\, j\left(\sin\theta\right) T_s = \frac{2}{3} V_d T_a + \frac{1}{3} V_d T_b + j\frac{1}{\sqrt{3}} V_d T_b \tag{3.50}$$

Splitting Equation (3.50) into the real component and imaginary components:

$$\text{Real}: \ V_{ref} \left(\cos\theta\right) T_s = \frac{2}{3} V_d T_a + \frac{1}{3} V_d T_b \tag{3.51}$$

$$\text{Imaginary}: \ V_{ref} \left(\sin\theta\right) T_s = \frac{1}{\sqrt{3}} V_d T_b$$

Solving for T_a and T_b from Equation (3.51)

$$T_a = \frac{3 V_{ref} T_s \cos\theta}{2 V_d} - T_b \tag{3.52}$$

$$T_b = \frac{\sqrt{3} T_s V_{ref}}{V_d} \sin\theta \tag{3.53}$$

Substituting T_b into T_a the rearranged value of T_a can be: -

$$T_a = \frac{3V_{ref} T_s \cos\theta}{2V_d} - \frac{\sqrt{3} T_s V_{ref}}{V_d} \sin\theta$$

$$T_a = \frac{\sqrt{3}\, T_s V_{ref}}{V_d} \frac{\left(\sqrt{3}\cos\theta - \sin\theta\right)}{2} \tag{3.54}$$

$$T_a = \frac{\sqrt{3}\, T_s V_{ref}}{V_d} \sin\left(\frac{\pi}{3} - \theta\right) \tag{3.55}$$

Equation (3.49) can be solved for T_0:

$$T_0 = T_s - T_a - T_b \tag{3.56}$$

T_a value from Equation (3.55) and T_b value from Equation (3.53) is derived when V_{ref} is in sector I, for the reaming 5 sectors Equation (3.57) will be used.

$$\theta' = \theta - (k-1)\frac{\pi}{3} \quad \text{for } 0 < \theta < \frac{\pi}{3} \quad k = 1, 2, ..., 6 \tag{3.57}$$

Table 3.8 shows the location of V_{ref} and its corresponding dwell time value for one sector.

Table 3.8 V_{ref} location and dwell times

V_{ref} location	$\theta = 0$	$0 < \theta < \frac{\pi}{6}$	$\theta = \frac{\pi}{6}$	$0 < \theta < \frac{\pi}{3}$	$\theta = \frac{\pi}{3}$
Dwell times	$T_a > 0$ $T_a = 0$	$T_a > T_b$	$T_a = T_b$	$T_a < T_b$	$T_a = 0$ $T_b > 0$

Figure 3.15 shows the Simulink MATLAB representation for calculating the dwell time for each sector.

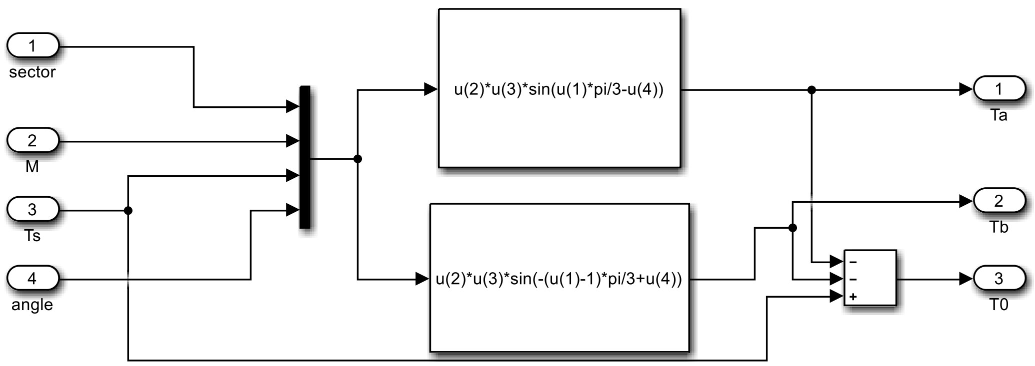

Figure 3.15 Dwell time calculation of MATLAB Simulink block diagram

Using the modulation in Equation (3.45), (3.55), and (3.53) can be updated as: -

$$T_a = T_s M_a \sin\left(k\frac{\pi}{3} - \theta\right) \quad (3.58)$$

$$T_b = T_s M_a \sin\left(\theta - (k-1)\frac{\pi}{3}\right)$$

Step 5: Switching sequence generation:

Using the calculated dwell times and the sector reference signal will be generated and compared with the carrier signal to generate the gating pulses.

The switching sequence should satisfy the following two requirements for the minimization of the device switching frequency:

1. The transition from one switching state to the next must involve only two switches in the same inverter leg, one being switched on and the other being switched off.
2. The transition for V_{ref} moving from one sector in space vector diagram to the next must require no or minimum number of switching.

From Figure 3.16 it can be shown that the transition from [0 0 0] to [1 0 0] is accomplished by turning S1 on and S4 off, which involves only two switches therefore design requirement (1) is satisfied.

The redundant switching sates for V_0 are utilized to reduce the number of switching per sampling period. For the $T_0/2$ segment in the center of sampling period, the switching state [1 1 1] is selected, whereas for the $T_0/2$ segments on both sides, the state [0 0 0] is used.

Each of the switches in the inverter turns on and off once per sampling period. The switching frequency f_{sw} of the device is thus equal to the sampling frequency f_{sp} that is, $f_{sw} = f_{sp} = 1/T_s$.

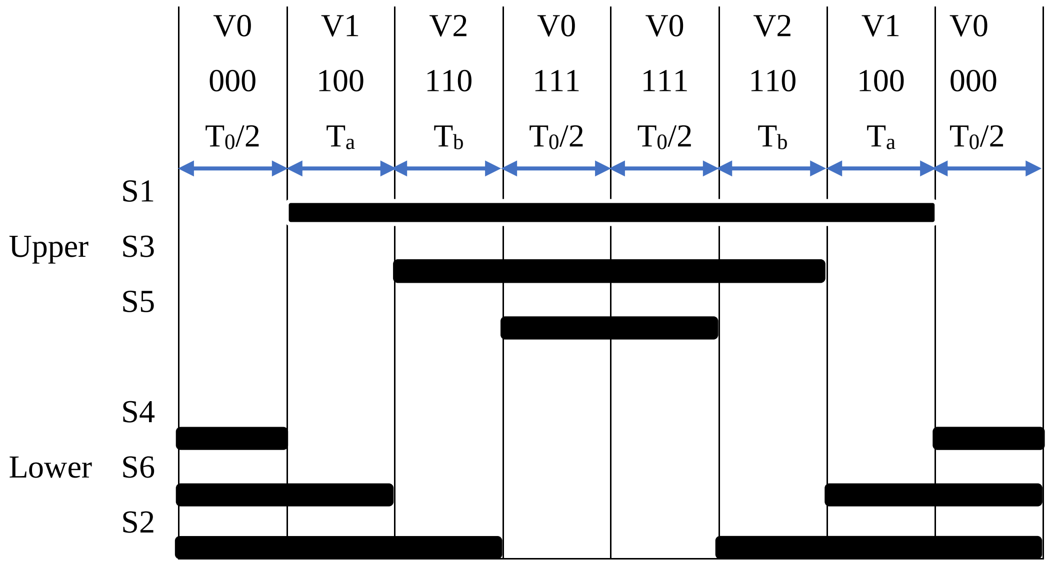

Figure 3.16 Typical seven-segment switching sequence for sector I

Table 3.9 Seven-segment switching sequence [50]

Sector	1	2	3	4	5	6	7
I	V0 0 0 0	V1 1 0 0	V2 1 1 0	V0 1 1 1	V2 1 1 0	V1 1 0 0	V0 0 0 0
II	V0 0 0 0	V3 0 1 0	V2 1 1 0	V0 1 1 1	V2 1 1 0	V3 0 1 0	V0 0 0 0
III	V0 0 0 0	V3 0 1 0	V4 0 1 1	V0 1 1 1	V4 0 1 1	V3 0 1 0	V0 0 0 0
IV	V0 0 0 0	V5 0 0 1	V4 0 1 1	V0 1 1 1	V4 0 1 1	V5 0 0 1	V0 0 0 0
V	V0 0 0 0	V5 0 0 1	V6 1 0 1	V0 1 1 1	V6 1 0 1	V5 0 0 1	V0 0 0 0
VI	V0 0 0 0	V1 1 0 0	V6 1 0 1	V0 1 1 1	V6 1 0 1	V1 1 0 0	V0 0 0 0

Table 3.9 gives the seven-segment switching sequence for V_{ref} residing in all six sectors. It can be noted that all the switching sequence starts and end with switching state [0 0 0] which indicates that the transition for V_{ref} moving from one sector to the next does not require any switching's which satisfies the sequence design requirement (2) this rule help in limiting the number of switching actions and there is a reduction in the switching losses. The switching time at each sector is listed in Table 3.10.

Table 3.10 Switching time calculation at each sector [51].

Sector	Upper Switches ($S1$, $S3$, $S5$)	Lower Switches **($S4$, $S6$, $S2$)**
1	$S1 = T_a + T_b + T_0/2$ $S3 = T_b + T_0/2$ $S5 = T_0/2$	$S4 = T_0/2$ $S6 = T_a + T_0/2$ $S2 = T_a + T_b + T_0/2$
2	$S1 = T_a + T_0/2$ $S3 = T_a + T_b + T_0/2$ $S5 = T_0/2$	$S4 = T_b + T_0/2$ $S6 = T_0/2$ $S2 = T_a + T_b + T_0/2$
3	$S1 = T_0/2$ $S3 = T_a + T_b + T_0/2$ $S5 = T_b + T_0/2$	$S4 = T_a + T_b + T_0/2$ $S6 = T_0/2$ $S2 = T_a + T_0/2$
4	$S1 = T_0/2$ $S3 = T_a + T_0/2$ $S5 = T_a + T_b + T_0/2$	$S4 = T_a + T_b + T_0/2$ $S6 = T_b + T_0/2$ $S2 = T_0/2$
5	$S1 = T_b + T_0/2$ $S3 = T_0/2$ $S5 = T_a + T_b + T_0/2$	$S4 = T_a + T_0/2$ $S6 = T_a + T_b + T_0/2$ $S2 = T_0/2$
6	$S1 = T_a + T_b + T_0/2$ $S3 = T_0/2$ $S5 = T_a + T_0/2$	$S4 = T_0/2$ $S6 = T_a + T_b + T_0/2$ $S2 = T_b + T_0/2$

3.6 Vector Control of Induction Motor

As discussed in the literature review mainly there are two types of vector control methods of induction motor namely FOC and DTC. DTC SVM is selected to control the speed of the induction motor due to its advantage over the other speed control methods of IM.

3.6.1 DTC with SVM

The control algorithm in DTC-SVM methods are based on averaged values whereas the switching signals for the inverter are calculated by space vector modulator. In DTC-SVM the flux and torque hysteresis controller replaced by PI controller and the vector selection table is replaced by SVM to decrease the torque ripple in conventional DTC [33]. A block diagram of the method with close-loop torque and flux control in stator flux coordinate system is presented in Figure 3.17.

The output of the PI flux and torque controllers can be interpreted as the reference stator voltage components V_d and V_q in the stator flux-oriented coordinates. These dc voltage commands are then transformed into αβ stationary frame, the commanded values V_α, V_β are delivered to SVM. SVM generates the gating pulses to the switches. How a Space vector pulse width modulation generates the switching signals for the inverter detailly discussed in Section 3.6.2.

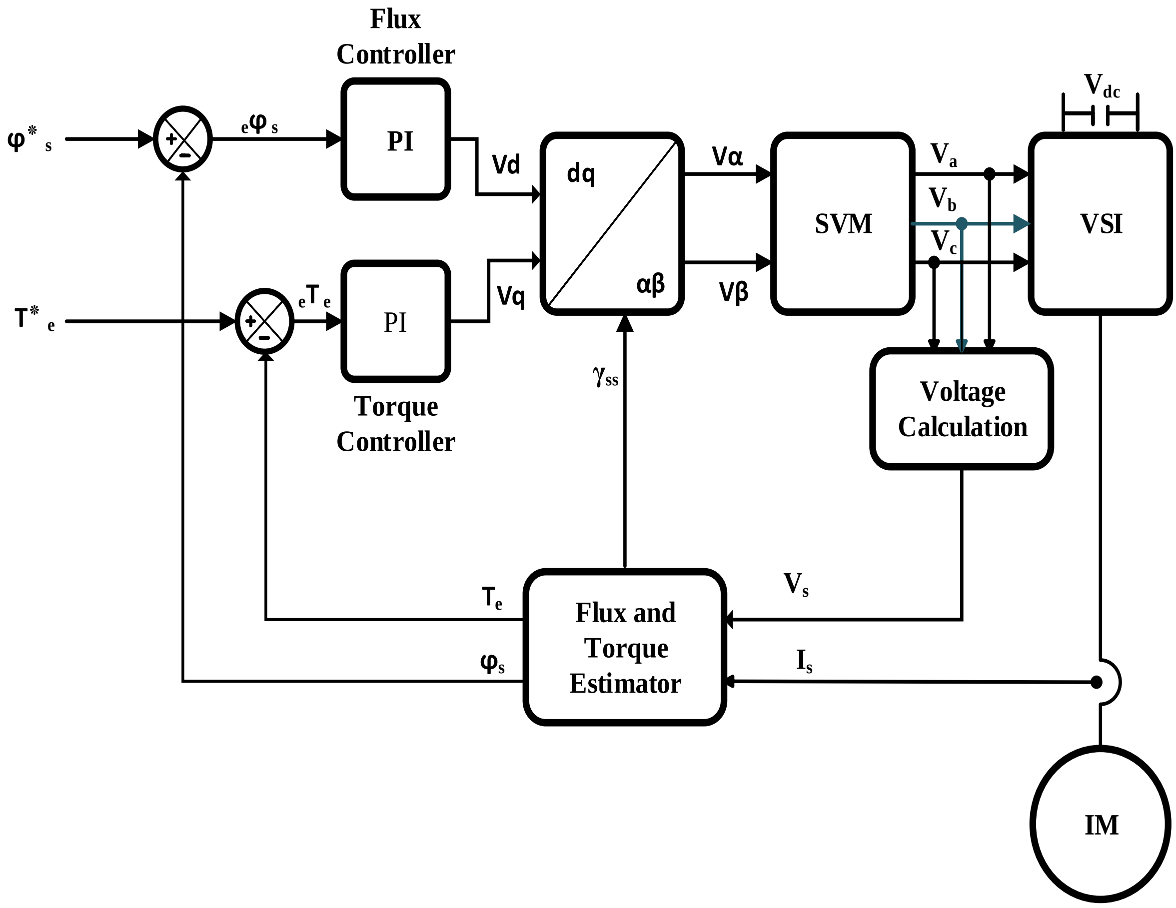

Figure 3.17 Block diagram of the space vector pulse width modulation DTC method

3.6.1.1 Flux and Torque Estimator

The flux and torque are estimated from the measured machine terminal voltage and current by using 3-phase to 2-phase transformation in dq stator reference frame with d-axis fixed along a-axis and then calculating the flux and torque from the two-phase variables.

Flux estimation: From the equation of stator voltage, it can be shown that the variation of flux is directly affected by the applied voltage vector Vs. Basing on the induction motor model in dq stator reference frame, the stator flux equation can be expressed as follows. In stator reference frame the reference frame angular velocity ω_g becomes zero.

Equation (3.30) and (3.31) in dq stator reference frame becomes: -

$$v_{ds} = R_s i_{ds} + \frac{d\varphi_{ds}}{dt} \quad (3.59)$$

$$v_{qs} = R_s i_{qs} + \frac{d\varphi_{qs}}{dt} \quad (3.60)$$

The speed of the reference frame $\omega_g = 0$ since dq is in a stationary frame. Equation (3.59) and (3.60) can be rewrite for φ_{dqs} in the dq plane as: -

$$\varphi_{ds} = \int (v_{ds} - R_s i_{ds})\, dt \quad (3\ 61)$$

$$\varphi_{qs} = \int (v_{qs} - R_s i_{qs})\, dt \quad (3.62)$$

The average stator flux vector will be

$$\varphi_s = \sqrt{\varphi_{ds}^2 + \varphi_{qs}^2} \quad (3.63)$$

The stator flux position can be obtained from: -

$$\tan^{-1}\theta = \left(\frac{\varphi_{qs}}{\varphi_{ds}}\right) \quad (3\ 64)$$

Torque estimation: The produced electromagnetic torque of the induction motor can be determined using the cross product of the stator quantities (i.e., stator flux and stator currents). It can be seen that the calculated torque is depended on the current measurement accuracy and stator flux estimation method. The torque formula is expressed as the follows:

$$T_e = \frac{3}{2} p \left(\varphi_{ds} i_{qs} - \varphi_{qs} i_{ds} \right) \tag{3.65}$$

MATLAB Simulink implementation of the torque and flux estimation and stator flux position determination block is shown in Figure 3.18.

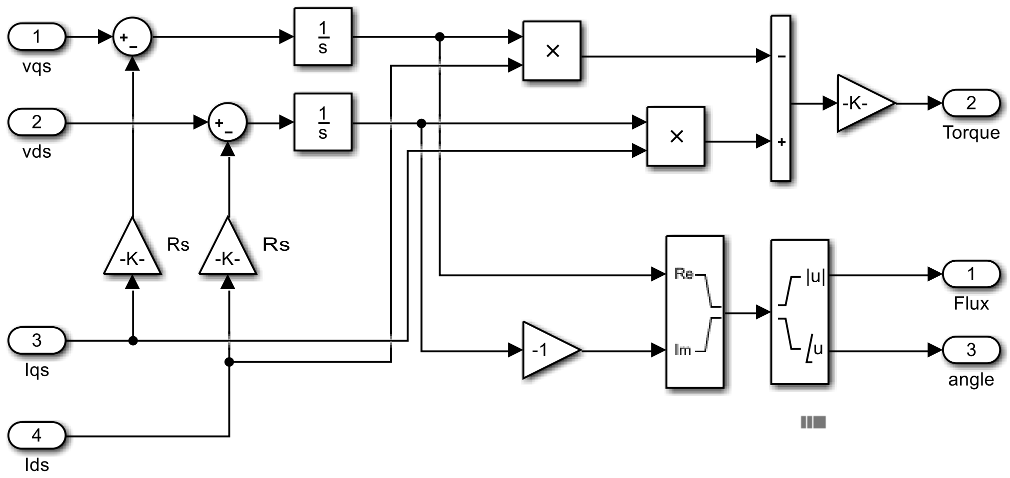

Figure 3.18 MATLAB Simulink block diagram of flux and torque estimator

3.6.1.2 PI Flux and Torque Controller Design

A controller should be simple and cost effective as possible. In order to design the flux and torque PI controller the motor model equations must be considered. The complete set of motor model equations from Equation (3.30 - 3.33) can be written in stator flux coordinate synchronous rotating reference frame dq. This system of coordinates dq rotates with the stator flux angular speed ($\omega_g = \omega_s$) this angular speed is defined as follows:

$$\omega_s = \frac{d\gamma_{ss}}{dt} \tag{3.66}$$

Where ω_s is the stator flux angular speed and γ_{ss} is the stator flux vector angle.

In stator flux coordinate synchronous rotating reference frame φ_{qs} become zero therefore $\varphi_{ds} = \varphi_s$ since the complex space vector for the stator flux is $\varphi_s = \varphi_{ds} + j\varphi_{qs}$. In order to relate the mechanical speed of the motor to the electrical Equation (3.67) is used.

$$\omega_e = p * \omega_r \tag{3.67}$$

Where p is number of pole pair, ω_r is the rotor angular speed and ω_e is electrical speed

The general equation of induction motor in Equations (3.30 - 3.33) in stator flux coordinate synchronous rotating reference frame can be expressed as:

$$v_{ds} = R_s i_{ds} + \frac{d\varphi_{ds}}{dt} \tag{3.68}$$

$$v_{qs} = R_s i_{qs} + \omega_s \varphi_{ds} \tag{3.69}$$

$$0 = R_r i_{dr} + \frac{d\varphi_{dr}}{dt} + \left(\omega_r - \omega_s\right)\varphi_{qr} \tag{3.70}$$

$$0 = R_r i_{qr} + \frac{d\varphi_{qr}}{dt} + \left(\omega_s - \omega_r\right)\varphi_{dr} \tag{3. 71}$$

The transfer function of PI controllers is given as follows:

$$G_c\left(s\right) = K_p + \frac{K_i}{s} \tag{3.72}$$

The transfer function can be also expressed in a more general form as: -

$$G_c\left(s\right) = k_p\left(1 + \frac{1}{sT_i}\right) \tag{3.73}$$

Where k_p is proportional gain, k_i is integral gain and T_i is controller integrating time and can be obtained as: - $T_i = \frac{k_p}{k_i}$

3.6.2.1.1 Flux Controller Design

The flux equation from Equation (3.26) can be rearranged for the rotor current: -

$$i_{dr} = \frac{\varphi_s - L_s i_{ds}}{L_m} \tag{3. 74}$$

But from Equation (3.68) i_{ds} becomes:

$$i_{ds} = \frac{1}{R_s}\left(V_{sd} - \frac{d\varphi_s}{dt}\right) \tag{3. 75}$$

Therefore, substituting Equation (3.75) in to (3.74) yields: -

$$i_{dr} = \left(\frac{R_s \varphi_s - L_s \left(V_{ds} - \frac{d\varphi_s}{dt} \right)}{R_s L_m} \right) \tag{3. 76}$$

From Equation (3.27), the rotor current in the q axis can be obtained as:

$$i_{qr} = \frac{-L_s i_{qs}}{L_m} \tag{3.77}$$

Equation (3.36) in stator flux coordinate synchronous rotating frame

$$v_{dr} = R_r i_{dr} + \frac{d}{dt}\left(L_r I_{dr} + L_m I_{ds}\right) + \left(L_r I_{qr} + L_m I_{qs}\right)\left(p\omega_r - \omega_s\right) \tag{3. 78}$$

Substituting for i_{ds}, i_{dr} and i_{qr} from Equation (3.75), (3.76), and (3.77) respectively and collecting terms for V_{ds} and φ_s, Equation (3.78) becomes:

$$\left(R_r L_s + \frac{d}{dt}\left(L_r L_s - L_m^2\right)\right)\frac{V_{ds}}{R_s L_m} = \left(\begin{matrix} R_r R_s + \frac{d}{dt}\left(R_r L_s + L_r R_s\right) + \\ \left(\frac{d}{dt}\right)^2 \left(L_r L_s - L_m^2\right) \end{matrix} \right) \frac{\varphi_s}{R_s L_m} - i_{qs}\left(\frac{L_r L_s + L_m^2}{L_m} \right)\left(p\omega_r - \omega_s\right) \tag{3.79}$$

Multiplying Equation (3.79) by $R_s L_m$

$$\left(R_r L_s + \frac{d}{dt}\left(L_r L_s - L_m^2\right)\right) V_{ds} = \left(\begin{matrix} R_r R_s + \frac{d}{dt}\left(R_r L_s + L_r R_s\right) + \\ \left(\frac{d}{dt}\right)^2 \left(L_r L_s - L_m^2\right) \end{matrix} \right) \varphi_s - R_s i_{qs}\left(L_r L_s + L_m^2\right)\left(p\omega_r - \omega_s\right) \tag{3.80}$$

Substituting σ for $\left(1 - \frac{L_m^2}{L_r L_s}\right)$

$$\left(R_rL_s + \frac{d}{dt}L_rL_s\sigma\right)V_{ds} = \left(R_rR_s + \frac{d}{dt}\left(R_rL_s + L_rR_s\right) + \left(\frac{d}{dt}\right)^2 L_rL_s\sigma\right)\varphi_s + R_si_{qs}L_rL_s\sigma\left(p\omega_r - \omega_s\right) \quad (3.81)$$

By taking assumption $R_si_{qs}L_rL_s\sigma\left(p\omega_r - \omega_s\right) \approx 0$ [28] the close loop flux transfer function can be obtained as in Equation (3.82).

$$\frac{\varphi_s}{V_{ds}} = \frac{\left(\frac{R_r}{L_r\sigma} + \frac{d}{dt}\right)}{\left(\left(\frac{d}{dt}\right)^2 + \frac{d}{dt}\frac{\left(R_rL_s + L_rR_s\right)}{L_sL_r\sigma} + \frac{R_rR_s}{L_sL_r\sigma}\right)} \quad (3.82)$$

The open-loop flux transfer function of Equation (3.82) in s domain can be obtained as: -

$$G_\varphi(s) = \frac{\left(\frac{R_r}{L_r\sigma} + s\right)}{\left((s)^2 + \frac{\left(R_rL_s + L_rR_s\right)}{L_sL_r\sigma}s + \frac{R_rR_s}{L_sL_r\sigma}\right)} \quad (3.83)$$

From the motor parameter the flux transfer function becomes: -

$$G_\varphi(s) = \frac{(s - 0.01255)}{\left(s^2 - 0.01276s - 1.331\right)} \quad (3.84)$$

The flux control loop is shown in Figure 3.20, where $G_\varphi(s)$ is a transfer function of the flux and $G_c(s)$ is the transfer function of PI controller given by Equation (3.72).

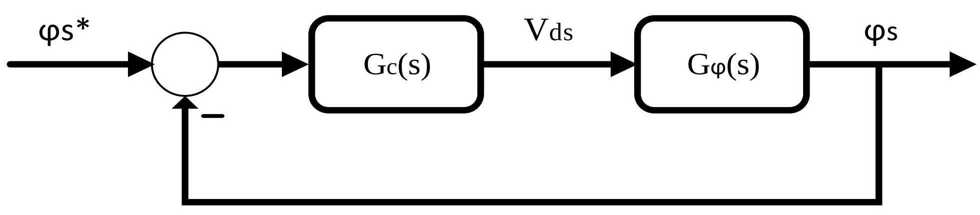

Figure 3.19 Flux closed control loop

PID gain tuning techniques:

If a mathematical model of the plant can be derived than it is possible to apply various design techniques for determining parameters of the controller that will meet the transient and steady state specification of the closed loop system. If the plant is complicated that its mathematical model cannot be easily obtained then the experimental approach of tuning the gains performed using Ziegler and Nichols tuning method. If the system has a known mathematical model such as the transfer function the gain can be easily obtained using different tuning methods but they are not efficient. Ziegler and Nichols tuning method can also be used for system that their transfer function is known. This method applies if the system response to a step input exhibits 's' shaped curve or for some value of kp the system must exhibits sustained oscillation otherwise this method does not apply.

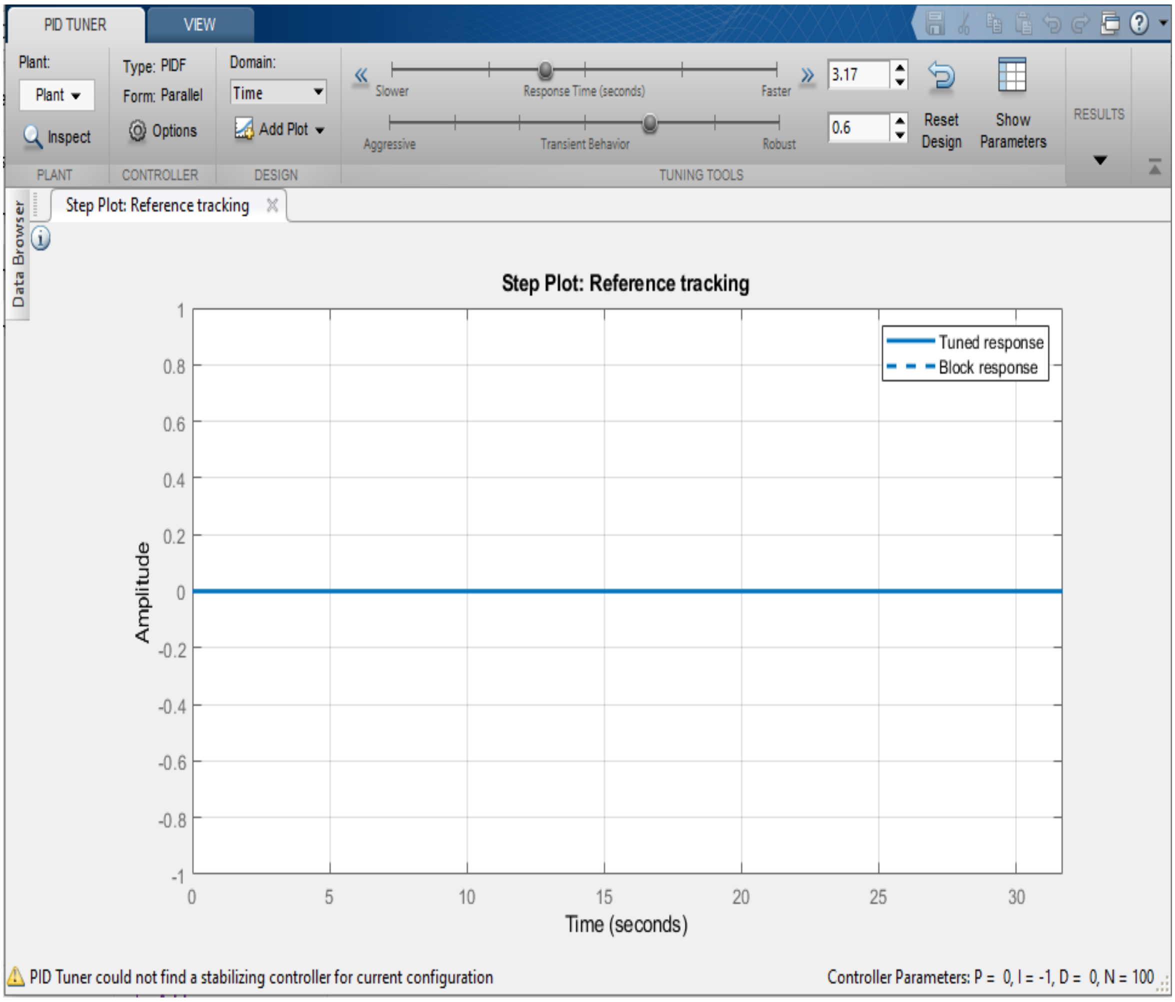

Figure 3.20 PID tuner Tool

MATLAB provides tools for automatically obtaining optimal PID gains which makes the trial and error process unnecessary. It can be accessed directly using PID tune inside PID/PI block it can also accused from the APPS menu. Using a PID tuner tool the PI gain can be adjusted for the required performance by adjusting the response time and transient behavior of the system but faster and robust controller cannot be achieved without sacrificing one for the other therefore the designed controller needs to be compensated.

PID tuning is a control system designer application MATLAB build in tool that helps to automatically tune single input single output compensators. The example window of PID design tool is shown in Figure 3.20. In the upper middle area of the window, the response time (second) and transient behavior is displayed, the doted point moved to right and to the left until the nicely damped response is obtained. More on the left the show parameter icon is visible which displays the block and tuned response as well as controller parameter, and below them the step plot is shown, here the block and the tuned response will be compared.

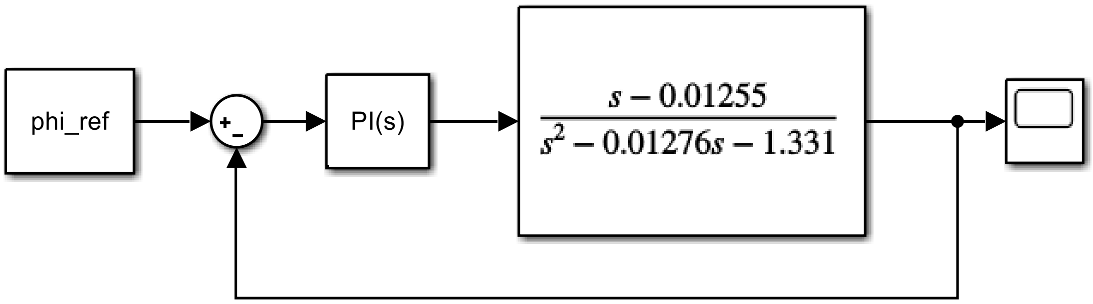

Figure 3.21 MATLAB Simulink representation of closed loop PI flux control

The linear flux transfer function is implemented on MATLAB Simulink as shown in Figure 3.21. Using a PID tuner tool the optimal PI gains are obtained. Figure 3.22 shows the step response of the flux control system from Figure 3.19 described by Equation (3.84), with the PI controller parameters setting as: kp = 134.6, and ki = 5024. The tuned response has a settling time of 0.0752, a rise time of 0.0106, and an overshoot of 14.5% trying to decrease the overshoot by making the transient behavior of the plant more robust will increase the steady state error.

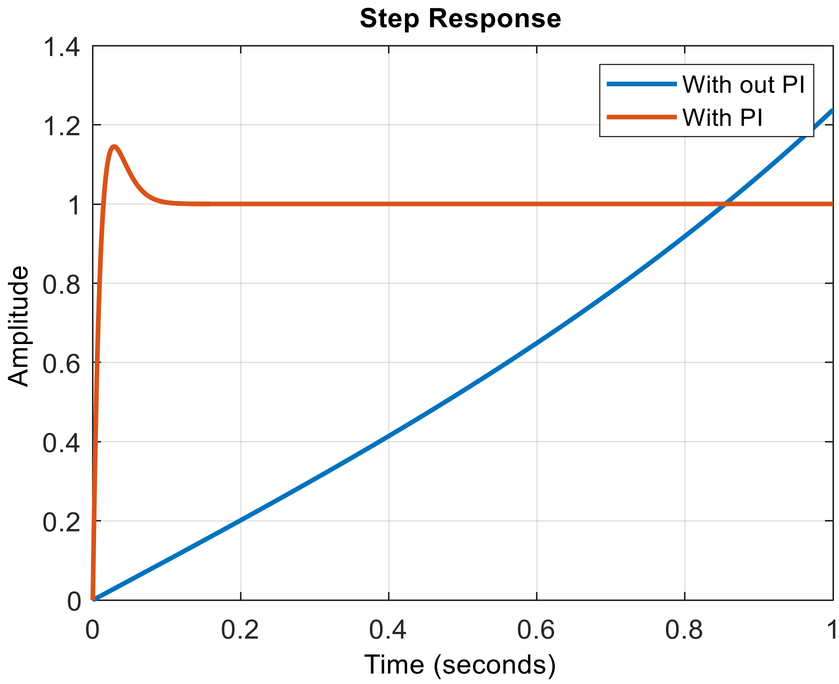

Figure 3.22 Step response of the flux transfer function using a PI tuner App

3.6.2.1.2 Torque Controller Design:

From Equation (3.69), φ_s become: -

$$\varphi_s = \frac{V_{qs} - R_s i_{qs}}{\omega_s} \tag{3.85}$$

Therefore substituting φ_s from Equation (3.85) in to Equation (3.74) i_{dr} becomes:

$$I_{dr} = \frac{V_{qs} - R_s i_{qs} - L_s I_{ds}\omega_s}{\omega_s Lm} \tag{3.86}$$

From Equation (3.27), the rotor current in the q axis can be obtained as:

$$I_{qr} = \frac{-L_s I_{qs}}{L_m} \tag{3.87}$$

Equation (3.36) in stator flux coordinate synchronous rotating frame

$$0 = R_r i_{dr} + \frac{d}{dt}\left(L_r I_{dr} + L_m I_{ds}\right) + \left(L_r I_{qr} + L_m I_{qs}\right)\left(p\omega_r - \omega_s\right) \tag{3.88}$$

Substituting for i_{qr} and i_{dr} from Equation (3.87) and (3.86) respectively in to Equation (3.88)

$$0 = R_r i_{qr} + \frac{d}{dt}\left(L_r I_{qr} + L_m I_{qs}\right) - \left(L_r I_{dr} + L_m I_{ds}\right)\left(\omega_s - p\omega_r\right) \quad (3.89)$$

$$= -L_s R_r i_{qr} - i_{qs}\frac{d}{dt}\left(L_r L_s - L_m{}^2\right) + \left(\begin{matrix} \dfrac{L_r V_{qs} - L_r R_s i_{qs}}{w_{ss}} \\ -L_r L_s i_{ds}\left(L_r L_s - L_m^2\right) + L_m I_{ds} \end{matrix}\right)\left(\omega_s - p\omega_r\right) \quad (3.90)$$

Simplifying Equation (3.90) and substituting σ for $\left(1 - \frac{L_m^2}{L_r L_s}\right)$

$$\left(\left(L_s R_r + L_r R_s\right) + L_r L_s \sigma \frac{d}{dt}\right) i_{qs} = L_r V_{qs} - p_b \omega_m L_r \varphi_s + i_{ds} L_r L_s \sigma\left(\omega_s - p\omega_r\right) \quad (3.91)$$

By taking assumption that, the last term in Equation (3.91) is very small, $i_{ds} L_r L_s \sigma\left(\omega_s - p\omega_r\right) \approx 0$ [28] the Equation (3.91) becomes:

$$\left(\left(L_s R_r + L_r R_s\right) + L_r L_s \sigma \frac{d}{dt}\right) i_{qs} = L_r V_{qs} - p\omega_r L_r \varphi_s \quad (3.92)$$

Equation (3.39) in stator flux-oriented coordinate system can be expressed as: -

$$T_e = \frac{3}{2} p\left(\varphi_{ds} i_{qs}\right) \quad (3.93)$$

Under the assumption that the motor is not loaded $T_L = 0$ the Equation (3.40) becomes:

$$\frac{d\omega_r}{dt} = \frac{1}{J} T_e \quad (3.94)$$

Substituting Equation (3.93) in to (3.94) gives:

$$\frac{d\omega_r}{dt} = \frac{1}{J}\frac{3}{2} p \varphi_{ds} i_{qs} \quad (3.95)$$

From torque, Equation (3.93) the stator current i_{qs} becomes:

$$i_{qs} = \frac{2T_e}{3p\varphi_{ds}} \tag{3.96}$$

Differentiating both side of Equation (3.92)

$$\left((L_s R_r + L_r R_s)\frac{d}{dt} + L_r L_s \sigma \left(\frac{d}{dt}\right)^2 \right) i_{qs} = L_r \frac{dV_{qs}}{dt} - pL_r \varphi_s \frac{d\omega_r}{dt} \tag{3.97}$$

Substituting Equation (3.95) in to Equation (3.97)

$$\left(\left(\frac{d}{dt}\right)^2 + \frac{(L_s R_r + L_r R_s)}{L_r L_s \sigma}\frac{d}{dt} + \frac{3L_r p^2 \varphi_{ds}^2}{2JL_s \sigma} \right) i_{qs} = \frac{1}{L_s \sigma}\frac{dV_{qs}}{dt} \tag{3.98}$$

Substituting Equation (3.96) in to (3.98) and expressing in s domain the open-loop torque transfer function can be obtained as:

$$G_T(s) = \frac{T_e}{V_{qs}} = \frac{\frac{3p\varphi_{ds}}{2L_s\sigma} s}{s^2 + \frac{(L_s R_r + L_r R_s)}{L_r L_s \sigma} s + \frac{3p^2 \varphi_{ds}^2}{2JL_s \sigma}} \tag{3.99}$$

From the motor parameter the torque transfer function becomes:

$$G_T(s) = \frac{T_e}{V_{qs}} = \frac{s - 0.01606}{s^2 + 0.02511s - 2.891} \tag{3.100}$$

The torque control loop is shown in Figure 3.23, where $G_T(s)$ is a transfer function of the torque and $G_c(s)$ is the transfer function of PI controller given by Equation (3.72).

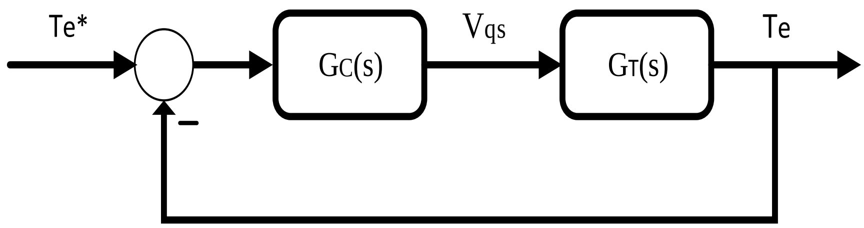

Figure 3.23 Torque control loop

The closed loop PI torque control linear transfer function is implemented on MATLAB Simulink as shown in Figure 3.24. Using a PID tuner tool the optimal PI gains are obtained. Figure 3.25 shows the step response of the torque control system from Figure 3.24 described by Equation (3.100), with the PI controller parameters setting as: kp = 88.5054, and ki = 1121.3. The tuned response has a settling time of 0.155, a rise time of 0.0178, and an overshoot of 10.8% trying to decrease the overshoot by making the transient behavior of the plant more robust will increase the steady state error.

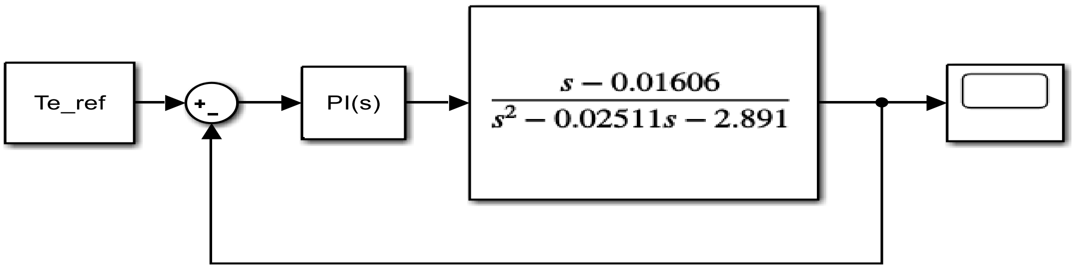

Figure 3.24 MATLAB Simulink representation of closed loop PI torque control

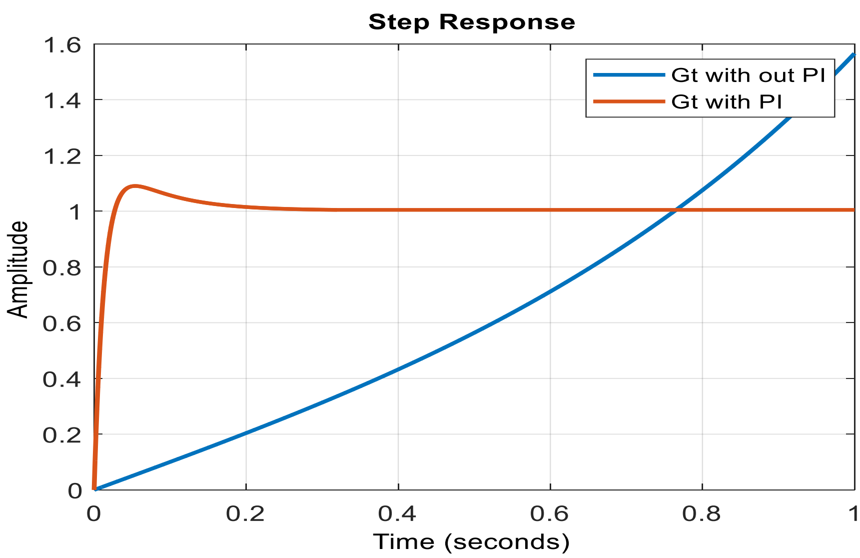

Figure 3.25 Step response of the torque transfer function using PID tuner

3.7 Speed Controller Design

3.7.1 PID Controller

A PID controller is a feedback control system, which calculates an error value as the difference between the reference value and a measured variable and applies a correction based on proportional, integral, and derivative terms continuously [52]. The controller attempts to minimize the error signal by adjustment of a control variable to a new value determined by a weighted sum. The output of a PID controller, which is equal to the control input to the plant, is calculated in the s domain from the feedback error as follow:

$$k_P + k_I \frac{1}{s} + sk_D \tag{3.101}$$

Increasing the proportional gain (k_p) will reduce the rise time but never eliminates the steady-state error. Introducing the integral gain (k_i) will help to reduce the steady state error, but it makes the system very sluggish (and oscillatory), thereby making the transient response very poor. The effect of adding a derivative gain (k_d) is increase in the stability of the system, reduction in the overshoot, and improvement in the transient response (but no effect on the steady-state error). The general effect of each controller parameter (k_p, k_i, k_d) independently on a closed loop feedback system have been summarized in Table 3.11.

Table 3.11 Effects of the parameters Kp, Ki, Kd on closed loop system [52]

CL response	Rise time	Overshoot	Settling time	S-s error
k_p	decrease	increase	small change	decrease
k_i	decrease	increase	increase	decrease
k_d	small change	decrease	decrease	no change

Based on the Equations (3.40) the dynamic of IM can be described as:

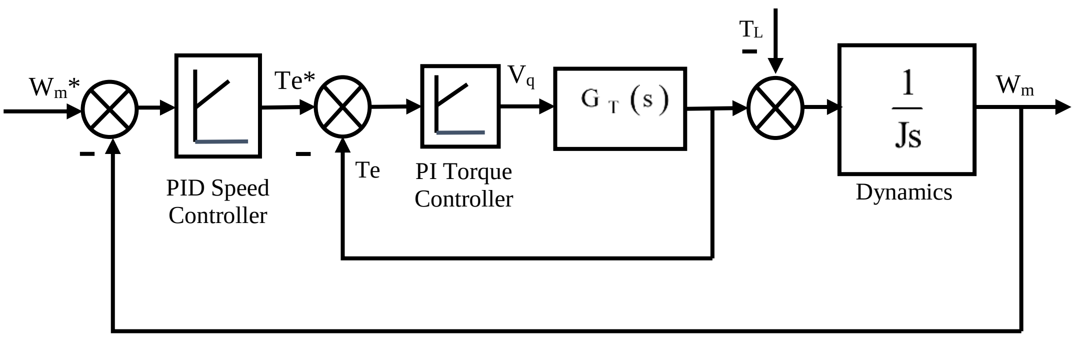

$$\frac{d\omega_r}{dt} = \frac{1}{J}\left(T_e - T_L\right) \tag{3.102}$$

Figure 3.26 Block diagram of the speed control loop

In DTC method the speed is controlled through the torque which means the output of PID controller is input to the torque system transfer function which is shown in Figure 3.26. where $G_T(s)$ is the open loop torque transfer function from Equation (3.100). MATLAB/Simulink representation of closed loop PID speed control is shown in Figure 3.27.

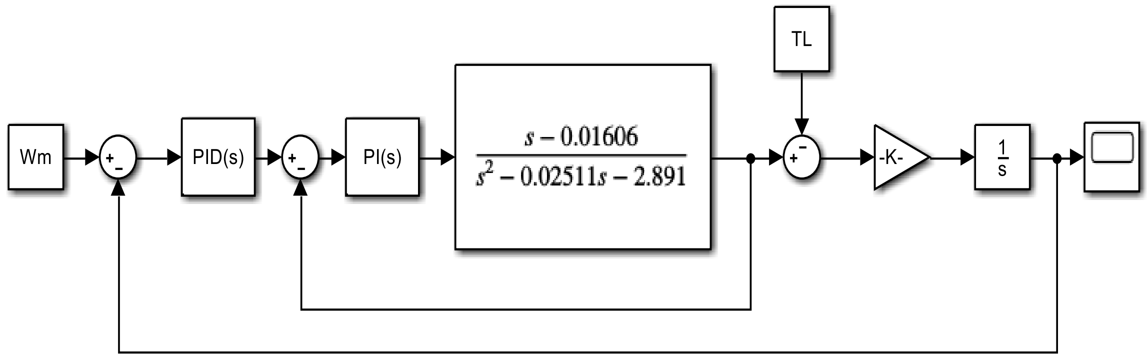

Figure 3.27 MATLAB representation of linear model closed loop PID speed control

The closed loop torque transfer function using the kp and kd value from torque controller design can be obtained as: -

$$\frac{T_e}{T_e^*} = G_c(s) \times G_T(s) \tag{3. 103}$$

$$G_{Tc}(s) = \frac{T_e}{T_e^*} = \frac{89.9s^2 + 1120s - 18.01}{s^3 + 89.87s^2 + 1117s - 18.01} \tag{3. 104}$$

Therefore, the closed loop speed control transfer function in Figure 3.27 will be reduced to Figure 3.28.

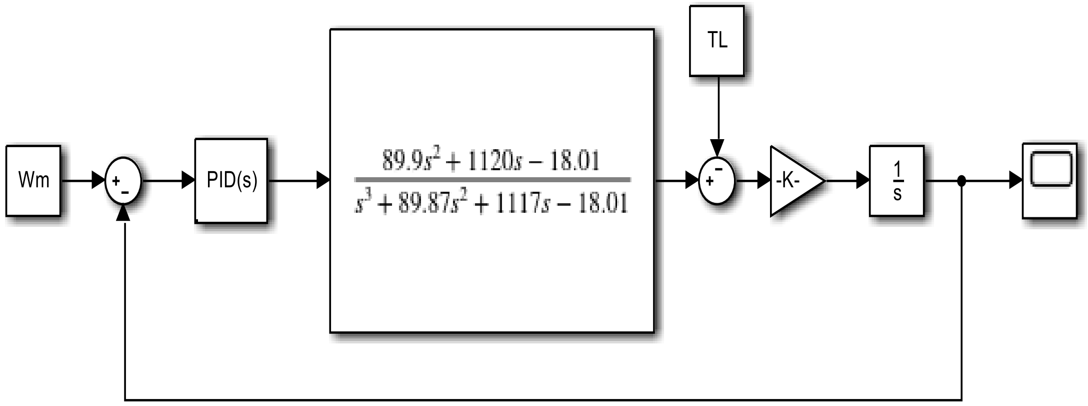

Figure 3.28 MATLAB representation of reduced linear model closed loop PID speed control

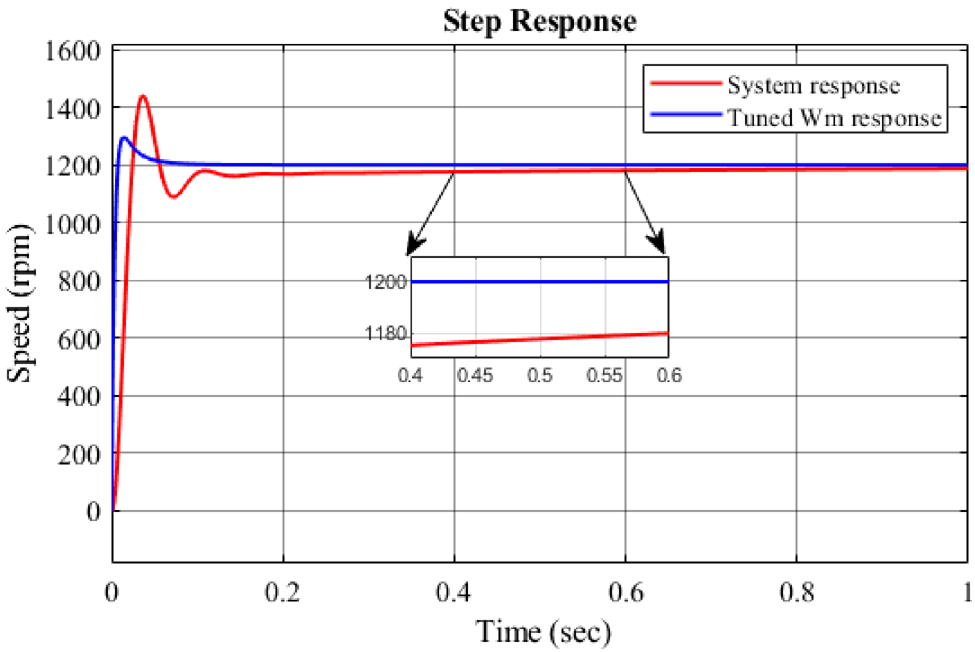

Figure 3.29 PID speed control step response

Using a PID tuner tool the optimal PID gains are obtained. Figure 3.29 shows the step response of the tuned and the system. With the PI controller parameters setting as: kp = 4.625, ki = 121.229 and kd=0.03612 the tuned response has a settling time of 0.0441, a rise time of 0.00499, and an overshoot of 8.78% trying to decrease the overshoot by making the transient behavior of the plant more robust will increase the steady state error.

Table 3.12 summarizes the parameter Kp, Ki, and Kd values for flux and torque PI controller and PID speed controller from the tuner response.

Table 3.12 Summery of controller design

Controller gain	Flux	Torque	Speed
Kp	134.6	88.5054	4.625
Ki	5024	1121.3	121.229
Kd	-	-	0.03612

3.7.2 Fuzzy Logic based Speed Controller

In this work, Mamdani type fuzzy logic controller is applied in the speed control loop and it produces the torque reference. As compared to a PID controller, FLC does not need an accurate mathematical model of the system and it will adjust itself corresponding to the situation. FLC has human-like thinking to produce output from the known values of input and it eliminates control issues of a conventional controller for IM. FLC is unique control techniques for uncertain and inaccurate nonlinear systems [53].

FLC consists of fuzzification of input variables, fuzzy inference system for the mapping of input and output variables and defuzzification of output variables as shown in Figure 3.30. Triangular membership function involves less computation, simple and easy to implement. Therefore, the triangular membership function has been used for input/output variables. The membership functions are over lapped to get out of discontinuity with respect to the minor changes in the input/output functions.

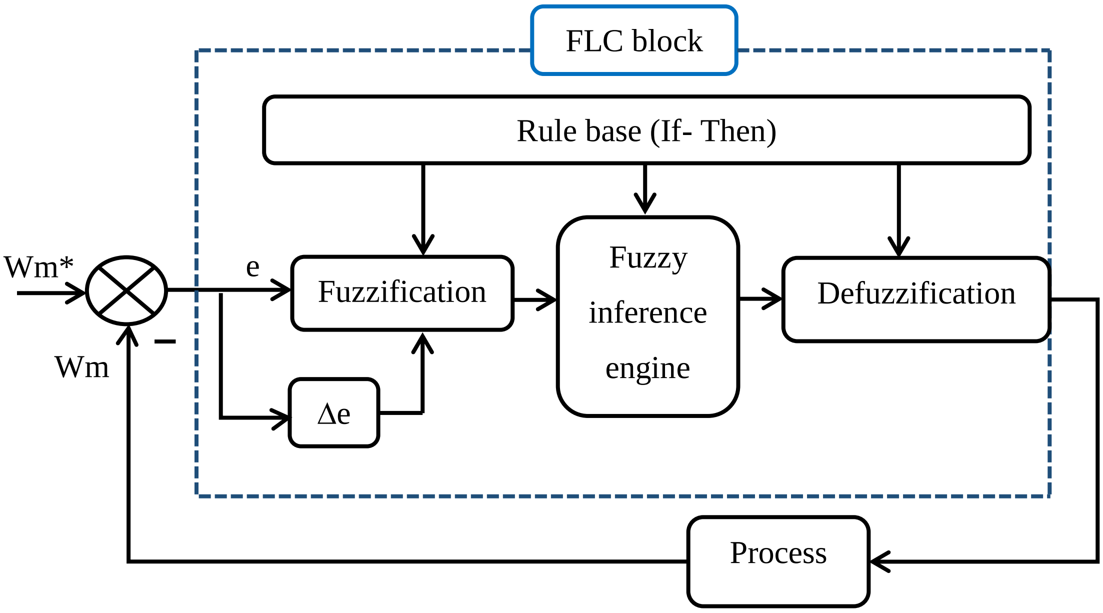

Figure 3.30 Fuzzy logic controller block diagram

3.7.2.1 Fuzzification of Input Variables

In fuzzification process a crisp input value converted to a fuzzy value that is performed by the use of the information in the knowledge base. Seven linguistic variables, NB (Negative Big), NM (Negative Medium), NS (Negative Small), ZE (Zero), PS (Positive Small), PM (Positive Medium) and PB (Positive Big) are selected for each input fuzzy set as given in Figure 3.31 and Figure 3.32.

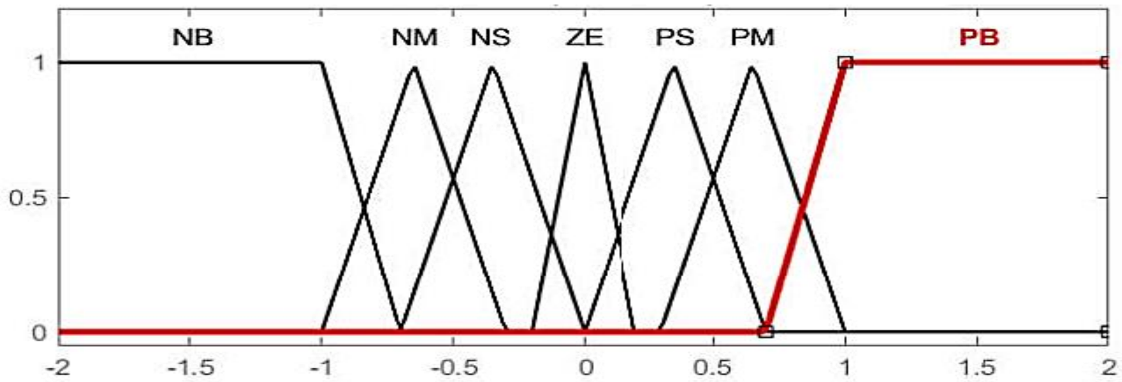

Figure 3.31 Input error membership function

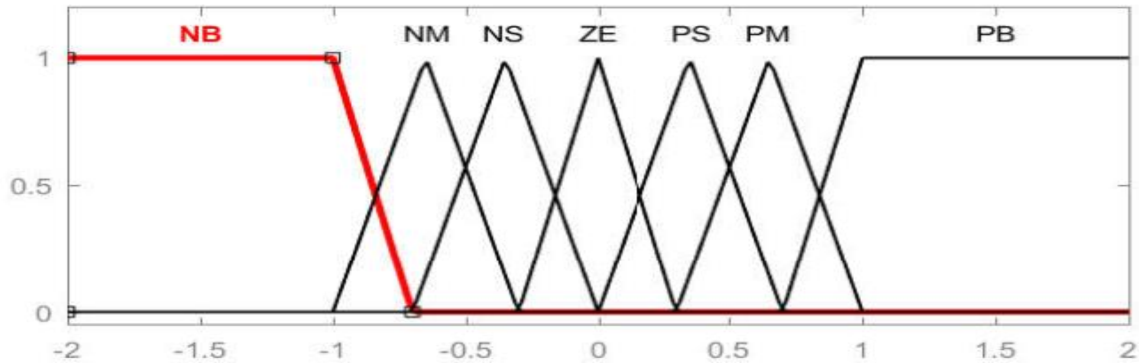

Figure 3.32 Input change in error membership function

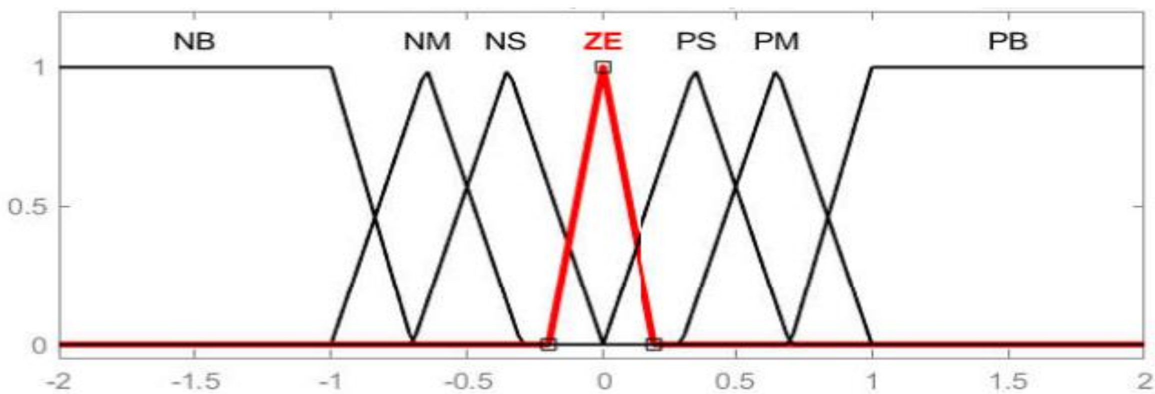

Figure 3.33 Output membership function

Seven variables are introduced in the output fuzzy set as given in Figure 3.33. These are NB (Negative Big), NM (Negative Medium), NS (Negative Small), ZE (Zero), PS (Positive Small), PM (Positive Medium), and PB (Positive Big).

3.7.2.2 Fuzzy Inference Engine

After fuzzification of input/outputs variables, the fuzzy rule base is formed as given in Table 3.13. The Mamdani type fuzzy inference system has been used because of its intuitive property. Totally, 49 rule bases (7 x 7 = 49) are generated with fuzzy If-Then rules.

Table 3.13 Fuzzy rule

e/Δe	NB	NM	NS	ZE	PS	PM	PB
NB	NB	NB	NB	NB	NM	NS	ZE
NM	NB	NB	NB	NM	NS	ZE	PS
NS	NB	NB	NM	NS	ZE	PS	PM
ZE	NB	NM	NS	ZE	PS	PM	PB
PS	NM	NS	ZE	PS	PM	PB	PB
PM	NS	ZE	PS	PM	PB	PB	PB
PB	ZE	PS	PM	PB	PB	PB	PB

3.7.2.3 Defuzzification

In defuzzification step the resultant fuzzy values transform into numerical values (crisp output). Based on the rule base output variables are selected for defuzzification. The centroid type defuzzification method is used in this proposed approach. A graphic view of output response and rule viewer according to the inputs are shown in Figure 3.34 and Figure 3.35 respectively. The entire output surface of the system, that is, the entire span of the output set based on the entire span of the input set is shown in Figure 3.34.

The rule viewer in Figure 3.35 shows the entire fuzzy inference process at once it plots every part of every rule. The shape of certain membership functions influences the overall result. For a given error and change in error membership function it yields the appropriate output membership function value based on the rule base and defuzzification process.

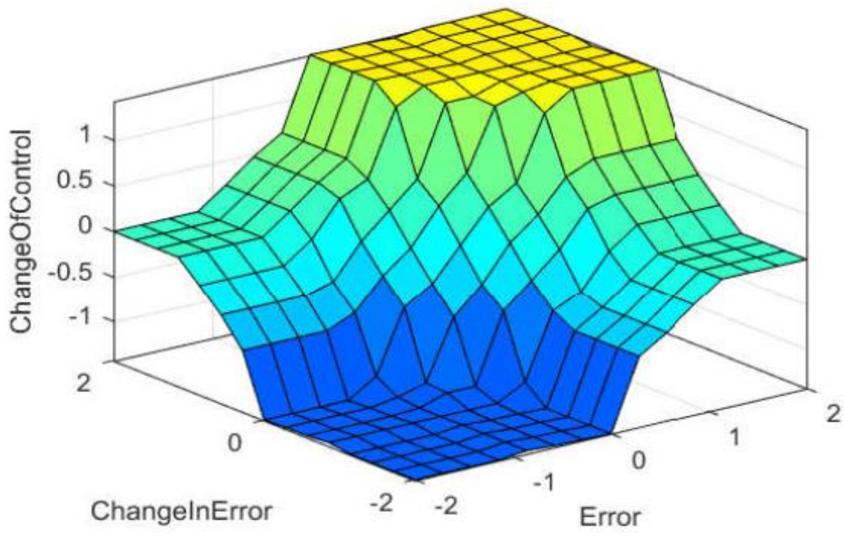

Figure 3.34 Control surface view

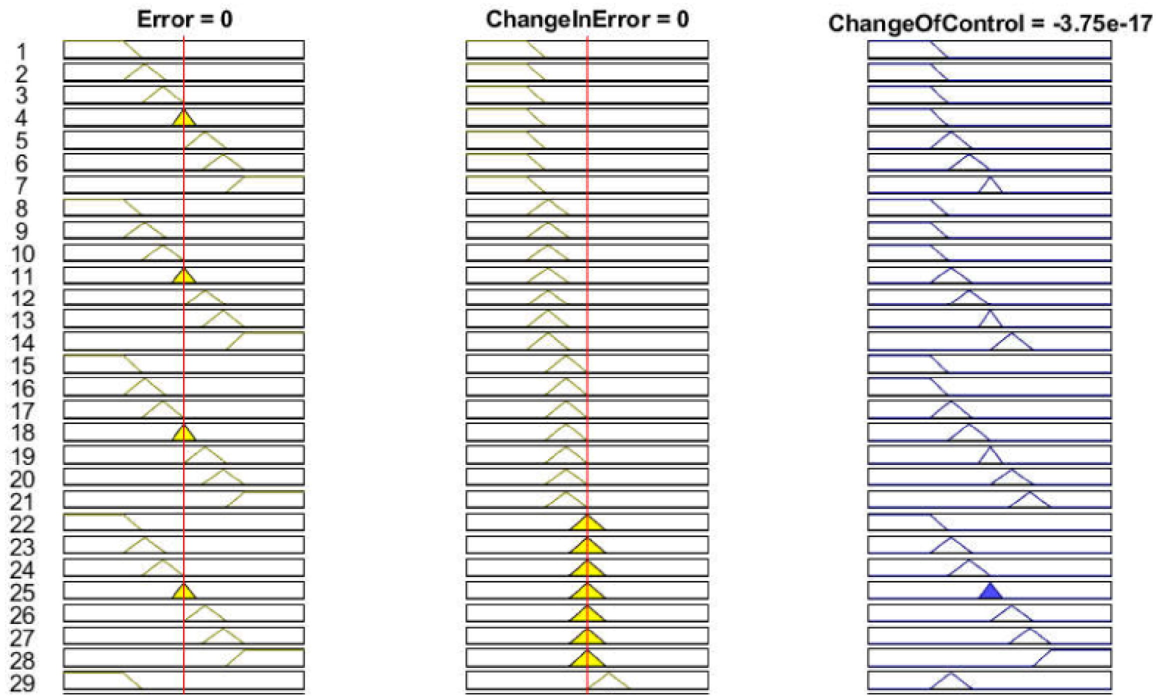

Figure 3.35 Control rule view

CHAPTER 4

RESULT AND DISCUSSION

4.1 Chapter Overview

This chapter explains the simulation result and analysis of the proposed control system that performed for the same value of the system under the study. The system is simulated with different load torque and set speeds, by using the speed controller parameters values specified in chapter three. The proposed PID and fuzzy speed controller are compared. The motor electromagnetic torque and flux are compared with their estimated values.

4.2 SVM results

The first thing in generating the modulating voltage signals Va, Vb, and Vc for SVM is transformation to obtain the magnitude and the position of the reference voltage. Usually Clarke transformation which transforms three phase voltage to two phase voltage is used but here in DTC-SVM technique the input to the SVM is Vd, Vq and the stator flux vector position therefore instead of Clarke transformation inverse Park transformation is used. The modulating signal in Figure 4.1 generated from SVM algorithm compared with the carrier signal and the gating pulse in Figure 4.2 generated in order to switch the IGBT so that the required 3 phase voltage that drive the motor can be generated.

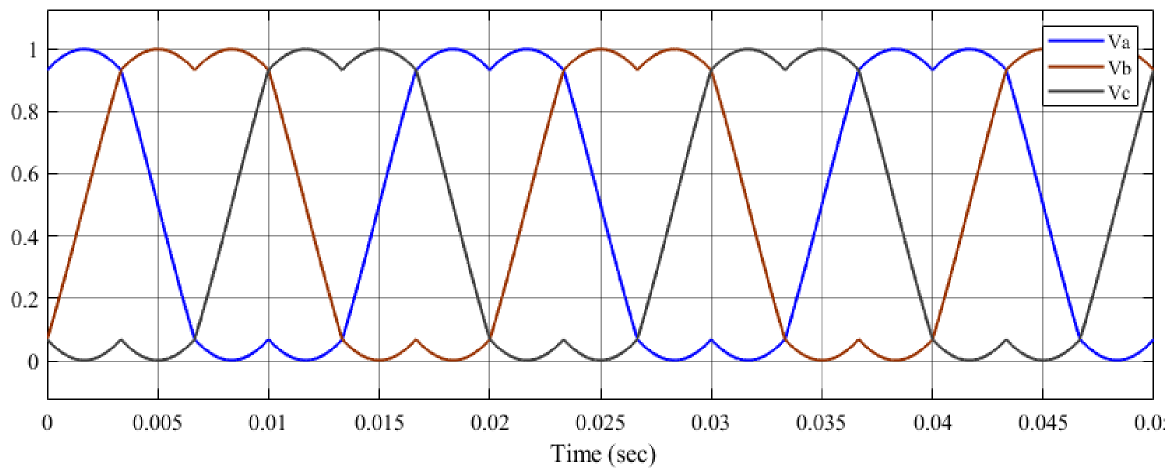

Figure 4.1 Generated SVPWM signal.

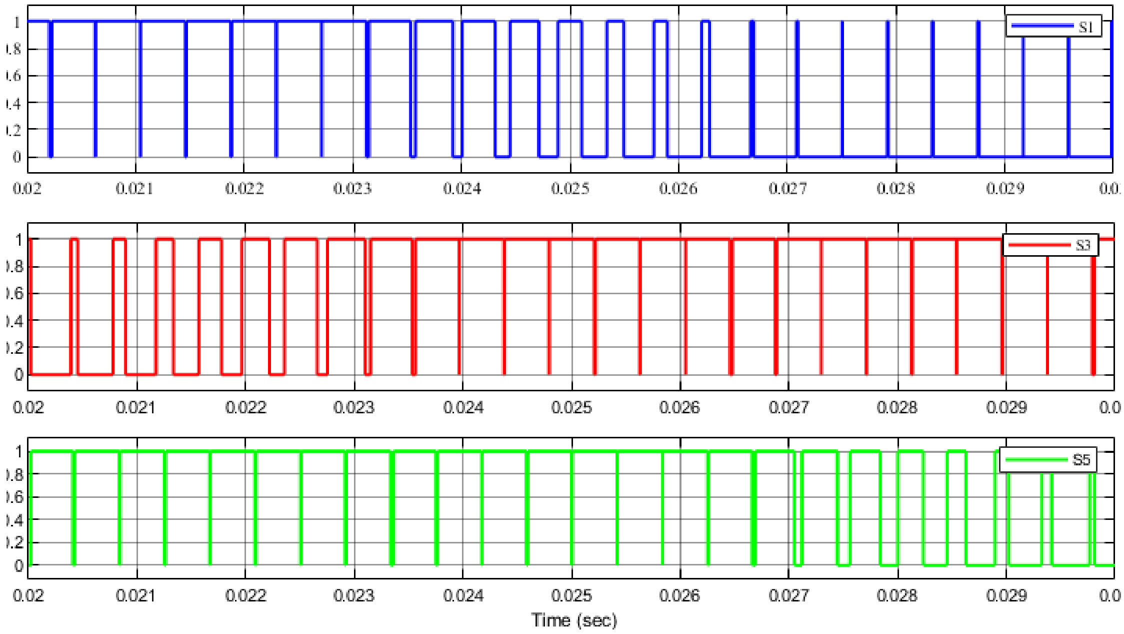

Figure 4.2 Generated gate pulse

The gating pulses for switch 1, 3 and 5 are shown in Figure 4.2 the remaining switches S4, S6 and S2 have a gating pulse of exactly opposite to S1, S3 and S5 respectively to avoid the switching of IGBT's in the same leg at the same time so that circuit will not be shorted.

4.3 SVM-DTC Based Fuzzy Logic Speed Controller Response

In this work fuzzy speed controller with PI flux and torque controller is proposed. The following result is obtained with proposed speed controller technique for different set speed MATLAB/Simulink model of the proposed drive control system is shown in Appendix B.1.

4.3.1 Motor Speed Response for a Load Torque of 48.5 Nm

The reference and actual speed waveform are shown in Figure 4.3 The system is simulated under different speed setpoint values because the vehicle moves at different speed. From Figure 4.3 it can be observed that the proposed speed controller has a better dynamic response (settling time, rise time, peak time, overshoot, and steady state error) of the IM drive as reference speed is tracked by actual speed only at 0.05 sec when compared with PID speed controller which takes 0.3 sec which is shown in Figure 4.12. The result also shows that the speed overshoot is 0%.

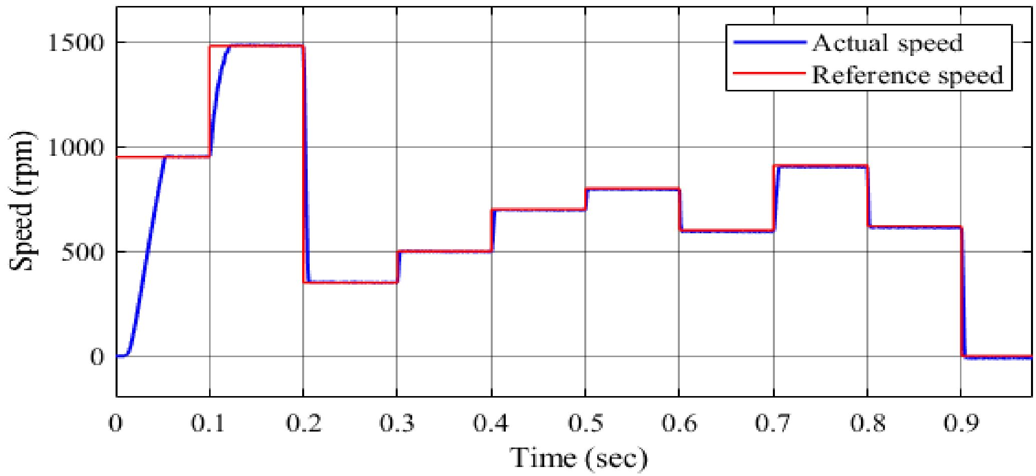

Figure 4.3 The speed response of IM with the proposed controller at 48.5Nm load torque

4.3.2 IM Stator Current Result

Figures 4.4, illustrate stator current of IM, oscillations appear at each period corresponding to changes in speed of the motor but it takes much less time to settle down at steady value.

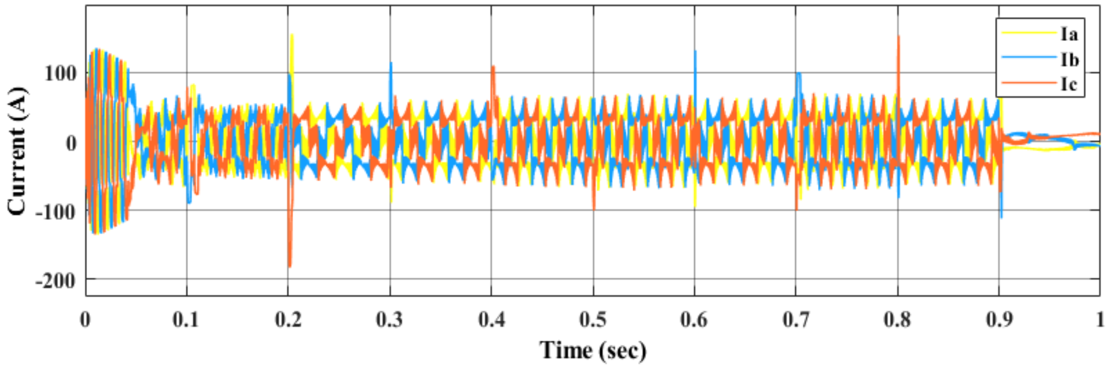

Figure 4.4 Stator current of IM during each speed change

Figures 4.5, illustrate the stator voltage of IM

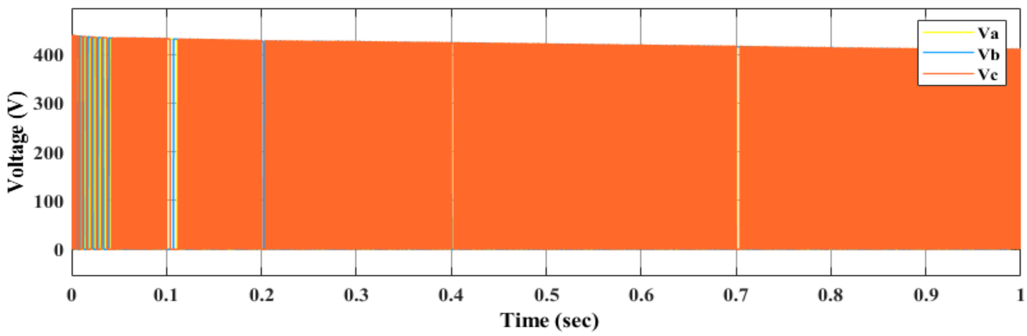

Figure 4.5 Stator voltage of IM during each speed change

4.3.3 Electromagnetic Torque of the Motor

Figure 4.6 shows the electromagnetic torque response with PI torque and flux controller and fuzzy speed controller, there are variations in the torque that corresponds to the variation of the reference speed at different times because the motor needs more toque to accelerate but once the motor reaches its new speed the torque will back off to its original value. Torque ripples in steady state response are about ±2 Nm. From Figure 4.6 it can be observed that throughout the speed range the torque developed is kept constant. The system is simulated with a load torque of 48.5 Nm for different speed setpoints below its base speed. Hence in speed versus torque characteristics below base speed, the torque is constant.

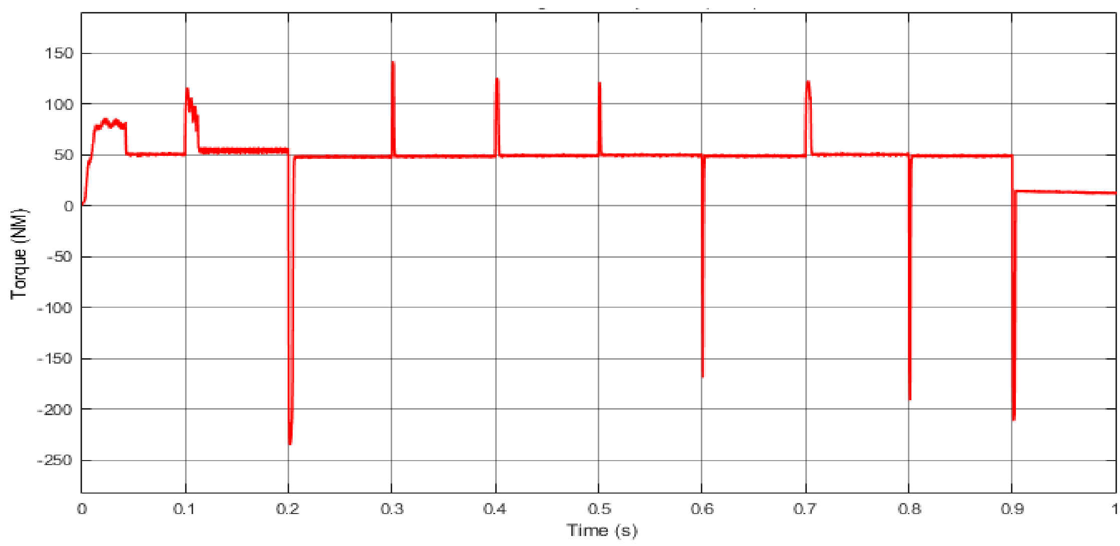

Figure 4.6 The electromagnetic torque of the motor

4.3.4 Output Power of the Motor

Figure 4.5 depicts the result of the output power of the IM with the proposed controller. The product of the speed and electromagnetic torque of the motor results in output power for the corresponding speed and electromagnetic torque. For instance, when the speed of the motor equals to 500 rpm (52.33 rad/sec) from 0.3 sec to 0.4 sec as shown in Figure 4.3 with a load torque of 48.5 Nm then the output power is 2538 W. The system is simulated about a constant load for different speed setpoints below its base speed. Hence in the speed versus torque characteristics curve below base speed, the power is variable. The result also shows the power is variable below the rated speed.

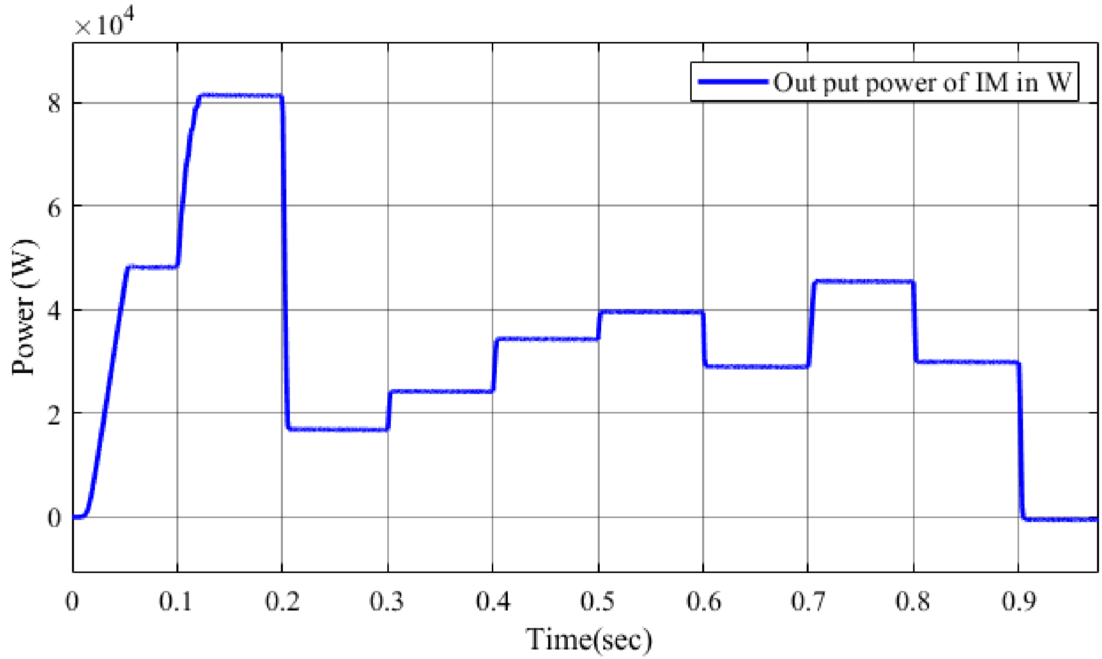

Figure 4.5 The power output of IM motor under the proposed drive system at Tl=48.5Nm

4.3.5 Estimated and Set Electromagnetic Torque

The estimation algorithm is tested in various speed regions. As shown in Figure 4.7, the estimator has seen to work well under various circumstances. It can be seen from the figure the estimated motor torque and the actual electromagnetic torque of the motor is equal with a torque pulsation of ±2 Nm.

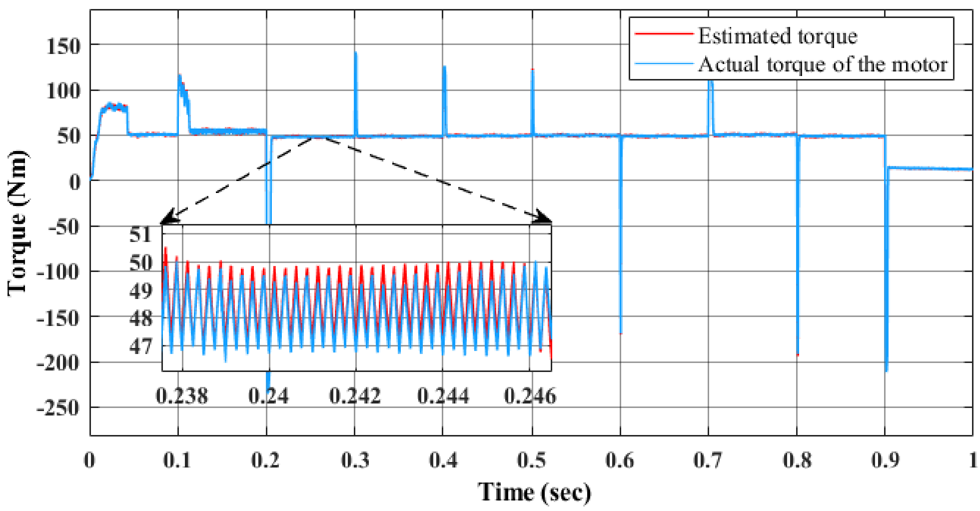

Figure 4.7 Estimated and actual torque of the motor

4.3.6 Estimated and Set Motor Flux

Figure 4.8 shows the stator flux, at the beginning of the operation the amplitude of the flux increases. Then, the amplitude remains constant and equal to its reference value with a low ripple, thus revealing a correct regulation of the flux decoupled from that of the torque during the steady state.

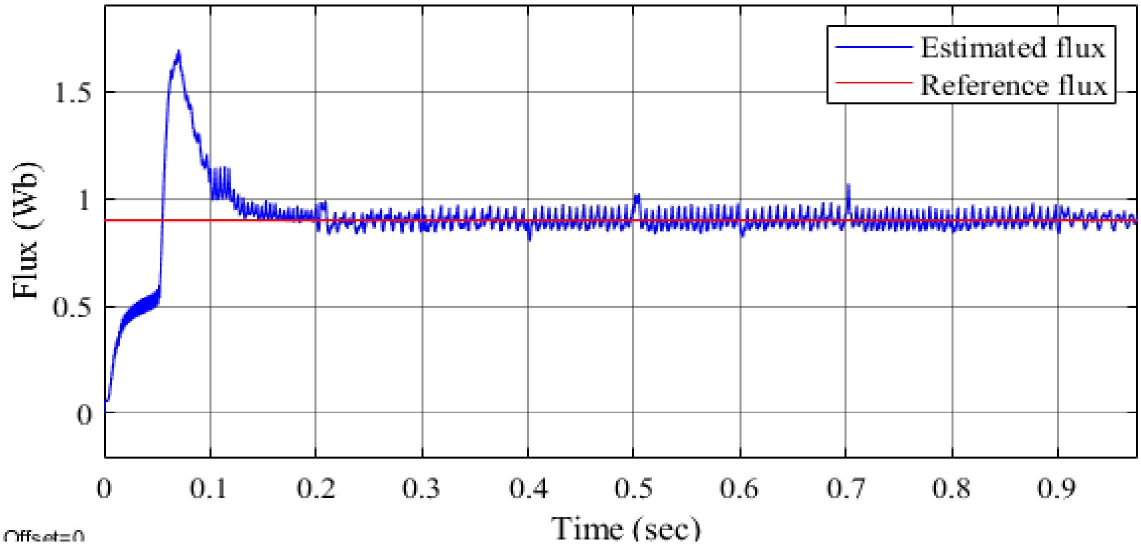

Figure 4.8 Estimated and reference stator flux

4.3.7 Stator Flux Response

Stator flux waveforms are shown in Figure 4.9. The waveforms are in quadrature nature with respect to each other and sinusoidal. The stator flux maintained constant irrespective of the change speed.

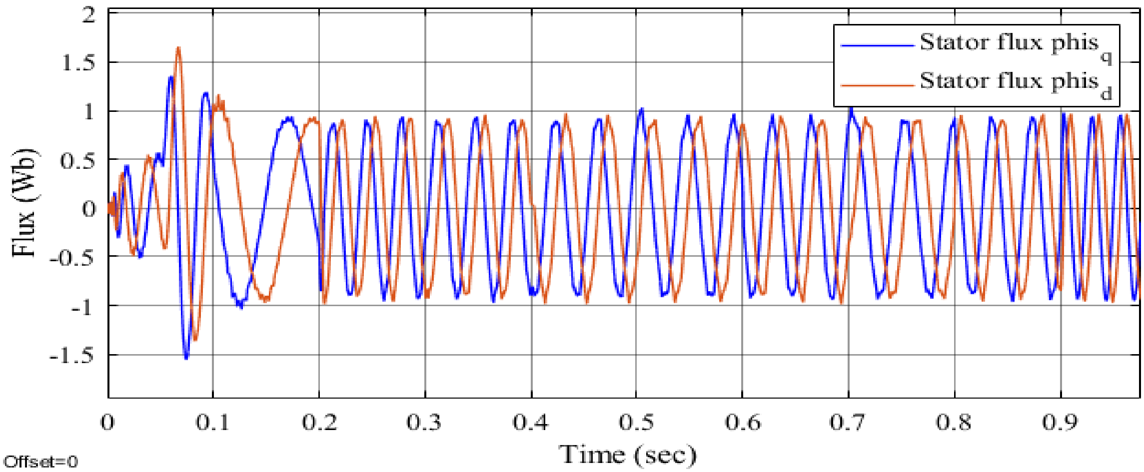

Figure 4.9 Stator flux magnitude

4.3.8 Vehicle Speed vs Battery State of Charge

Figure 4.10 and Figure 4.11 shows vehicle speed in km/hr and battery state of charge respectively. The speed of the vehicle follows its command speed with a better dynamic performance. In addition, the state of charging in the range of the different motor speed performance is also shown in this Figure 4.11. Accordingly, in the case when the speed of the motor is increasing the discharging rate of the battery also increases. Whenever the vehicle is accelerating the discharging rate of the battery increases but when the vehicle is at rest or when it stops moving which is from 0.9sec to 1sec the battery stops discharging.

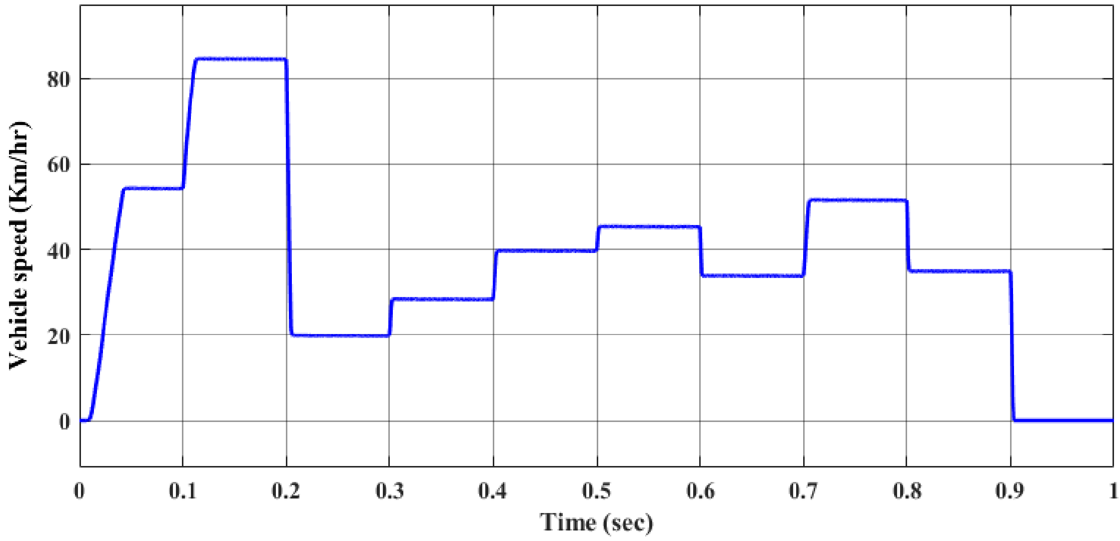

Figure 4.10 Vehicle speed in km/hr

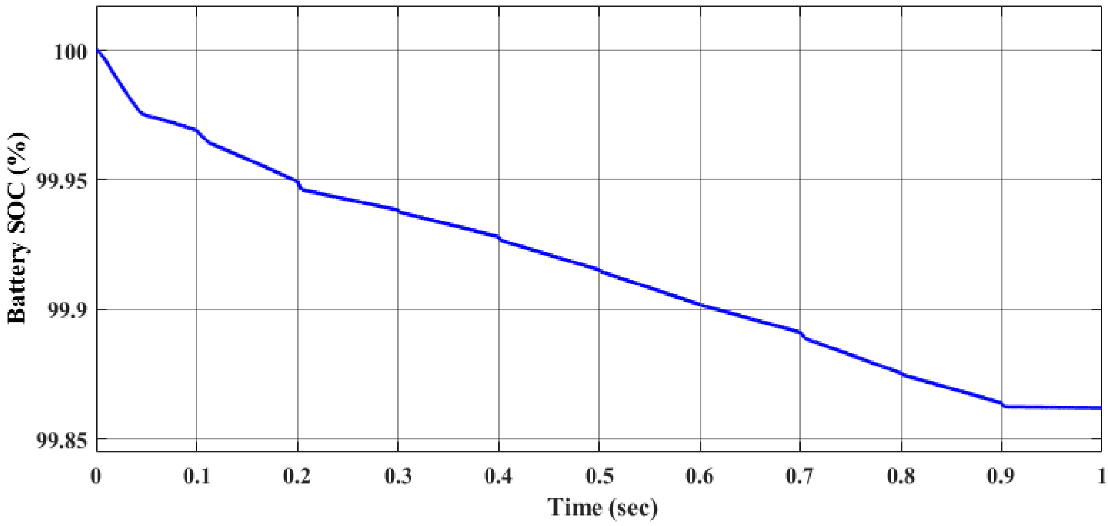

Figure 4.11 Battery state of charge in percent

4.4 SVM-DTC Based PID Speed Controller Response

Figure 4.12 shows the actual and reference speed of the IM using a PID controller at 48.5 Nm load torque. Although, the reference speed is tracked by the actual speed it can be seen clearly in the Figure 4.12 that it has a very poor transient response since it has a high overshoot of 48.564% and the time taken by actual speed to track reference is 0.3sec. The settling time of the proposed fuzzy controller is less than PID controller. The fuzzy speed controller has no overshoot. The electromagnetic torque of the motor in Figure 4.13 simulated under a load torque of 48.5Nm with a PID speed controller. The result shows that the electromagnetic steady state response have above ±10 Nm torque pulsation.

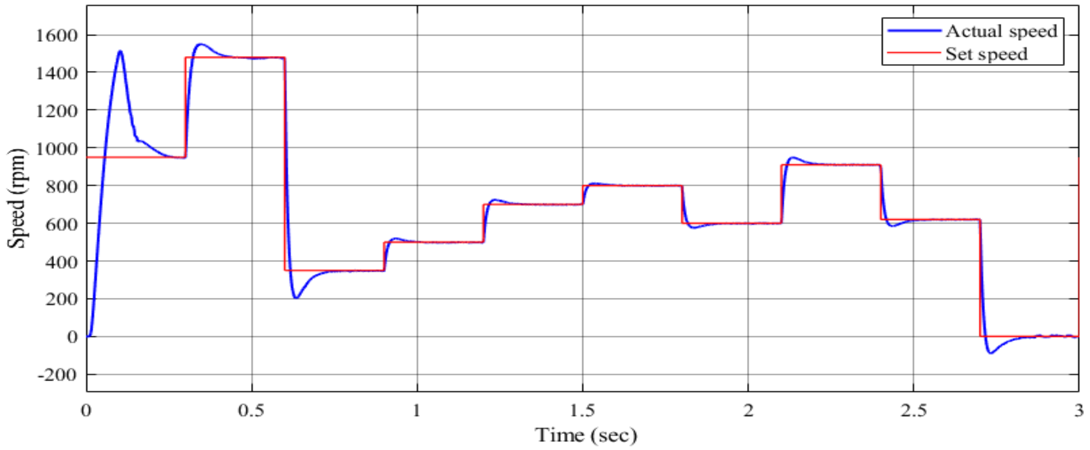

Figure 4.12 The speed response of IM using a PID controller at 48.5 Nm load torque

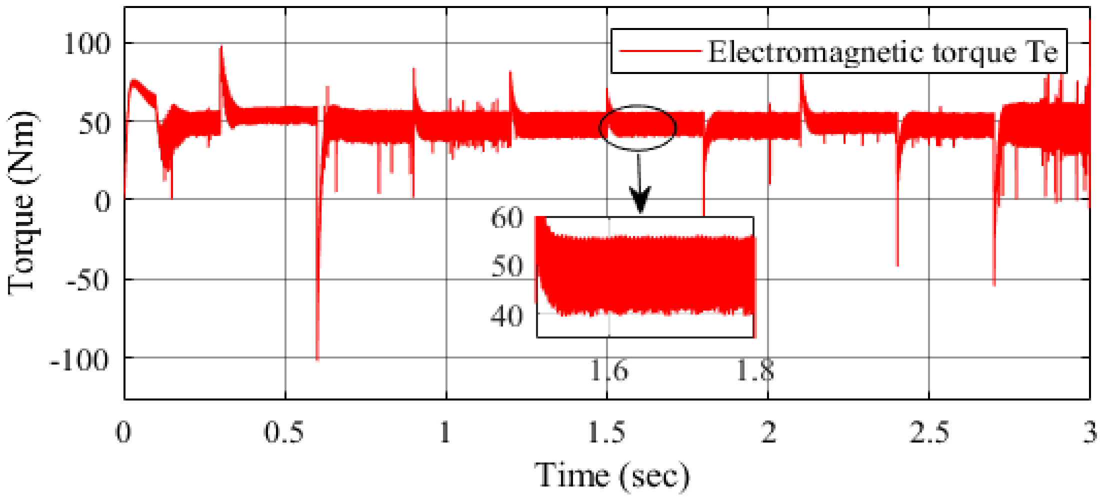

Figure 4.13 Electromagnetic torque response of IM using a PID controller at 48.5 Nm load torque

4.5 Performance Comparison of Speed Controllers

4.5.1 Fuzzy Speed Controller Response at No Load

At first the motor is at rest and then it is made to run at 500rpm for about 0.05 sec. The motor further accelerates to 1000 rpm before decelerating to 750 rpm. From the response of the actual motor speed during all this time interval it can be concluded that the controller has very good transient and steady state response at no load. The electromagnetic torque of the motor in Figure 4.15 also have less pulsation ±1.5 Nm when it is compared with PID controller result at no load.

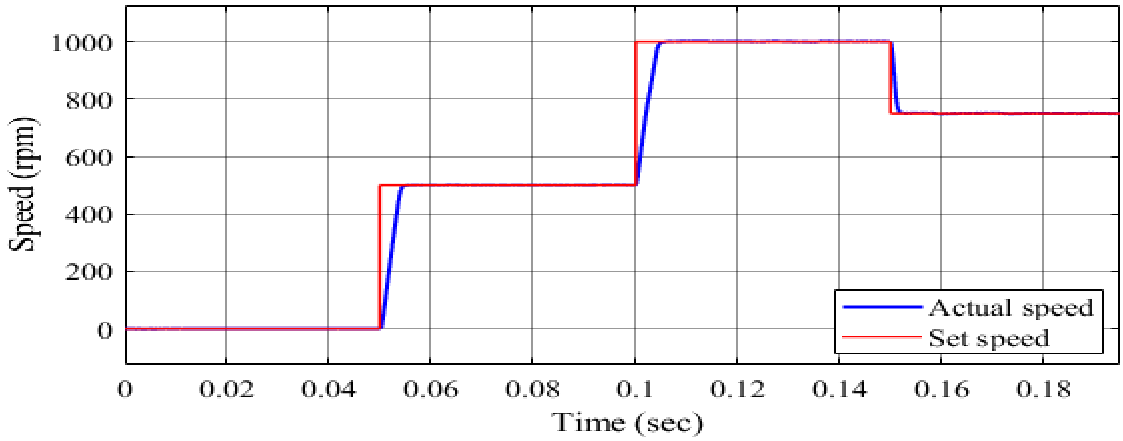

Figure 4.14 The speed response of IM using a Fuzzy controller at no load torque

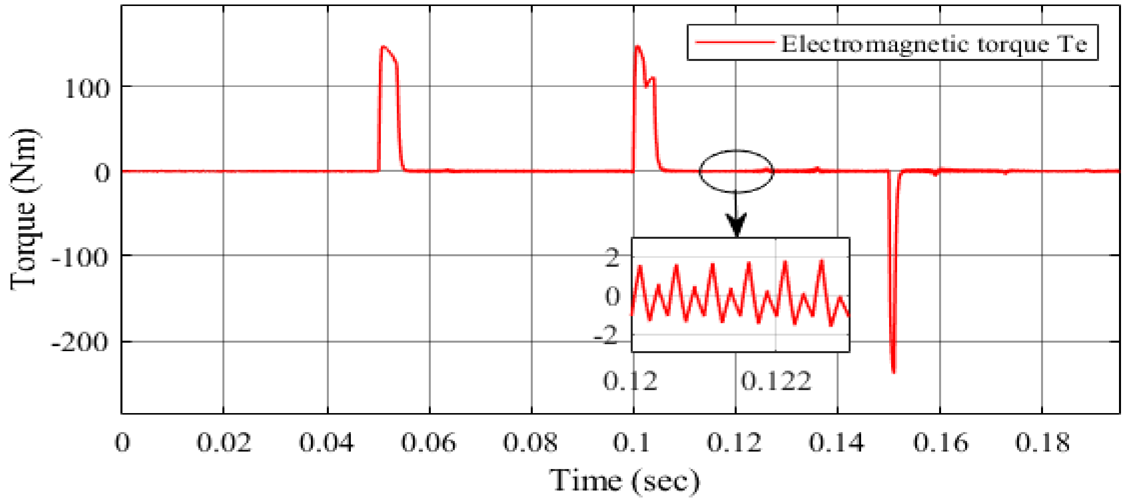

Figure 4.15 Electromagnetic torque response of IM using a fuzzy controller at no load

4.5.2 PID Speed Controller Response at No Load

The speed and torque response of the PID controller at no load is shown in Figure 4.16 and Figure 4.17 respectively. Initially the motor is at rest and made to run at 500 rpm for about 0.3 sec after that it accelerates to 1000 rpm and finally riches 750 rpm during this speed change the controller have a percentage overshoot. The electromagnetic torque of the motor is shown in Figure 4.17 and it shows ±3 Nm pulsating.

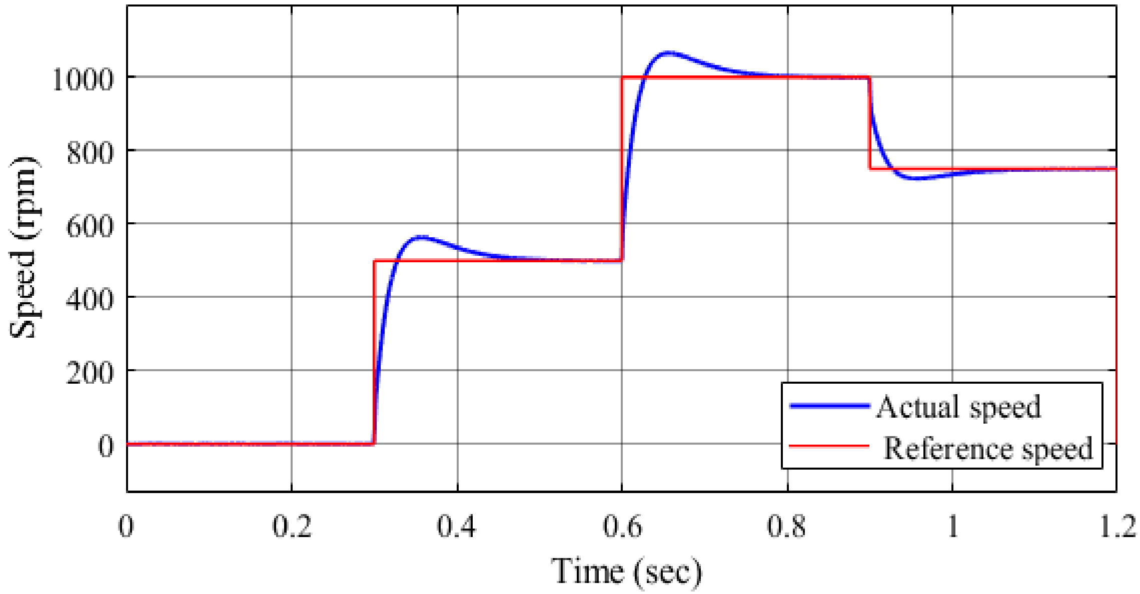

Figure 4.16 The speed response of IM using a PID controller at no load

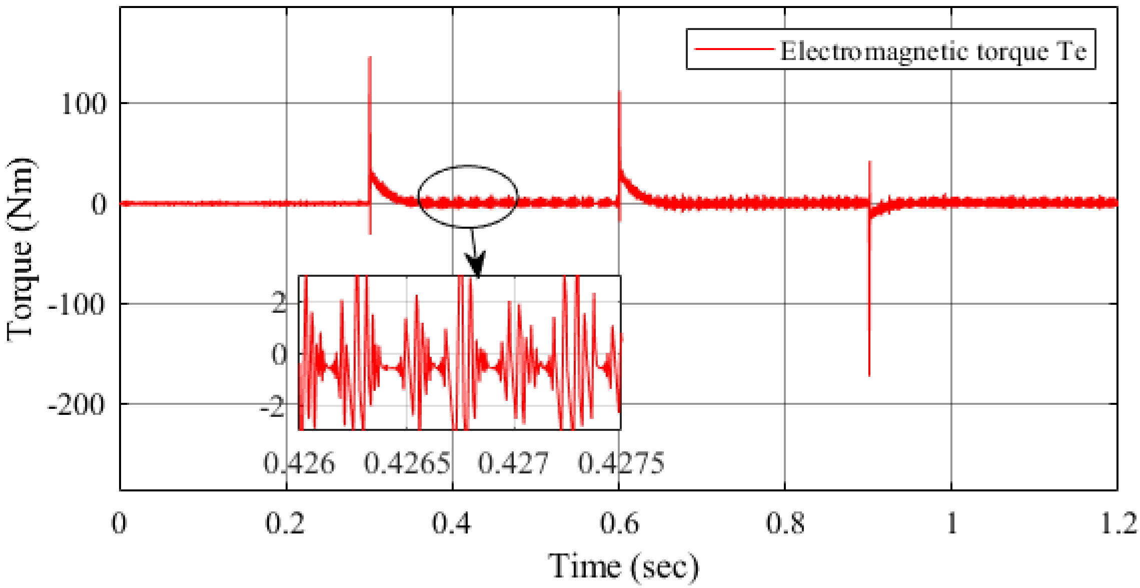

Figure 4.17 The torque response of IM using a PID controller at no load

4.5.3 Fuzzy Speed Controller Responses for Ramp Input

Figure 4.18 and 4.19 shows the speed and electromagnetic torque response of the motor for a ramp speed input respectively. From 0 to 0.4 sec the motor is accelerating from 0 rpm to 1200 rpm during this time the motor torque has a value of 3Nm. Once the speed reaches 1200 rpm it gets constant for 0.4 sec. From 0.8 sec -1.2 sec the motor is decelerating resulting in negative torque.

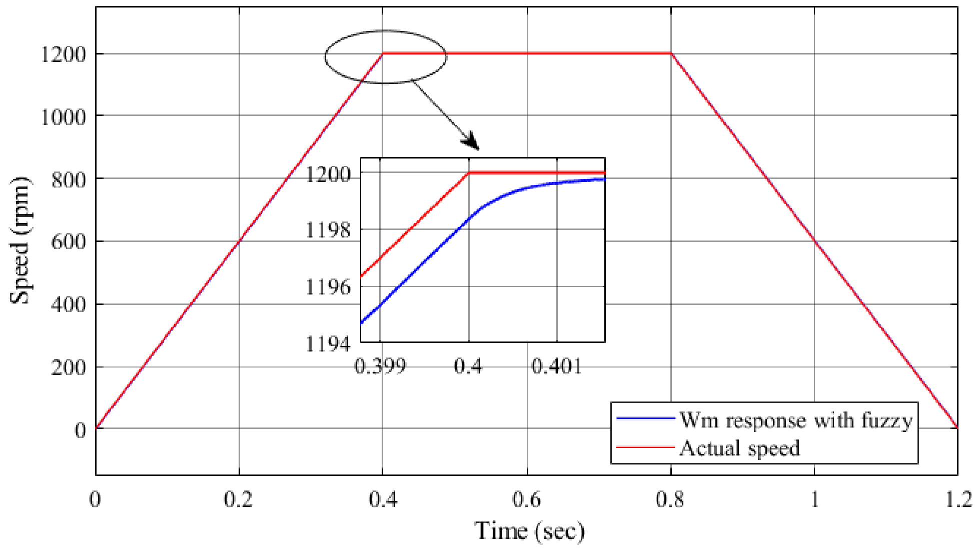

Figure 4.18 The speed response of IM using a fuzzy controller at no load for a ramp input

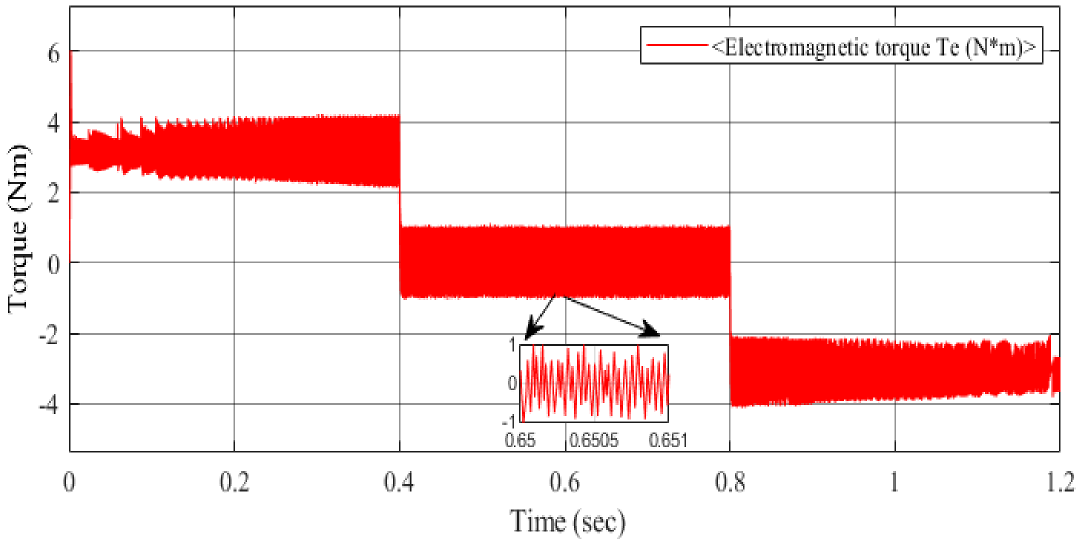

Figure 4.19 The torque response of IM using a fuzzy controller at no load for a ramp input

The performance of the induction motor is compared for PID and fuzzy speed controller at no load and at load torque of 48.5 Nm. Table 4.1 summarizes the performance comparison of PID and fuzzy controller considering the transient and steady state response.

Table 4.1 Speed controller comparison of performance parameter results

Performance parameter	Speed Controller			
	PID		Fuzzy	
	At no load	At 48.5Nm	At no load	At 48.5Nm
Rise time in sec	0.0268	0.0348	0.02451	0.035528
Settling time in sec	0.255	0.3	0.026	0.05
Peak time in sec	0.08	0.1	0	0
Percentage overshoot	21.34%	48.564%	0	0
Steady state error	0	0	0	0

Figure 4.20 demonstrates the speed dynamic performance parameters (settling, rise, and peak times) graphical results of PID and fuzzy speed controllers under a load torque of 48.5Nm.

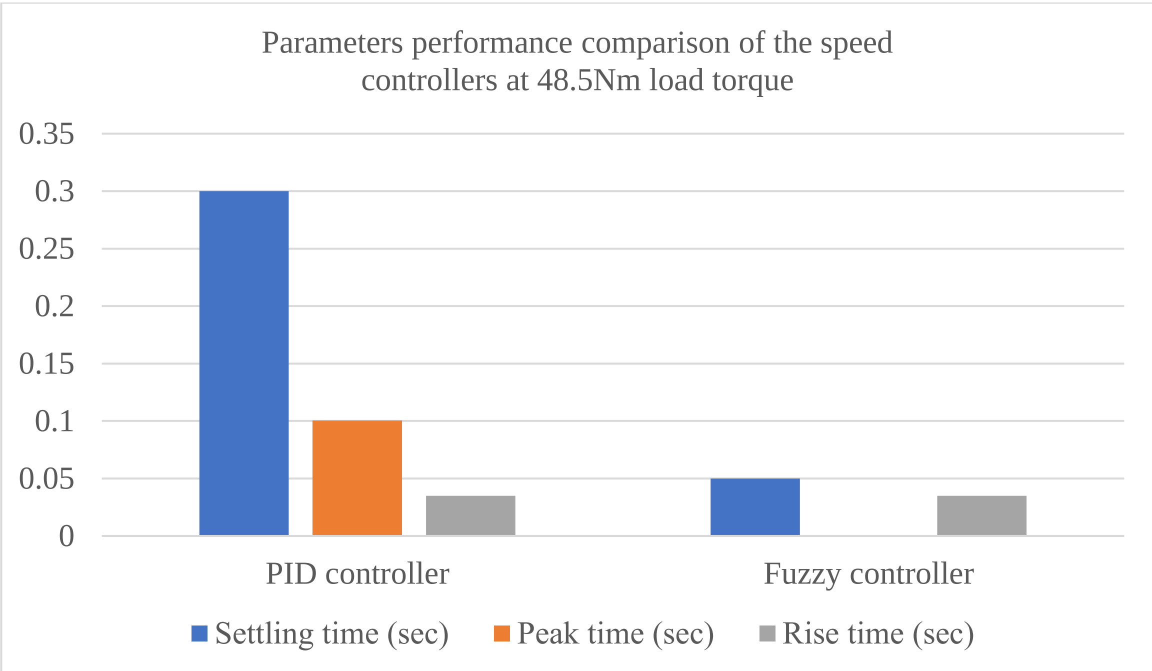

Figure 4.20 Graphical representation of speed controller parameter result

From the graph in Figure 4.20 and from the Table 4.1 it can be concluded that the fuzzy speed controller has better performance parameters than PID controller. Therefore, the proposed fuzzy controller enhanced the direct torque control performance induction motor. So, the proposed speed controller is better for controlling the speed of motor for the proposed electric vehicle.

CHAPTER FIVE

CONCLUSION AND RECOMMENDATION

5.1 Conclusion

In internal combustion engines, fuel is burned inside the cylinder therefore it emits carbon dioxide which is very harmful to the environment. So, fuel engine cars are highly characterized as one of the major polluting sources of the environment. Considering the number of fuel-based vehicles in the planet we live in, it is easy to observe how badly human beings are treating the environment. Electric vehicles are a solution to the environmental problems caused by vehicles with internal combustion engines. The advantages of EVs include energy efficiency, no pollution or emits no greenhouse gas, and it uses renewable energy source. Different researchers have been researching about different electric motors and their drive that are used in electric vehicles. The motor is the main part of the EV. The most important requirements of the EV motors are high efficiency, high dynamic response (fast torque and speed response), high torque at low speeds, high torque/power to size ratio, low production cost, and many more others. The rapid development in the field of power electronics and control techniques has created a space for various types of electric motors to be used in electric vehicles. Induction motor is favored due to its rigidness, high reliability, mature manufacturing and power converter technologies. Induction motor drives are well suited for cost sensitive mass production EV applications.

The control techniques of induction motor were presented in Chapter 2: Scaler and vector control. Scaler control only controls the magnitude of a variable. However, an induction motor has a rotating magnetic field produced by three magnetic fields therefore, the position of those fluxes should have been controlled this drawback can be eliminated by vector control method. A vector control is divided in to two FOC and DTC. FOC implementation depends critically on a very accurate coordinate transformations and flux angle estimation, which are complex and depending on the variation of machine parameters. Thus, DTC based direct flux and torque control with space vector modulation (DTC-SVM) were analyzed and investigated in simulation. The flux and torque are estimated and the result shows that the estimated torque and flux are almost the same with the motor flux and torque. The PID gains Kp, Ki, and Kd are obtained from flux, voltage and torque equation of the induction motor.

The proposed fuzzy speed controller based SVM-DTC system was implemented in MATLAB Simulink. Then, the output performance of the induction motor was analyzed during the time of speed variation. From the performance analysis, it is been found that the proposed fuzzy controller-based speed control provides a better performance than a PID speed controller. Hence, the proposed fuzzy controller based SVM-DTC method is better for controlling the speed of an induction motor for the proposed vehicle.

5.2 Recommendation

The IM drive system can be further improved by adding the application of four quadrant DC-DC drive for fast dynamic braking operation. Instead of taking the rotor resistance (Rs) value from the induction motor parameter it can be improved by applying an estimation mechanism. The torque ripple can be further reduced by using an intelligent control method for the torque and flux pi controller that are used in the proposed DTC-SVM method. Appling artificial neural network, Adaptive Neuro-Fuzzy, particle swarm optimization and other intelligent controls for the speed control also improves the steady state and transient response of the system. Furthermore, it is also recommended to practice and implement the proposed control system using real time operating systems like digital signal processor (DSP).

Acknowledgements: This research thesis was funded by Adama Science and Technology University under the grant number of **ASTU/SM-R/078/19**, Adama, Ethiopia.

REFERENCES

[1] J. Y. Yong, K. M. Tan, and N. Mithulananthan, "A review on the state-of-the-art technologies of electric vehicle, its impacts and prospects," *Elsevier*, pp. 365-385, 2015.

[2] C. C. Chan, "The rise and fall of electric vehicles in 1828-1930: lesson learned," *IEEE*, vol. 101, January 2013.

[3] Zhi Shang, "Simulation and Experiment for Induction Motor Control Strategies," Electronic Theses Dissertations, 2011.

[4] M. A. W. Begh, and H. Georg Herzog, "Comparison of Field Oriented Control and Direct Torque Control," Technical University of Munich, Germany, 2018.

[5] Bazaz, Shoeb Hussain and Mohammad Abid, "Review of Vector Control Strategies for Three Phase Induction Motor Drive," in *International Conference on Recent Developments in Control, Automation and Power Engineering (RDCAPE)*, India, 2015.

[6] I. Abdelhakim, K. Madjid, Z. Mimoune and A. Aimad, "A Comparative Study between DTC, SVM-DTC and SVM-DTC with PI Controller of Induction Motor," in *Université M'Hamed Bougara de Boumerdès,* Algeria.

[7] T. Elwert, D. Goldmann, F. Römer, M. Buchert, C. Merz, D. Schueler, and J. Sutter, "Current Developments and Challenges in the Recycling of Key Components of (Hybrid) Electric Vehicles," *Recycling,* vol. 01, pp. 25-60, October 2015.

[8] A. K. Balaji, T. Raj, F. Patel, P. and K. Soori, "Intelligent Inductive Power Transfer Systems for Electric Vehicles," in *IEEE International Conference on Emerging Technologies and Innovative Business Practices for the Transformation of*, United Arab Emirates, 2016.

[9] J. Nerg, M. Rilla, V. Ruuskanen, J. Pyrhönen, and S. Ruotsalainen, "Design of Direct-Driven Permanent Magnet Synchronous Motors for an Electric Sports Car," *IEEE,* pp. 177-182, 2012.

[10] Y.K. Chin, J. Soulard, "A Permanent Magnet Synchronous Motor for Traction Applications of Electric Vehicles," *IEEE*, 2003.

[11] C. Ulu, O. Korman, and G. Kömürgöz, "Electromagnetic and Thermal Analysis/Design of an Induction Motor for Electric Vehicles," *International Journal of Mechanical Engineering and Robotics Research*, vol. 07, no. 06, pp. 617-623, November 2018.

[12] B. Kim, J. Lee, Y. Jeong, B. Kangi, K. Kim, Y. Kim, and Y. Parki, "Development of 50kW Traction Induction Motor for Electric Vehicle (EV)," in *IEEE Vehicle Power and Propulsion Conference*, Seoul, Korea, Oct. 9-12, 2012.

[13] G. Pellegrino, A. Vagati, B. Boazzo, and P. Guglielmi, "Comparison of Induction and PM Synchronous Motor Drives for EV Application Including Design Examples," *IEEE Transactions on Industry Application*, vol. 48, no. 06, pp. 2322-2332, DECEMBER 2012.

[14] Riley,C.P. et al., "Simulation based design of reluctance motors for traction applications in hybrid and electric vehicles," in *7th IET International Conference on Power Electronics, Machines and Drives (PEMD 2014)*, 2014.

[15] Dr. K.V. Vidyanandan, "Batteries for Electric Vehicles," *International Journal of Engineering Research and Technology* , 19 November november 2019.

[16] M. Lowe, S. Tokuoka, T. Trigg and G. Gereffi, "Lithium-ion Batteries for Hybrid and All-Electric Vehicles: the U.S. Value Chain," Center on Globalization, Governance & Competitiveness, October 2010.

[17] C. Iclodean, B. Varga, N. Burnete, D. Cimerdean, and B. Jurchiș, "Comparison of Different Battery Types for Electric Vehicle," *IOP Conference Series: Materials Science and Engineering*, pp. 103 - 105, 2017.

[18] W. Cao, A. A. Shah Bukhari, and L. Aarniovuori, "Review of Electrical Motor Drives for Electric Vehicle Applications," *Mehran University Research Journal of Engineering & Technology*, vol. 38, no. 03, pp. 525-540, July 2019.

[19] X. D. Xue, K. W. E. Cheng, and N. C. Cheung, "Selection of electric motor drives for electric vechile," *International Journal of Engineering Research and Technology* .

[20] David G. Dorrell, Mircea Popescu, David A. Staton and Lyndon Evans, "Comparison of Different Motor Design Drives for Hybrid Electric Vehicles," *IEEE*, pp. 3352-3359, 2010.

[21] Luthra, Gagandeep, "comparison of characteristics of various motor drives currently used in electric vehicle propulsion system," in *SARC-ACN International Conference*, New Delhi, India, 12th March, 2017.

[22] K. T. chua, Wenlong Li, "Over view of electric machine for electic and hybrid vechile".

[23] Hemish R. Choksi, Hemant I. Joshi, "Experimental Results of Variable Frequency Drive for Three Phase Induction Motor Using Microcontroller," *International Journal of Innovative Research in Electrical, Electronics, Instrumentation and Control Engineering*, vol. 03, no. 03, March 2015.

[24] S. R. Jape, and A. Thosar, "Comparsion of electric motors for electric vehicle application," *International Journal of Research in Engineering and Technology*, vol. 06, no. 09, Sep-2017.

[25] Sen Li, "A Review of Electric Motor Drives for Applications in Electric and Hybrid Vehicles," *International Journal of Engineering Research and Technology* , March 2017.

[26] P. N. Bhatta, H. Meharb, and M. Sahajwanib, "Electrical Motors for Electric Vehicle – A Comparative Study," in *SSRN-ELSEVIER*, India, 2018-2019.

[27] Ali Saghafinia, "Introduction on IM drive," *Nova Science Publisher*, pp. 1-10, 2016.

[28] Zelechowski, Marcin, Space Vector Modulated – Direct Torque Controlled (DTC – SVM) Inverter – Fed Induction Motor Drive, Poland: Warsaw University of Technology, 2005.

[29] S. Hemza, N. Mansour, and M. Abdelhamid, "Electric Vehicle Speed Control using Three Phase Inverter operated by DSP-based Vector Pulse Width Modulation Technique," *Mohamed Boudiaf University of Science and Technology*.

[30] Mr. Anurag M. Lulhe and Prof. Tanuja N. Date, "A Design & MATLAB Simulation of Motor Drive usedfor Electric Vehicle," in *2015 International Conference on Control,Instrumentation, Communication and Computational Technologies (lCCICCT)*, India, 2015.

[31] Sharma, A. Raj and Rahul, "Improved Direct Torque Control for Induction Motor in Electric Vehicle Application," *IEEE*, no. 18, 2018.

[32] Latif, F. Sedaghati and S. Hadi, "Application of a Three-Phase Multilevel Inverter for DTC Based Induction Motor Drive," in *IEEE*, Ardabil, Iran, 2018.

[33] L. Narasimha, R. Yalavarthi and Dr. R. Gurram, "Modeling, analysis and ANFIS control for DTC-SVM of induction motor of an electric vehicle using electrical differential.," *International Journal of Electrical Engineering & Technology (IJEET),* vol. 10, no. 02, pp. 57-68, April 2019.

[34] Ta, Thanh Vo-Duy and Minh C, "A signal hardware in the loop model," *Robomech*, p. 6, 2016.

[35] S. M. Goda, Y. S. Elkoteshy, A. N. Ouda and A. E. Elawa, "Scalar Control Technique for Three Phase Induction Motor for Electric Vehicle," in *Twentieth International Middle East Power Systems Conference (MEPCON)*, Cairo University, Egypt, 2018.

[36] A. D. a. P. K. Amit Kumar Singh, "Analysis of Induction Motor for Electric Vehicle Application Based on Drive Cycle Analysis," in *IEEE International Conference on Power Electronics, Drives and Energy Systems*, 2014.

[37] A. Smallbonea, B. Jiab, P. Atkinsc, and A. P. Roskilly, "The impact of disruptive powertrain technologies on energy consumption and carbon dioxide emissions from heavy-duty vehicles," *Elsevier*, pp. 4-5, 2020.

[38] M. Ravi Teja Reddy, C. Sai Virinchy, T.S.A. Suryakumari, "Investigation of Capacity of Motor and its Simulation for an Electric Vehicle," *Journal of Chemical and Pharmaceutical Sciences,* no. 05, 2016.

[39] R, Shabin and Bindu, "Induction motor based drive for hybrid electric vehicle application," *International Journal Of Electrical, Electronics And Data Communication,* vol. 05, no. 07, pp. 31-32, Jul.-2017.

[40] T. Porselvi, M. K. Srihariharan, and J. Ashok, "Selection of Power Rating of an Electric Motor for Electric Vehicles," *International Journal of Engineering Science and Computing,* vol. 7, no. 4, 2017.

[41] *Standard Motor Catalogue.* [Performance]. TECO e motors.

[42] G. D. a. G. S. P. Nandawadekar Ajit Dattu, "Multifunctional Induction Machine," in *IEEE International WIE Conference on Electrical and Computer Engineering (WIECON-ECE),* Pune, India, December 2016.

[43] H. Kantari, "K Direct Torque Control of Induction Motor Using Space Vector," *International Journal of Modern Engineering Research (IJMER),* vol. 02, no. 05, pp. 3747-3768, 2012.

[44] Hussein, A. I. jaber and H. Idan, "Mathematical driving model of three phase induction motor in stationary coordinate frame," *Diyala Journal of Engineering Sciences,* pp. 255-265, December. 2015.

[45] M. J. Asif, T. Shahbaz, S. U. Hassan and S. Rizvi, "Mathematical Modelling of 3-phase Induction motor to study the Torque vs. Speed Characteristics using MATLAB Simulink," *Institute of Electrical and Electronics Engineers (IEEE),* 2016.

[46] P. D. M. Ahmad, High Performance AC Drives, India: Springer-Verlag London Limited , 2010.

[47] L. Aarniovuori, H. Kärkkäinen and M. Niemelä, "Modelling a Vector Controlled Induction Motor in Simulink," in *International Journal of Engineering Research and Technology,* October 2018.

[48] Vijay Kumar Singh, Ravi Nath Tripathi and Tsuyoshi Hanamoto, "HIL Co-Simulation of Finite Set-Model Predictive Control Using FPGA for a Three-Phase VSI System," *Energies*, 12 April 2018.

[49] Prasad, G.Naga Jyothi and P.Ram, "Controlling of three level diode clamped multi-level inverter fed induction motor using space vector PWM," *International Journal of Professional Engineering Studies*, vol. 10, no. 01, Jun 2018.

[50] G. Abdalrahman, O. H. Abdalla, and M. I. Jibril, "Space Vector Pulse Width Modulation Technique Applied to Two Level Voltage Source Inverter," *SUST Journal of Engineering and Computer Science (JECS)*, vol. 09, no. 02, 2018.

[51] Z. B. Ibrahim, Md. L. Hossain, and I. B. Bugis, "Simulation Investigation of SPWM, THIPWM and SVPWM Techniques for Three Phase Voltage Source Inverter," *International Journal of Power Electronics and Drive System (IJPEDS)*, 2014.

[52] O. M. Meetei, "Advanced Control Methods of Induction Motor: A Review," *ADBU Journal of Electrical and Electronics Engineering (AJEEE)*, vol. 01, no. 01, 2017.

[53] M. Boutouba, A. E. Ougli, and S. Miqoi, "Asymmetric Fuzzy Logic Controlled DC-DC Converter for Solar Energy system," *Journal of Renewable Energy and Sustainable Development (RESD)*, vol. 02, no. 01, 2016.

References Link

[L1] Ethiopian energy situation (accused on March 9 2020)

https://energypedia.info/wiki/Ethiopia_Energy_Situation#Energy_Situation

[L2] Link for Figure 2.1 parts of electric vehicle (accused on January 14 2020)

https://afdc.energy.gov/vehicles/how-do-all-electric-cars-work

[L3] Types of motor for EV (accused on February 6 2020)

https://circuitdigest.com/article/different-types-of-motors-used-in-electric-vehicles-ev

APPENDIEX

Appendix A: Related to analysis of data

MATLAB code for the analysis of aerodynamics force vs speed in Km/hr (Figure 3.5)

```
clear all;
m=1360; % mass of the Vehicle
g=9.81;
a=1.8; % acceleratin in m/s^2
r=0.2539; % Radius of the wheel in meter 1142/70-R12
K_friction=0.01; %Coefficient of friction for asphalt road
F_tot=0;
v=23.6; %speed of the car in m/s
Tot_effcen.M=0.95;
Adnsty=1.2041; %air density Kg/m^3
Af=2.688; %area in m^2
vo=0; %air velocity in m/s
Cd=0.25; % drag coefficient
%Initial condition
Vkph=0;
Vkph1=0;
d_Vkph=1e-2; %unit step increment
Vkph_final=85; %final value in km/hr.
x=1;
n=1;
while(Vkph<Vkph_final),
Vmps=Vkph*(1000/3600);
Fadyna=0.5*Adnsty*Cd*Af*(Vmps+vo)^2;
if Vkph<=85*d_Vkph;
statfric=0.2;
else
statfric=0;
end
F_tot=m*g*(K_friction+statfric)+Fadyna+m*a; % Total force(Nm)
```

```
Power=F_tot*Vmps/0.95; % Required input power (Watt)
Torque=(Power*r/Vmps);% Nm
Vkph=Vkph+d_Vkph;
Vkph1=Vkph1+d_Vkph;
if x>0,
F_totn(n)=F_tot;
Torquen(n)=Torque;
Powern(n)=Power/1000; %Power in KW
Fadynan(n)=Fadyna;
Vkphn(n)=Vkph;
n=n+1;
x=1;
end
x=x+1;
end

plot(Vkphn,Fadynan,'r','LineWidth',2);
axis([0 95 0 230]);
grid
xlabel('Speed of the car (Km/hr)')
ylabel('Aerodynamic (Drag) Resistance Force (N)')
```

MATLAB code for the analysis of power required to drive EV vs speed in Km/hr (Figure 3.6)

```
clear all;
close all;
m=1360; % mass of the Vehicle
fric=0.01;
g=9.81;
a=1.8; % acceleratin in m/s^2
r=0.2539; % Radius of the wheel in meter 1142/70-R12
K_friction=0.01; %Coefficient of friction by considering asphalt road
F_tot=0;
v=23.6; %speed of the car in m/s
Tot_effcen.M=0.95;
```

```
Adnsty=1.2041; %air density Kg/m^3
Af=2.688; %area in m^2
vo=0; %air velocity in m/s
Cd=0.25; % drag coefficient
%Initial condition
Vkph=0;
Vkph1=0;
d_Vkph=1e-2; %unit step increment
Vkph_final=100; %final value in km/hr.
x=1;
n=1;
while(Vkph<Vkph_final),
Vmps=Vkph*(1000/3600);
Fadyna=0.5*Adnsty*Cd*Af*(Vmps+vo)^2;
if Vkph<=100*d_Vkph;
statfric=0.2;
else
statfric=0;
end
F_tot=m*g*(K_friction+statfric)+Fadyna+m*a; % Total force(Nm)
Power=F_tot*Vmps/0.95; % Required input power (Watt)
Torque=(Power*r/Vmps);% Nm
Vkph=Vkph+d_Vkph;
Vkph1=Vkph1+d_Vkph;
if x>0,
F_totn(n)=F_tot;
Torquen(n)=Torque;
Powern(n)=Power/1000; %Power in KW
Fadynan(n)=Fadyna;
Vkphn(n)=Vkph;
n=n+1;
x=1;
end
x=x+1;
end

plot(Vkphn,Powern,'r','LineWidth',2);
set(gca,'FontSize',12)
axis([0 100 0 80]);
grid
xlabel('Speed of the of the car(Km/hr)')
ylabel('Power (KW)')
```

MATLAB code for the analysis of torque speed and power characteristics of the motor (Figure 3.7)

```
Ratedpower=75000; %Rated power in Watt
wrpm_final=6000; %final value in RPM
wrpm=0; %initial condition
d_wrpm=1e-2; %unit step increment
x=1;
n=1;
while(wrpm<wrpm_final),
wm=(wrpm*2*pi)/60;
Torque= Ratedpower/wm;
if Torque>=480,
Torque=480;
end
if Torque<480,
Torque= Torque;
end
Power=Torque*wm;
wrpm=wrpm+d_wrpm;
if x>16,
wrpmn(n)=wrpm;
Torquen(n)=Torque;
Powern(n)=Power/1000;
n=n+1;
x=1;
end
x=x+1;
end
figure(1);
[AX,Torque,Power]=plotyy(wrpmn,Torquen, wrpmn,Powern);
axis([0 6000 0 500]);
set(get(AX(1),'ylabel'), 'string','Torque(Nm)')
```

```
set(get(AX(2),'ylabel'), 'string','Power(KW)')
set(Torque,'LineStyle','--')
set(Power,'LineStyle','-')
set(gca, 'FontName','TimesNewRoman')
set(gca, 'FontSize',12)
set([Torque,Power],'LineWidth',1.5)
xlabel('w_m(rpm)')
grid
legend('Torque','Power')
```

Appendix B: Related to system modeling

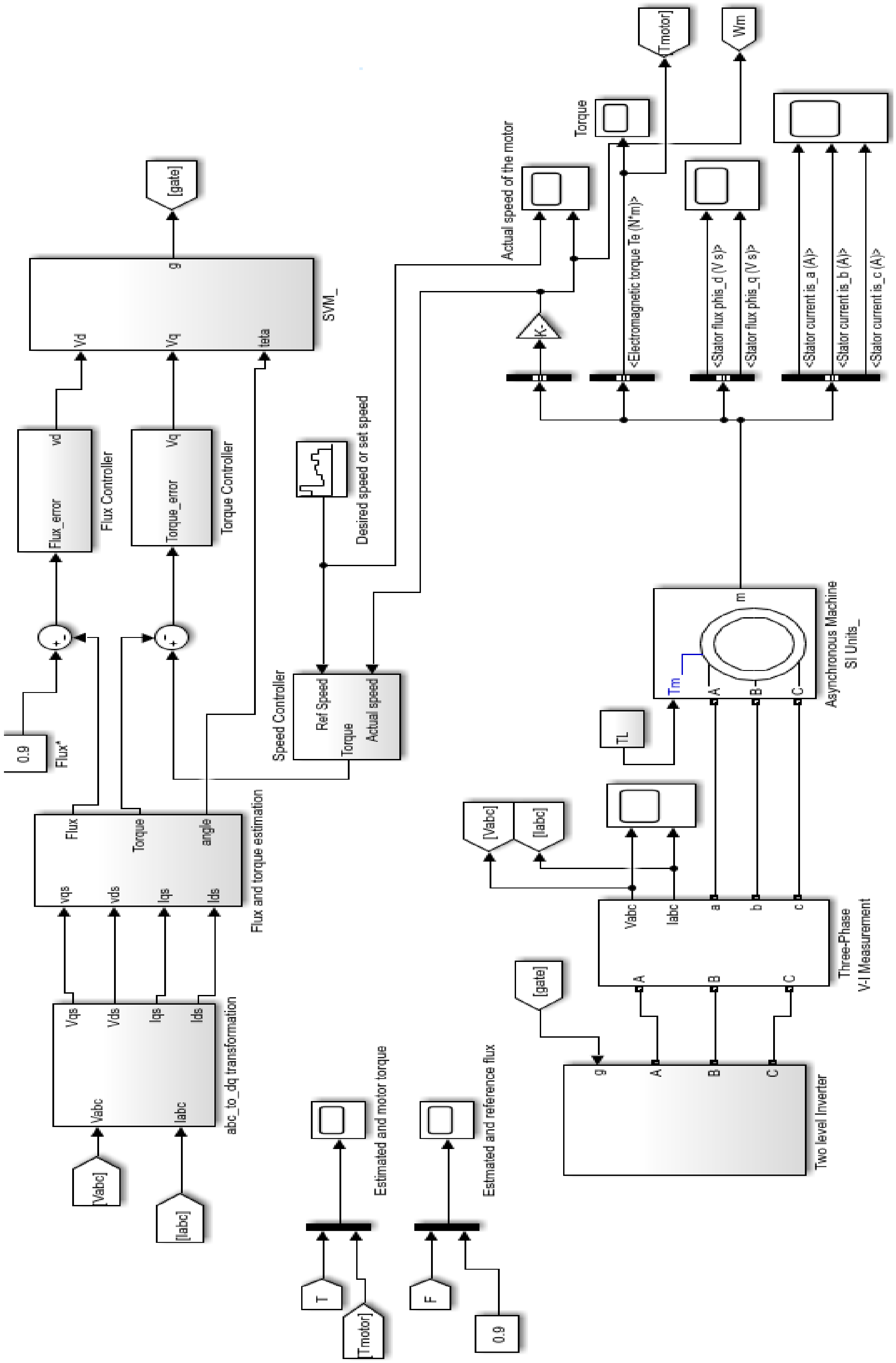

Figure B.1 MATLAB/Simulink model of the proposed drive control system

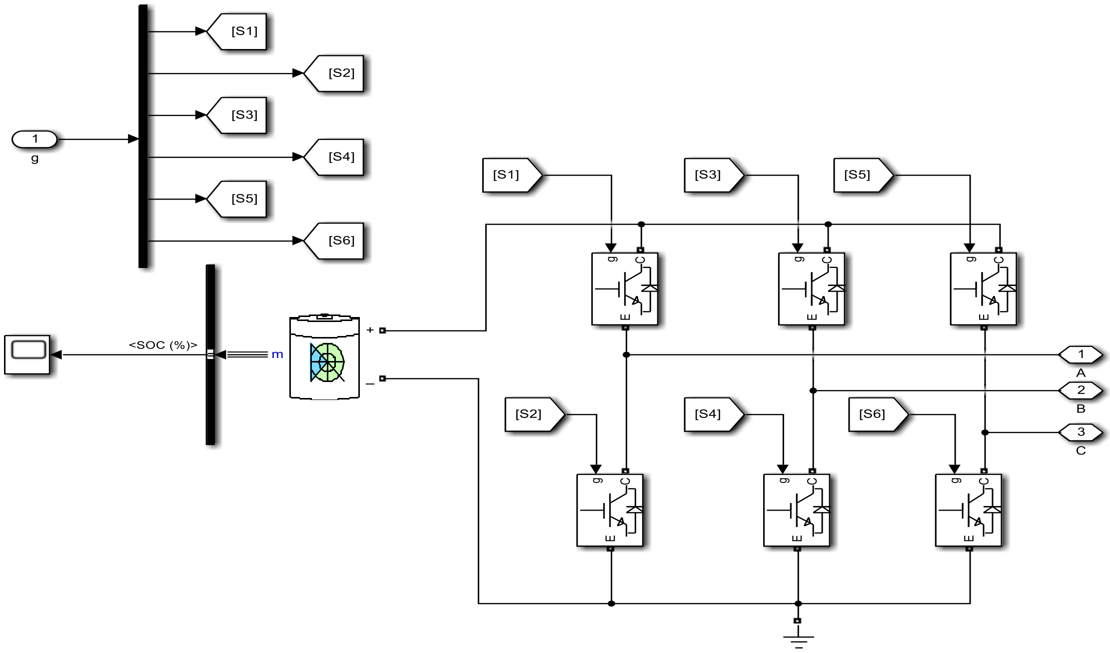

Figure B.2 Three phase two level inverter with battery system

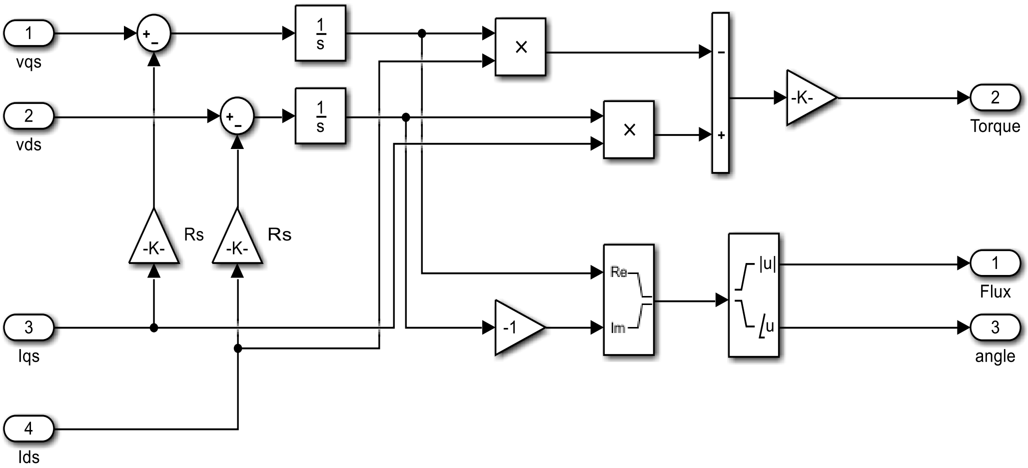

Figure B.3 MATLAB Simulink block diagram of flux and torque estimator

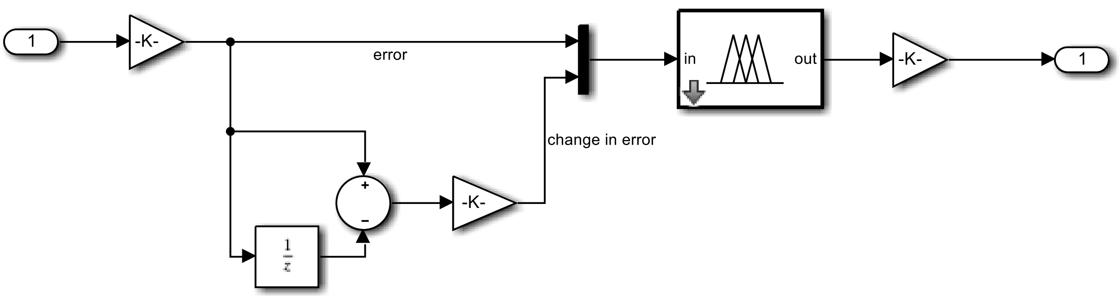

Figure B.4 MATLAB Simulink block diagram of fuzzy logic controller

Appendix C: Related to implementation of SVPWM

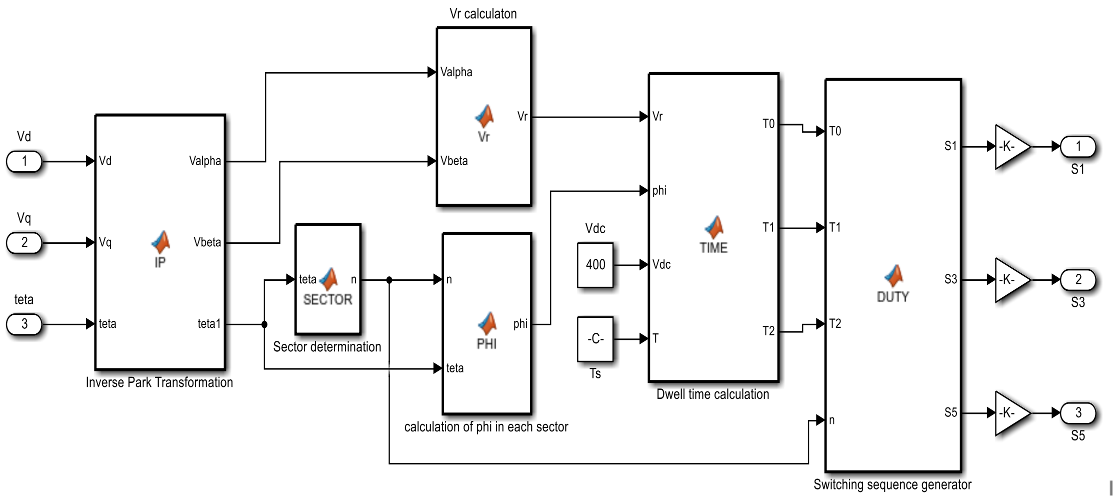

Figure C.1 MATLAB Simulink block of SVPWM

MATLAB code for inverse park transformation

```
function [Valpha, Vbeta, teta1] = IP(Vd, Vq, teta)
Valpha= Vd*cos(teta)-Vq*sin(teta);
Vbeta= Vd*sin(teta)+Vq*cos(teta);
teta1= atan2(Vbeta, Valpha);
```

MATLAB code for sector determination

```
function n = SECTOR(teta)
n=0;
if(teta>0)&&(teta<=pi/3)
    n=1;
end
if(teta>pi/3)&&(teta<=2*pi/3)
    n=2;
end
if(teta>2*pi/3)&&(teta<=pi)
    n=3;
end
if(teta<=0)&&(teta>-1*pi/3)
    n=6;
end
if(teta<=-1*pi/3)&&(teta>-2*pi/3)
    n=5;
end
if(teta<=-2*pi/3)&&(teta>-1*pi)
    n=4;
end
```

MATLAB code for calculation of the magnitude of Vr

```
function Vr = Vr(Valpha, Vbeta)
Vr=0;
Vr=sqrt(Valpha^2+Vbeta^2);
```

MATLAB code for calculation of phi in each sector

```
function phi = PHI(n, teta)
phi=0;
if(n==1)
    phi=teta;
end
if(n==2)
    phi=teta-pi/3;
end
if(n==3)
    phi=teta-2*pi/3;
end
if(n==6)
    phi=teta+pi/3;
end
if(n==5)
    phi=teta+2*pi/3;
end
if(n==4)
    phi=teta+pi;
end
```

MATLAB code for dwell time calculation

```
function [T0, T1, T2] = TIME(Vr,phi,Vdc, T)

a=sqrt(3)*(Vr/Vdc);
T1=T*a*sin(pi/3-phi);
T2=T*a*sin(phi);
T0=T-T1-T2;
```

MATLAB code for switching sequence generator

```
function [S1, S3, S5] = DUTY(T0, T1, T2, n)
S1=0;
S3=0;
S5=0;
if (n==1)
    S1=T1+T2+T0/2;
    S3=T2+T0/2;
    S5=T0/2;
end
```

```
if(n==2)
    S1=T1+T0/2;
    S3=T1+T2+T0/2;
    S5=T0/2;
end
if(n==3)
    S1=T0/2;
    S3=T1+T2+T0/2;
    S5=T2+T0/2;
end
if(n==4)
    S1=T0/2;
    S3=T1+T0/2;
    S5=T1+T2+T0/2;
end
if(n==5)
    S1=T2+T0/2;
    S3=T0/2;
    S5=T1+T2+T0/2;
end
if(n==6)
    S1=T1+T2+T0/2;
    S3=T0/2;
    S5=T1+T0/2;
End
```

Appendix D: Related to data collection

Daewoo-Damas-II specification accused from the internet on (January 18 2020).

https://www.autoevolution.com/cars/daewoo-damas-ii-2003.html#aeng_daewoo-damas-ii-2003-08-lpg

Parameter	Value
Fuel type	Hybrid
Fuel system	Electronic injection
Maximum speed of the car	112km/hr
Length	3485mm
Width	1400mm
Height	1920mm
Unladen weight	880kg
Front/rear track	1219/1209mm
Wheel base	1839mm
Tire size	155R12
Maximum gradient angle	23^0
Combined	9.4L/100km
CO_2 emission	224g/km